Theoretical evaluation of the nonlinear optical properties of extended π-conjugated chromophores

A Dissertation
Presented to
The Academic Faculty

by

Ohira, Shino

In Partial Fulfillment
of the Requirements for the Degree
Doctor of Philosophy in the
School of Chemistry and Biochemistry

Georgia Institute of Technology
August 2009

Theoretical evaluation of the nonlinear optical properties of extended π-conjugated chromophores

Approved by:

Dr. Jean-Luc Brédas, Advisor
School of Chemistry and Biochemistry
Georgia Institute of Technology

Dr. Jiří Janata
School of Chemistry and Biochemistry
Georgia Institute of Technology

Dr. Seth R. Marder
School of Chemistry and Biochemistry
Georgia Institute of Technology

Dr. David C. Sherrill
School of Chemistry and Biochemistry
Georgia Institute of Technology

Dr. Bernard Kippelen
School of Electrical and Computer Engineering
Georgia Institute of Technology

Date Approved: June 12, 2009

ACKNOWLEDGEMENTS

I gladly take this opportunity to express my sincere thanks to my colleagues and friends who have personally and practically supported this dissertation. I would like to express the deepest appreciation to my advisor, Professor Jean-Luc Brédas. His commitment to high standards always motivated me. I thank him for his helpful direction and guidance in my research. He was the most important contributor in this dissertation. I also would like to thank my committee members: Professors Jiri Janata, Bernard Kippelen, Seth R. Marder, and David C. Sherrill for their support and teachings.

My sincere gratitude goes to my colleagues and collaborators; Professors Harry L. Anderson and Joe W. Perry; Doctors Stephen Barlow, Veaceslav Coropceanu, Joel Hales, Mariacristina Rumi, Indranil Rudra, Karin Schmidt; and Jonathan D. Matichak, Susan Odom, Karl Thorley, and Xuan Zhang; and Brédators! Their efforts and work have enabled the completion of the dissertation.

In addition, I am pleased to acknowledge Susan Bossa, Sayaka Fujishige, Yuko Kato, Geoffrey Rollins, Yuriko Suzuki, Yumiko Tsutsumi, and Sho Yamamoto, the people whose support was really important for me. Finally, I would like to thank my family for believing in me and my decision for seven years since I left my home country at the age of eighteen.

TABLE OF CONTENTS

LIST OF TABLES

LIST OF FIGURES

Page

SUMMARY

Organic materials with large two-photon absorption (TPA) cross-sections, δ, are of interest due to potential applications in optics, materials fabrication, and biology. These applications exploit the advantages of a two-photon process compared to a one-photon process, in particular, the improved penetration depth, reduced scattering, and higher spatial selectivity in three dimensions. Also, TPA can be used to investigate the nature of electronic states that are one-photon forbidden in a compound with high symmetry.

In this dissertation, we discuss structure – non-linear optical (NLO) properties relationships in chromophores with enhanced third-order poralizability and/or two-photon absorption response, on the basis of highly correlated quantum-mechanical methods. Chapter 1 will introduce the general linear and non-linear optical processes in organic chromophores, and present the major computational methodologies (including *ab initio* Hartree-Fock and Density Functional Theory as well as the semi-empirical Intermediate Neglect of Differential Overlap methods) we have used to compute the NLO properties. Our main results are discussed in the following chapters. In Chapter 2, we focus on first- and third-order polarizabilities in cyanine and alkyne-cyanine compounds that have been recently synthesized. In Chapter 3, we discuss the TPA response as a function of the electronic coupling between porphyrin moieties in porphyrin dimers. Finally, Chapter 4 is devoted to a study of TPA in squaraine and cyanine compounds, and presents and analysis of the vibronic origin of the TPA response in some of

these molecules. Our general conclusions and outlook are given in the final Chapter.

CHAPTER 1:

Introduction

Two-photon absorption (TPA) is the process by which a system, for instance a molecule, absorbs two photons simultaneously; this excites the molecule from one electronic state to a (high) excited state. The TPA cross-sections are measured in the units of Göppert-Mayer (1 GM = 10^{-50} cm^4 s $photon^{-1}$ $molecule^{-1}$), after Maria Göppert-Mayer[1] who first predicted the phenomenon in 1931, *30 years* before it was experimentally observed.[2] TPA can be described in terms of the imaginary part of the third-order nonlinear electric susceptibility, $\chi^{(3)}$. The electric susceptibility is a measure of how easily a material polarizes in response to an electric field, F. The relationship between the susceptibility and polarization, P and F is:

$$P = \chi F \tag{1.1}$$

where χ has linear and nonlinear components as shown in Figure 1.1.

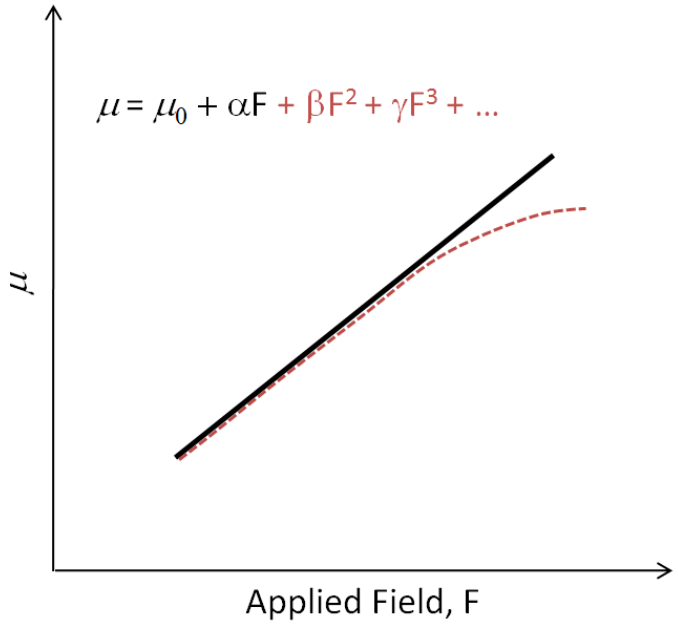

Figure 1.1. Plots of the molecular dipole moment μ versus applied electric field with: (i) only the linear term (black, straight line); and (ii) upon appearance of non-linear terms (red, dotted line).

When χ and P are expanded in a power series:

$$\chi = \chi^{(1)} + \chi^{(2)} \cdot \mathrm{F} + \chi^{(3)} : \mathrm{F}^2 + \cdots \tag{1.2}$$

$$\mathrm{P} = \mathrm{P}_0 + \chi^{(1)} \cdot \mathrm{F} + \chi^{(2)} : \mathrm{F}^2 + \chi^{(3)} \vdots \mathrm{F}^3 + \cdots \tag{1.3}$$

The electric susceptibilities correspond to a macroscopic description of the molecular level. This enables the investigation of chemical structure–optical properties relationships, which can be used to better understand the NLO processes and to design chromophores with desired optical properties. In this case, we consider the evolution of the molecular dipole moment μ with the field:

$$\mu = \mu_0 + \alpha \cdot \mathrm{F} + \beta : \mathrm{F}^2 + \gamma \vdots \mathrm{F}^3 + \cdots \tag{1.4}$$

where μ_0 denotes the permanent electric dipole moment, and α, β, and γ denote first-, second-, and third-order polarizabilities. When an intense light beam propagates through a two-photon absorbing medium, the variation in beam intensity at a given frequency ω is given by:

$$\frac{dI_z(\omega)}{dz} = \alpha(\omega)I_z(\omega) - \beta(\omega)I_z^2(\omega) - \cdots \quad (1.5)$$

where I_z denotes a laser beam intensity propagating in the z-direction, $\alpha(\omega)$ the linear absorption (or one-photon absorption, OPA) coefficient, and $\beta(\omega)$ the non-linear absorption (or TPA) coefficient. Thus, the strength of absorption due to a TPA process depends on the square of the light intensity, which explains the high spatial resolution that can be achieved with a tightly focused laser beam (see Figure 1.2).

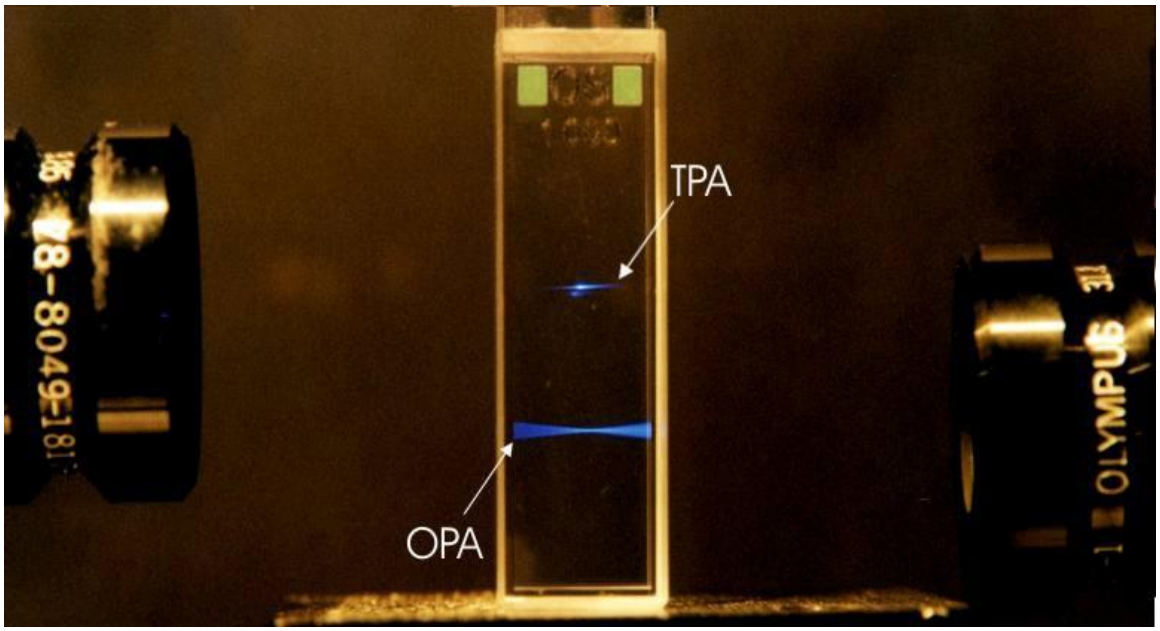

Figure 1.2. Difference between one-photon (OPA) and two-photon absorption (TPA) in a low absorbing medium. Reproduced from Ref. 30.

In this chapter, we first introduce the basic principles of quantum mechanics and modern computational chemistry in Section 1.1. Section 1.2 uses perturbation theory to describe the first-order polarizability α in the electric dipole approximation; we then provide a description of the third-order polarizability γ and TPA.

1.1 Quantum mechanics

Here, we first present the basic quantum mechanics expressions and then describe the general methodology we have followed to compute the NLO properties of the large chromophores we have investigated. We point out the difficulties and weaknesses of this approach and comment on alternative procedures that are still under development.

1.1.1 Schrödinger equation

We start with the time-independent Schrödinger equation:

$$H\Psi(\mathrm{r}_1, \mathrm{r}_2, \ldots, \mathrm{r}_\mathrm{n}; \mathrm{R}_\mathrm{A}, \mathrm{R}_\mathrm{B}, \quad \mathrm{aR}_\mathrm{N}) = E\Psi(\mathrm{r}_1, \mathrm{r}_2, \ldots, \mathrm{r}_\mathrm{n}; \mathrm{R}_\mathrm{A}, \mathrm{R}_\mathrm{B}, \quad \mathrm{aR}_\mathrm{N})$$

where H is the Hamiltonian describing the system; E is the total energy; and Ψ is the wavefunction of the system of particles with nn electrons and N nuclei. Note that Ψhas no physical meaning; its square does and represents the probability of finding the electron (or electron density) at a given place. While the solution of this equation can describe all the molecular properties, the equation can be solved exactly only for the hydrogen and hydrogenoid (He^+, Li^{2+} and so on) atoms.

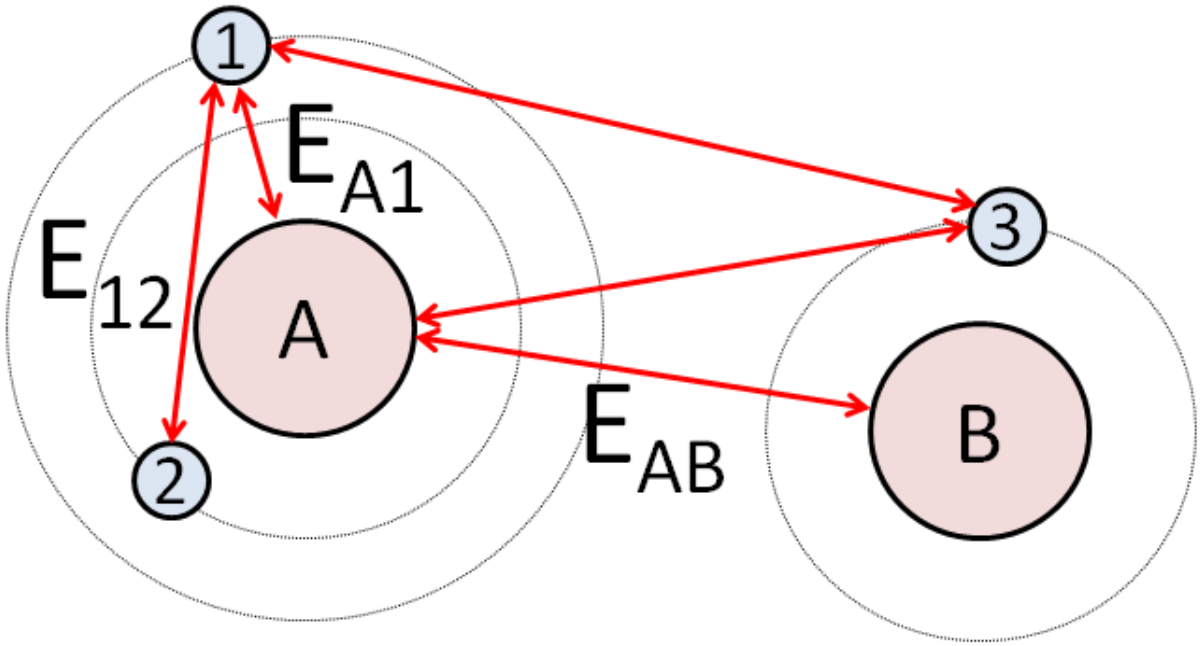

Figure 1.3. Illustration of the interactions between nuclei and electrons; *i.e.,* the nuclear-nuclear repulsion (E_{AB}), the electron-nuclear attraction (E_{A1}), and the electron-electron repulsion (E_{12}).

The energy for a system with nuclei and electrons can be considered as the summation of the nuclear kinetic energy, the electronic kinetic energy, the nuclear-nuclear repulsion energy, the electron-nuclear attraction energy, and the electron-electron repulsion energy (Figure 1.3).

$$\hat{H} = \hat{T}_{nuc} + \hat{T}_{el} + \hat{V}_{nuc} + \hat{V}_{nuc-el} + \hat{V}_{el}$$

Nuclear kinetic term ($\hat{T}_{nuc}$): $-\frac{1}{2M_A}\sum_i \nabla_A^2$

Electronic kinetic term ($\hat{T}_{el}$): $-\frac{1}{2}\sum_i \nabla_i^2$

Nuclear repulsion term ($\hat{V}_{nuc}$): $-\sum_{A>B}\frac{Z_A Z_B}{R_{AB}}$ *(1.6)*

Electron repulsion term ($\hat{V}_{el}$): $\sum_{i>j}\frac{1}{r_{ij}}$

Electron-nuclear attraction term ($\hat{V}_{nuc-el}$): $-\sum_{A,i}\frac{Z_A}{r_{Ai}}$

where i, j refer to electrons and A, B refer to nuclei. Since electrons are much lighter than nuclei, they are considered to be able to adjust their positions instantly as the nuclei move. This is called the Born-Oppenheimer approximation, which enables the consideration of the nuclear and electronic motions separately. The nuclei are put at rest, the nuclear kinetic energy is thus neglected, and the nuclear-nuclear repulsion energy becomes a constant. This reduces the computational complexity dramatically, since eqn 1.6 reduces to electronic energy and wavefunction with the nucleus positions as parameters:

$$\hat{H}^{el}\Psi^{el}(\mathrm{r};\mathrm{R}) = E^{el}\Psi^{el}(\mathrm{r};\mathrm{R})$$

where

$$\hat{H}^{el} = -\frac{1}{2}\sum_i \nabla_i^2 - \sum_{A,i}\frac{Z_A}{r_{Ai}} + \sum_{i>j}\frac{1}{r_{ij}} \quad (1.7)$$

The impossibility of treating exactly the many-body electronic repulsion term in the electronic Schrödinger equation leads to the next approximation in which each electron is considered to move in the mean field due to all other electrons:

the Hartree-Fock approximation. Eqn 1.7 can then be rewritten as a set of one-electron equations:

$$\begin{aligned} \hat{h}^{HF}(\mathrm{r}_1)\psi_1(\mathrm{r}_1) &= \epsilon_1\psi_1(\mathrm{r}_1) \\ \hat{h}^{HF}(\mathrm{r}_2)\psi_2(\mathrm{r}_2) &= \epsilon_2\psi_2(\mathrm{r}_2) \\ &\vdots \\ \hat{h}^{HF}(\mathrm{r}_i)\psi_i(\mathrm{r}_i) &= \epsilon_i\psi_i(\mathrm{r}_i) \end{aligned} \tag{1.8}$$

where $\hat{h}^{HF}$ refers to the Hartree-Fock (HF) operator; $\psi_i(\mathrm{r}_i)$ to a one-electron wavefunction called a spin-orbital; and $\epsilon_i(\mathrm{r}_i)$ to the one-electron energy. To satisfy the antisymmetry principle (Pauli Exclusion Principle), the total wavefunction can be expressed in the form of a Slater determinant:

$$\psi = \frac{1}{\sqrt{n!}}\begin{vmatrix} \Psi_1(1) & \Psi_2(1) & \cdots & \Psi_\mathrm{n}(1) \\ \Psi_1(2) & \Psi_2(2) & \cdots & \Psi_\mathrm{n}(2) \\ \vdots & \vdots & \ddots & \vdots \\ \Psi_1(\mathrm{n}) & \Psi_2(\mathrm{n}) & \cdots & \Psi_\mathrm{n}(\mathrm{n}) \end{vmatrix} \tag{1.9}$$

The Hartree-Fock operator consists of a kinetic term, nuclear attraction term, Coulomb repulsion term, and exchange term:

$$\hat{h}^{HF}(\mathrm{r}_i) = -\frac{1}{2}\nabla_i^2 - \sum_A \frac{Z_A}{r_{Ai}} + \sum_j^{occ} 2J_j(\mathrm{r}_i) - \sum_j^{occ} K_j(\mathrm{r}_i)$$

where occ refers to occupied orbitals

Kinetic term: $-\frac{1}{2}\nabla_i^2$

Nuclear attraction term: $-\sum_A \frac{Z_A}{r_{Ai}}$

Coulomb repulsion: $\sum_j^{occ} 2J_j(\mathrm{r}_i)$ *(1.10)*

where $J_j(\mathrm{r}_i)\psi(\mathrm{r}_i) = \left[\int dr_j \frac{\psi_j(\mathrm{r}_j)\psi_j(\mathrm{r}_j)}{r_{ij}}\right]\psi_i(\mathrm{r}_i)$

Exchange: $-\sum_j^{occ} K_j(\mathrm{r}_i)$

where $K_j(\mathrm{r}_i)\psi(\mathrm{r}_i) = \left[\int dr_j \frac{\psi_j(\mathrm{r}_j)\psi_i(\mathrm{r}_j)}{r_{ij}}\right]\psi_j(\mathrm{r}_i)$

Since in the HF approximation, electron-electron repulsion is taken into account as due to the average potential experienced by the i^{th} electron in the presence of all other electrons, the instantaneous correlation of the electron motions is neglected.

As a further approximation, the spin-orbitals are typically expanded as a linear combination of atomic orbitals (LCAO) that usually correspond to Gaussian functions centered on the various atoms:

$$\psi_i(r_i) = \sum_p^{\omega} C_{ip}\chi_p(r_i) \qquad (1.11)$$

where χ_p denotes a basis function or atomic orbital; the coefficients C_{ip} are now the unknowns in the HF equations:

$$\hat{h}^{HF}(\mathrm{r}_i)\sum_p C_{ip}\chi_p(r_i) = \epsilon_i \sum_p C_{ip}\chi_p(r_i) \qquad (1.12)$$

By multiplying by $\int d\tau\, \chi_q^*(r_i)$ on the left on each side of eqn. 1.12, we eventually obtain the following matrix expression:

$$\sum_p F_{pq}\, C_{ip} = \epsilon_i \sum_p S_{pq}\, C_{ip} \qquad (1.13)$$

where the Fock matrix element (F_{pq}) refers to $\int d\tau\, \chi_q^*(r_i)\hat{h}^{HF}(\mathrm{r}_i)\chi_p(r_i)$ and the overlap matrix element (S_{pq}) to $\int d\tau\, \chi_q^*(r_i)\chi_p(r_i)$. The HF equations can be written compactly in a matrix form as $\mathrm{FC} = \mathrm{SCE}$. By diagonalizing this (pseudo) eigenvalue equation, the LCAO coefficients and the spin-orbital energies can be determined (the matrix E collects the one-electron energies $\boldsymbol{\epsilon_i}$). The HF equations have to be solved iteratively by using an initial guess of the C matrix, as shown in Figure 1.4. According to the variational principle, the HF total energy is higher or equal to the exact total energy. In practice, the larger the number of basis functions included to describe a system, the more accurate the results. Note that if all the integrals appearing in eqn 1.13 in the expression of the Fock and overlap matrices are evaluated, the method is referred to as Hartree-Fock *ab initio*.

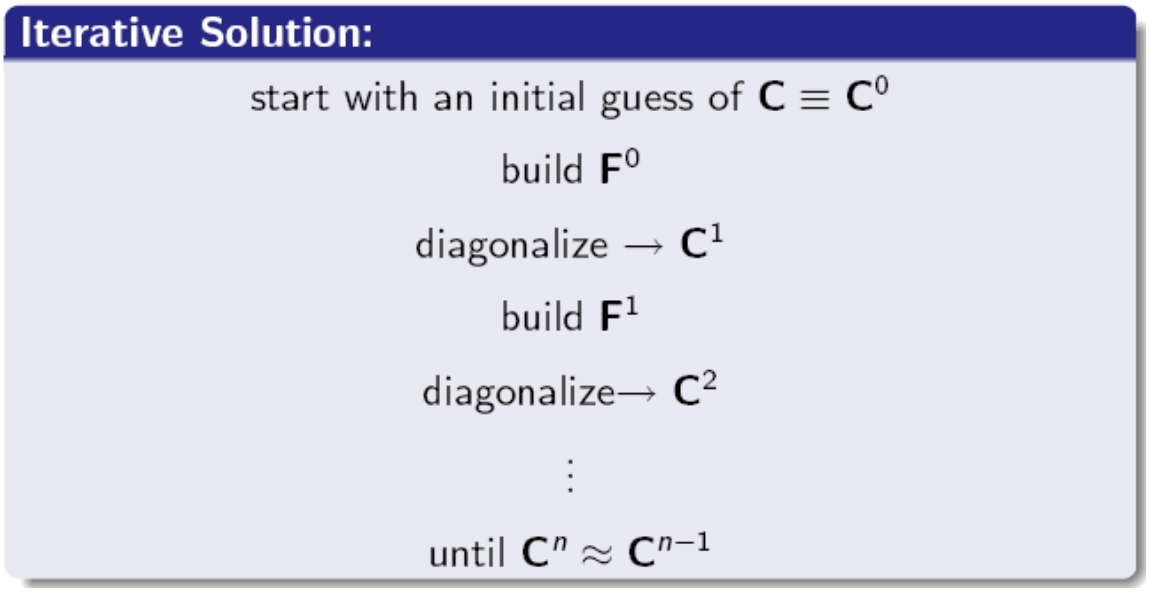

Figure 1.4. Self-consistent field method to obtain an iterative solution to the HF equations.

1.1.2 Post Hartree-Fock methods

In the HF method, the total wavefunction is described by a single Slater determinant, *i.e.*, a single electronic configuration. To take into account the electron correlation effects, several approaches employ multiple Slater determinants. The exact solution to the electronic Schrödinger equation can be obtained by using a "full configuration interaction (or full CI)" to express the wavefunction as a linear combination of all possible n-electron Slater determinants. Thus, full-CI calculations with an infinitely large basis set can lead to the exact solution. In practice, a full-CI approach can only be applied to very small systems. In molecules of the size we are interested in, electron correlation effects can only be partially taken into account and are based on choosing the most relevant Slater determinants. Given that the HF wavefunction is often a reasonable reference state, the accuracy of the post-HF methods, such as CI (or

limited CI in contrast to full CI), many-body perturbation theory, and coupled-cluster theory, depends on the selection of those 'essential' determinants. We will consider the CI method next.

The CI method has been widely used not only for calculating the ground-state correlation energy but also for determining the excited-state energies in many-electron atomic and molecular systems. The exact full CI wavefunction Ψ for any electronic state is formed as a linear combination of all possible Slater determinants in a given basis set:

$$\Psi = C_0|\Phi_0\rangle + \sum_{\mathrm{a,p}} C_a^p|\Phi_a^p\rangle + \sum_{\substack{\mathrm{a}<b \\ \mathrm{p}<q}} C_{ab}^{pq}|\Phi_{ab}^{pq}\rangle + \sum_{\substack{\mathrm{a}<b<c \\ \mathrm{p}<q<r}} C_{abc}^{pqr}|\Phi_{abc}^{pqr}\rangle + \cdots$$
$$= C_0|\Phi_0\rangle + C_S|S\rangle + C_D|D\rangle + C_T|T\rangle + \cdots \quad (1.14)$$

In Figure 1.5, a sample of singly, doubly, and triply excited determinants is shown: one, two, or three electrons have been promoted from occupied to unoccupied levels with respect to the HF determinant, respectively. When states are represented by a combination of singly [or singly and doubly] excited determinants, those calculations are referred to as singly [or singly and doubly] excited CI, SCI [or SDCI].

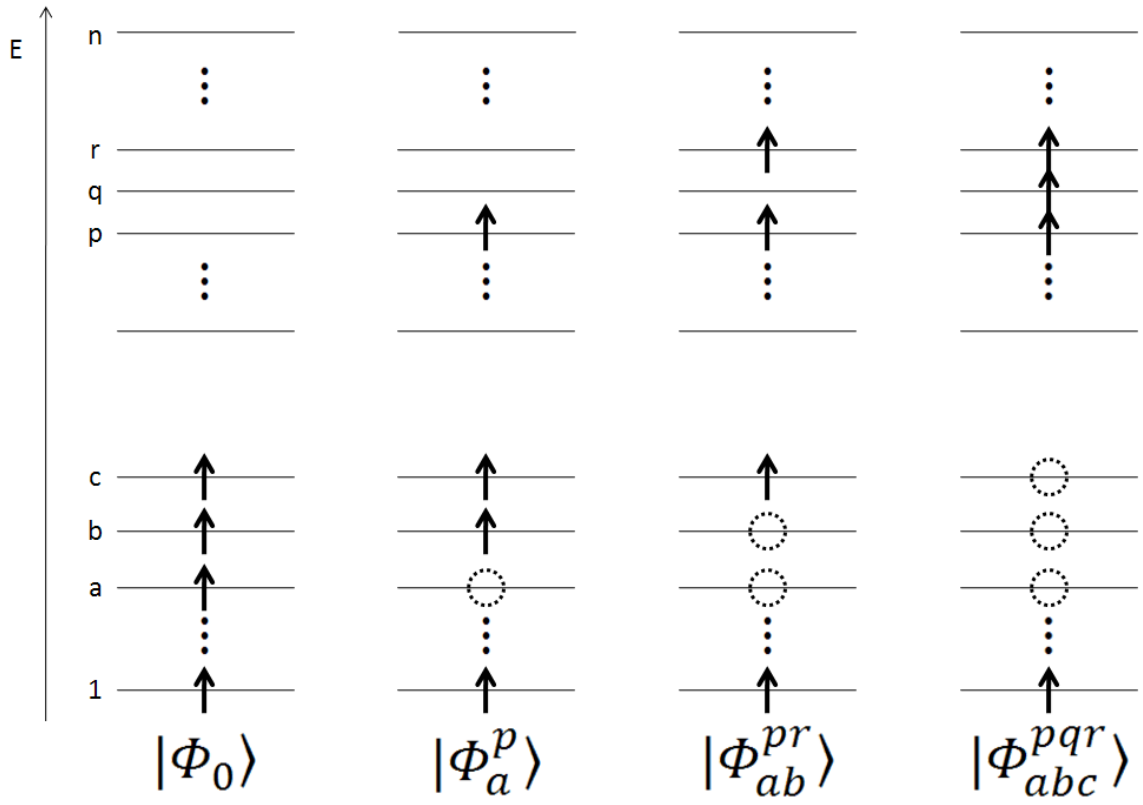

Figure 1.5. Excited determinants $|\Phi_a^p\rangle$, $|\Phi_{ab}^{pr}\rangle$, and $|\Phi_{abc}^{pqr}\rangle$ represent the promotion of one, two, or three electrons from occupied molecular orbital levels, *i.e.*, a, b and c, into unoccupied molecular orbital levels, *i.e.*, p, q and r, in comparison with the reference HF Slater determinant $|\Phi_0\rangle$.

Brillouin's theorem states that: (i) all matrix elements $\langle\Phi_0|\hat{H}|S\rangle$ are zero; and (ii) all matrix elements of the Hamiltonian between determinants that differ by more than 2 spin orbitals are zero. There is mixing between doubles and quadruples only when a and b are included in the set {c, d, e, f} and r and s included in the set {r, s, t, u} for $\langle\Phi_{ab}^{pr}|\hat{H}|\Phi_{cdef}^{rstu}\rangle$ ($\leftrightarrow \langle D|\hat{H}|Q\rangle$) to be nonzero. Point (i) means that there is no interaction between the HF reference state and single excitations. However, these still can indirectly mix since there is coupling between the HF

ground state and double excitations that interact with single excitations. Table 1.1 summarizes the structure of the CI matrix.

Table 1.1. Structure of the CI matrix.

	$\|\Phi_0\rangle$	$\|S\rangle$	$\|D\rangle$	$\|T\rangle$	$\|Q\rangle$
$\langle\Phi_0\|$	$\langle\Phi_0\|\hat{H}\|\Phi_0\rangle$	0	$\langle\Phi_0\|\hat{H}\|D\rangle$	0	0
$\langle S\|$		$\langle S\|\hat{H}\|S\rangle$	$\langle S\|\hat{H}\|D\rangle$	$\langle S\|\hat{H}\|T\rangle$	0
$\langle D\|$			$\langle D\|\hat{H}\|D\rangle$	$\langle D\|\hat{H}\|T\rangle$	$\langle D\|\hat{H}\|Q\rangle$
$\langle T\|$				$\langle T\|\hat{H}\|T\rangle$	$\langle T\|\hat{H}\|Q\rangle$
$\langle Q\|$					$\langle Q\|\hat{H}\|Q\rangle$

Multi-reference determinant configuration interaction (MRDCI)

The next approach to describe multi-determinantal eigenfunctions, is to set multiple Slater determinants, not only the ground state but also excited Slater determinants, as references. From those references, excitations are considered to better include electron correlation effects. This method is called multireference determinant configuration interaction (MRDCI).

Due to the large size of the systems under investigation, the SCI method is widely used to compute singlet state energies. In the methodology, we ignore the contribution from double excitation to both ground state and singlet excited states, and also that from triple excitation to the excited states. However, SCI is usually not sufficient for computing the non-linear optical properties beyond second order. So, either MRD-CI or CIS [or CISD] calculations are performed to describe multideterminantal eigenfunctions. By using multiple references, some

determinants that effectively correspond to double excitations can be obtained using single excitations of a singly excited reference (Figure 1.6). In this figure, it is shown that the determinant $|\Phi_{c\bar{c}}^{p\bar{p}}\rangle$ is obtained by CIS using the determinant $|\Phi_{c}^{p}\rangle$ as a reference state while the determinant is obtained by CISD from the HF determinant. Both of the methods are computationally demanding for large molecules, and we need to restrict the active MO space that is considered upon electron excitations.

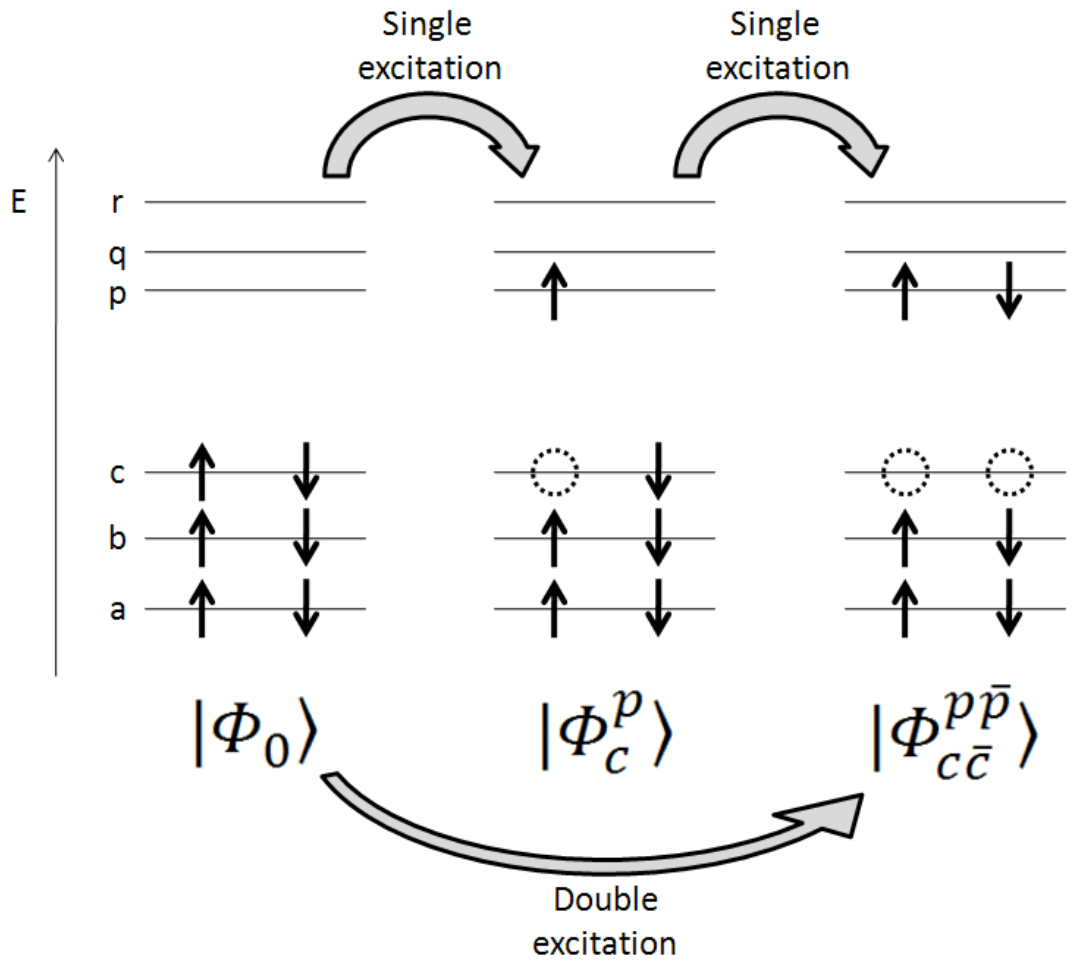

Figure 1.6. The determinant $|\Phi_{c\bar{c}}^{p\bar{p}}\rangle$ is obtained by CIS using determinant $|\Phi_c^p\rangle$ as a reference while is obtained by CISD from the HF determinant. Alpha electrons are represented as c and p, and beta electrons as $\bar{c}$ and $\bar{p}$.

1.1.3 Semiempirical methods

In the early days of quantum chemistry, *ab initio* calculations were computationally too expensive for large compounds and semiempirical methods were developed. These methods use parameters obtained from experimental data and include Hückel molecular orbital theory (HMO), Pariser-Parr-Pople method (PPP), complete neglect of differential overlap (CNDO), intermediate neglect of differential overlap (INDO), Zerner's INDO (ZINDO), modified intermediate neglect of differential overlap (MINDO), or neglect of diatomic differential overlap (NDDO) which includes the Austin model 1 (AM1) method. In this section, we concentrate on the INDO method since it has been widely used to compute the NLO properties of organic chromophores.

The major approximations in the INDO method are that: (i) only the valence electrons are explicitly included; and (ii) the zero differential overlap approximation (ZDO) is applied to reduce the number of two-electron integrals. ZDO ignores all the integrals that contain $\chi_i(r)\chi_j(r')$ with $i \neq j$ appearing in the Fock matrix elements:

$$\langle ij|kl\rangle = \delta_{ij}\,\delta_{kl}\langle ii|kk\rangle \tag{1.15}$$

where we define the two-electron integrals in bra-ket notation as:

$$\langle ij|kl\rangle = \int dr \int dr'\, \chi_i^*(r)\chi_j^*(r')\frac{1}{|r-r'|}\chi_k(\mathrm{r})\chi_l(\mathrm{r}') \tag{1.16}$$

The full application of the ZDO approximation leads to the CNDO method. In the INDO method, a number of integrals, neglected in CNDO, are considered. In the INDO method, two-electron integrals involving two centers are retained with

respect to the CNDO method. The parameters of the one-center two-electron integrals are obtained from spectroscopic values, and the two-center two-electron integrals are evaluated from empirical expressions including the Mataga-Nishimoto expression[3] we have considered. While the INDO method is restricted to organic molecules, the Zerner's Intermediate Neglect of Differential Overlap (ZINDO) was implemented for more elements.

1.1.4 Density functional theory

We now briefly turn our attention to density functional theory (DFT) which has become a popular alternative to HF *ab initio* methods. It indeed provides for the inclusion of correlation effects at a lower cost than post-HF methods. Hohenberg and Kohn stated that: (i) The ground state of a many-electron system in an external potential is defined by an electron density $\rho(\mathrm{r})$:

$$\int \rho(\mathrm{r})\mathrm{dr} = n \tag{1.17}$$

where n is number of electrons. (ii) The density $\rho(\mathrm{r})$ minimizes the total energy:

$$E[\rho] = T[\rho] + U[\rho] + V[\rho] \tag{1.18}$$

where $T[\rho]$ denotes kinetic energy, $U[\rho]$ denotes electron-electron interaction energy, and $V[\rho]$ denotes the external potential energy due to the nuclei.

Due to the difficulty in finding the correct solution from Hohenberg-Kohn theorem, Kohn-Sham introduced several approximations. Firstly, they set Kohn-Sham orbitals $\Psi_i(\mathrm{r})$, which are expanded within the LCAO approach (the expansion functions $\phi_j(r)$ are not necessarily AO's) and related to the density $\rho(\mathrm{r})$:

$$\rho(\mathrm{r}) = \sum_{i}^{n} |\Psi_i(\mathrm{r})|^2 = \sum_{i}^{n} \left| \sum_{j} c_{ji}\, \phi_j\,(r) \right|^2 \qquad (1.19)$$

Also, they considered a coupled set of equations to describe an interacting n-electron system in an external potential into n non-interacting functions in an effective potential. In their approximation, the electron-electron interaction potential is calculated from two parts: the Hartree potential; and the exchange-correlation potential. The major problem here is that no exact expression for the exchange-correlation potential in terms of the density is known, and, therefore, the exchange and correlation energies are approximated in the DFT method (while the HF method includes exchange energy exactly but neglects correlation energy completely).

1.1.5 Choice of methods

The geometries of all the molecules we considered were optimized at the DFT/B3LYP[4-8] level of theory using the SV(P), 6-31G*, or 6-31G** basis set. Based on DFT-optimized geometries, the excited-state energies and state- and transition-dipole moments were evaluated with the semiempirical Intermediate Neglect of Differential Overlap (INDO) Hamiltonian,[9,10] coupled to a multi-reference determinant single and double configuration interaction (MRD-CI with singles, S, or singles and doubles, SD)[11] scheme using the Mataga-Nishimoto potential to express the Coulomb repulsion term.[3,12] In all the MRD-CIS and MRD-CISD calculations, the configuration space was generated from the reference closed-shell Hartree-Fock (HF) ground state, three single-excitation

configurations HOMO-1 → LUMO, HOMO → LUMO, HOMO → LUMO+1, and one double-excitation configuration (HOMO, HOMO) → (LUMO, LUMO). The TPA cross-section values were computed with the perturbative sum-over-states (SOS) method, see below, considering the 300 lowest-lying states,[12] the S-tensor method,[13,14] and/or the correction vector method (CVM).[15]

We note that while using a TD-DFT based approach to compute the TPA cross-section in quadrupolar molecules could be an attractive alternative, we are unaware of any successful attempt in the literature of such applications to calculating the TPA of centrosymmetric quadrupolar molecules (such molecules have a zero permanent dipole moment but a non-zero quadrupole moment). We note that the nonlinear polarizabilities in TD-DFT-based approaches are often overestimated, which can be attributed to the lack of orbital-dependent terms in the exchange correlation potential or self-interaction error. Lately, there have been more successes in the evaluation of the NLO properties of dipolar molecules, compounds that have a non-zero permanent dipole moment, by using long-range correction schemes in the exchange correlation functional.[16,17] However, further improvements would be required to correctly reflect the multiple excitation character or the higher-lying excited states before such approaches can be applied to quadrupolar systems.

1.2. Linear and non-linear optical properties

In NLO, we deal with the interaction between matter and light, an electro-magnetic radiation, and consider the atomic or molecular response to the external field(s). We first introduce the molecular polarizabilities and then the perturbation technique used to derive a simplified model to describe polarizabilities and determine the NLO response in quantum mechanics.

1.2.1 Polarizabilities

The energy E of a molecule perturbed by an electric field F (such as that due to light) can be given in the form of a Taylor series expansion (Stark energy expression) as:

$$\begin{aligned} E &= E(0) + \left(\frac{dE}{dF}\right)_0 F + \frac{1}{2!}\left(\frac{\mathrm{d}^2E}{dF^2}\right)_0 F^2 + \frac{1}{3!}\left(\frac{\mathrm{d}^3E}{\mathrm{d}F^3}\right)_0 F^3 + \frac{1}{4!}\left(\frac{\mathrm{d}^4E}{\mathrm{d}F^4}\right)_0 F^4 + \cdots \\ &= E(0) - \mu_0 F - \frac{1}{2!}\alpha F^2 - \frac{1}{3!}\beta F^3 - \frac{1}{4!}\gamma F^4 + \cdots \end{aligned} \tag{1.20}$$

with:

$$\begin{aligned} \mu_{0i} &= -\left(\frac{dE}{dF_i}\right)_0 \\ \alpha_{ij} &= -\left(\frac{d^2E}{dF_i dF_j}\right)_0 \\ \beta_{ijk} &= -\left(\frac{d^3E}{dF_i dF_j dF_k}\right)_0 \\ \gamma_{ijkl} &= -\left(\frac{d^4E}{dF_i dF_j dF_k dF_l}\right)_0 \end{aligned} \tag{1.21}$$

where *ijkl* are Cartesian coordinates; μ_0 is the permanent dipole moment of the molecule; α, β, and , γ denote the first-, second-, and third-order polarizability, respectively.

Using time-independent perturbation theory with the perturbed Hamiltonian defined as $H = H^{(0)} + H^{(1)} = H^{(0)} - \mu \cdot F$, the energy of the perturbed molecule in the so-called electric dipole approximation can be expressed as:

$$E = E(0) - \langle 0|\mu|0\rangle F + \left\{\sum_{\mathrm{n}\neq 0} \frac{\langle 0|\mu|n\rangle\langle n|\mu|0\rangle}{E_0^0 - E_n^{(0)}}\right\} F^2 + \cdots \qquad (1.22)$$

Comparison of eqns 20 and 22 then allows to express the static (time or frequency independent) linear polarizability as:

$$\alpha_{ij}(0) = -2\sum_{n\neq 0} \frac{\langle 0|\mu|n\rangle\langle n|\mu|0\rangle}{E_0^{(0)} - E_n^{(0)}} = -2\sum_{n\neq 0} \frac{M_{0n}^2}{E_{0n}} \qquad (1.23)$$

From time-dependent perturbation theory, Orr and Ward derived the following expression for the dynamic α, which corresponds to the sum-over-states (SOS) method:[24]

$$\alpha_{\mathrm{ij}}(-\omega_\sigma;\omega) = \sum_{n\neq 0}\left\{\frac{\mu_{gn}^i \mu_{ng}^j}{(\Omega_{ng} - \hbar\omega)} + \frac{\mu_{gn}^j \mu_{ng}^i}{(\Omega_{ng}^* + \hbar\omega)}\right\} \qquad (1.24)$$

where ω is the frequency of incident photon with $\omega_\sigma = \omega$, $\Omega_{lm} = E_{lm} - i\Gamma_{lm}$, and $\Omega_{lm}^* = E_{lm} + i\Gamma_{lm}$ with E_{lm} the transition energy between states $|l\rangle$ and $|m\rangle$ and Γ_{lm} the damping factor related to the lifetime of the $|l\rangle$ to $|m\rangle$ transition. The summation is carried out over all excited states $|n\rangle$ while $|g\rangle$ denotes the ground state. The second term in eqn 1.24 is known as the antiresonant or counter-

rotating term; this can be neglected when ω is nearly resonant with the transition frequency ω_{ng}.

$$\alpha_{\mathrm{ij}}(-\omega_\sigma;\omega) = \frac{\mu_{gn}^i \mu_{ng}^j}{\left(\hbar\omega_{ng} - \hbar\omega\right) - i\Gamma_{\mathrm{ng}}} = \frac{\mu_{gn}^i \mu_{ng}^j}{\left(\hbar\omega_{ng} - \hbar\omega\right)^2 - \Gamma_{\mathrm{ng}}^2}\left\{\left(\hbar\omega_{ng} - \hbar\omega\right) + i\Gamma_{\mathrm{ng}}\right\} \tag{1.25}$$

We note that the polarizability is a complex quantity.

Sum-over-state expression for the third-order polarizability γ. Orr and Ward[12] derived the following expression for the third-order polarizability:

$$\gamma_{hijk}(-\omega_\sigma;\omega_1,\omega_2,\omega_3)$$

$$= \mathcal{P}\left[\sum_{vnml}\left\{\frac{\mu_{lv}^k \mu_{vn}^j \mu_{nm}^i \mu_{ml}^h}{(\Omega_{vl} - \hbar\omega_\sigma)(\Omega_{nl} - \hbar\omega_1 - \hbar\omega_2)(\Omega_{ml} - \hbar\omega_1)}\right.\right. \tag{1.26a}$$

$$+ \frac{\mu_{lv}^h \mu_{vn}^k \mu_{nm}^j \mu_{ml}^i}{(\Omega_{nv} + \hbar\omega_\sigma)(\Omega_{mv} - \hbar\omega_1 - \hbar\omega_2)(\Omega_{vl}^* + \hbar\omega_1)} \tag{1.26b}$$

$$+ \frac{\mu_{lv}^i \mu_{vn}^k \mu_{nm}^j \mu_{ml}^h}{(\Omega_{nv} - \hbar\omega_\sigma)(\Omega_{vm}^* + \hbar\omega_1 + \hbar\omega_2)(\Omega_{ml} - \hbar\omega_1)} \tag{1.26c}$$

$$+ \frac{\mu_{lv}^h \mu_{vn}^i \mu_{nm}^k \mu_{ml}^j}{(\Omega_{mv} + \hbar\omega_\sigma)(\Omega_{nl}^* + \hbar\omega_1 + \hbar\omega_2)(\Omega_{vl}^* + \hbar\omega_1)} \tag{1.26d}$$

$$+ \frac{\mu_{lv}^j \mu_{vn}^k \mu_{nm}^i \mu_{ml}^h}{(\Omega_{vn}^* + \hbar\omega_\sigma)(\Omega_{nl} - \hbar\omega_1 - \hbar\omega_2)(\Omega_{ml} + \hbar\omega_1)} \tag{1.26e}$$

$$+ \frac{\mu_{lv}^h \mu_{vn}^j \mu_{nm}^k \mu_{ml}^i}{(\Omega_{nm}^* + \hbar\omega_\sigma)(\Omega_{mv} - \hbar\omega_1 - \hbar\omega_2)(\Omega_{vl}^* + \hbar\omega_1)} \tag{1.26f}$$

$$+ \frac{\mu_{lv}^i \mu_{vn}^j \mu_{nm}^k \mu_{ml}^h}{(\Omega_{nm}^* + \hbar\omega_\sigma)(\Omega_{vm}^* + \hbar\omega_1 + \hbar\omega_2)(\Omega_{ml} - \hbar\omega_1)} \tag{1.26g}$$

$$+\frac{\mu_{lv}^{h}\mu_{vn}^{i}\mu_{nm}^{j}\mu_{ml}^{k}}{(\Omega_{ml}^{*}+\hbar\omega_{\sigma})(\Omega_{nl}^{*}+\hbar\omega_{1}+\hbar\omega_{2})(\Omega_{vl}^{*}+\hbar\omega_{1})}\Bigg\}\Bigg] \quad (1.26h)$$

where $\omega_\sigma = \omega_1 + \omega_2 + \omega_3$; $\mathcal{P}$ denotes the permutation operator that satisfies the intrinsic permutation symmetry of the polarization tensor; ω_1 , ω_2 , and ω_3 correspond to the frequencies of the incident photons.

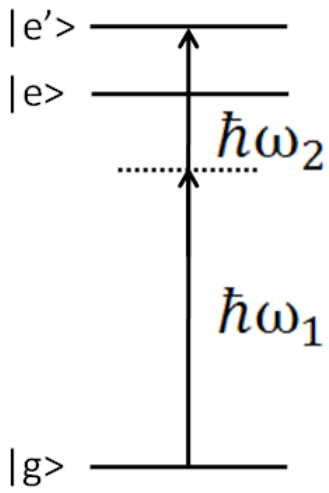

Figure 1.7. Non-degenerate TPA process with ground state $|g\rangle$, which is couple to only one excited state $|e'\rangle$ and the excited state $|e'\rangle$ is couple to excited states $|e\rangle$, where $\hbar\omega_1$is the energy of the high intensity pump beam while $\hbar\omega_2$ is the pump beam energy.

For a qualitative analysis of the cross-sections, the full expression of γ in the case of quasi-one-dimensional molecules (taken to extend along the x-axis; $h = i = j = k = x$) can be simplified. In the case of TPA, there are two incident photon frequencies, ω_1 and ω_2, see Figure 1.7. Assuming that there is only one excited state $|e\rangle$ strongly coupled to the ground state $|g\rangle$ and only a few excited states $|e'\rangle$ coupled to $|e\rangle$, we obtain:

$\gamma_{xxxx}(\omega_2;\omega_1,-\omega_1,\omega_2)$

$$\approx \frac{\mu_{ge}^x \bar{\mu}_{ee}^x \bar{\mu}_{ee}^x \mu_{eg}^x}{(\Omega_{eg}-\hbar\omega_1)(\Omega_{eg}-\hbar\omega_2)(\Omega_{eg}-\hbar\omega_1-\hbar\omega_2)} \quad (1.27a)$$

$$-\frac{\mu_{ge}^x \mu_{eg}^x \mu_{ge}^x \mu_{eg}^x}{(\Omega_{eg}-\hbar\omega_1)(\Omega_{eg}-\hbar\omega_2)^2} \quad (1.27b)$$

$$+\sum_{e'} \frac{\mu_{gm}^x \mu_{mg}^x \mu_{nm}^x \mu_{mn}^x}{(\Omega_{eg}-\hbar\omega_1)(\Omega_{eg}-\hbar\omega_2)(\Omega_{e'g}-\hbar\omega_1-\hbar\omega_2)} \quad (1.27c)$$

where $\bar{\mu}_{lm} = \mu_{lm} - \delta_{lm}\mu_{gg}$. The first term is called dipolar term (or simply D-term) since they are present only in dipolar (non-centrosymmetric) compounds (these terms involve the difference in state dipole moments between ground state $|g\rangle$ and excited state $|e\rangle$, their values vanish in centro-symmetric systems). The next negative term (N-term) does not contain two-photon resonances in the denominator, so the term only contribute to the total γ value when it is in a double resonance situation, $\hbar\omega_1 = \hbar\omega_2$. Thus, we omit the interpretation of the term here. The last term is called two-photon term (T-term), which is the dominant terms to describe γ and TPA in centro-symmetric compounds.

1.2.2 Spectroscopic properties

In this section, we establish the relationship between imaginary part of γ with experimentally measurable parameter, TPA cross-section δ. In a way similar to α_{ij} and $\chi_{ij}^{(1)}$, we can relate γ_{ij} and $\chi_{ijkl}^{(3)}$:

$$\gamma = \frac{\chi^{(3)}}{L_1^2 L_2^2 N} \quad (1.54)$$

where N is the number of molecules per unit volume and L_i is the local field factor ($L_1 = L_2$ in a degenerate process with with $\omega_1 = \omega_2$). The TPA cross-section δ is defined in terms of the imaginary part of γ:

$$\delta = \frac{3L_1^2 L_2^2}{n_1 n_2 c^2 \epsilon_0 \hbar} \frac{\hbar\omega_2^2 \hbar\omega_1}{\hbar(\omega_1 + \omega_2)} \, \mathrm{Im}\gamma(-\omega_2; \omega_1, -\omega_1, \omega_2) \tag{1.55}$$

We now extract imaginary part of γ from D- and T-terms in eqn 27 in the case of two-photon resonance situation:

$$\begin{aligned} \mathrm{Im}\gamma_{D-term} &= \frac{\mu_{ge}^2 \Delta\mu_{eg}^2}{\Gamma_{eg}} \left\{ \frac{(\hbar\omega_1)^2 - \Gamma_{eg}^2}{\left((\hbar\omega_1)^2 + \Gamma_{eg}^2\right)^2} + \frac{1}{(\hbar\omega_2)^2 + \Gamma_{eg}^2} \right. \\ &\quad \left. + \frac{2\hbar\omega_1 \hbar\omega_2}{\left((\hbar\omega_1)^2 + \Gamma_{eg}^2\right)\left((\hbar\omega_2)^2 + \Gamma_{eg}^2\right)} \right\} \\ &\approx \frac{\mu_{ge}^2 \Delta\mu_{eg}^2}{\Gamma_{eg}} \left\{ \frac{1}{(\hbar\omega_1)^2} + \frac{1}{(\hbar\omega_2)^2} + \frac{2}{\hbar\omega_1 \hbar\omega_2} \right\} \\ &= \frac{\mu_{ge}^2 \Delta\mu_{eg}^2}{\Gamma_{eg}} \left(\frac{\hbar\omega_1 + \hbar\omega_2}{\hbar\omega_1 \hbar\omega_2} \right)^2 \end{aligned} \tag{1.56}$$

and

$$\mathrm{Im}\gamma_{T-term} = \frac{\mu_{ge}^2 \mu_{ee'}^2}{\Gamma_{e'g}} \left\{ \frac{\left(\hbar\omega_{eg} - \hbar\omega_1\right) + \left(\hbar\omega_{eg} - \hbar\omega_2\right)}{\left(\hbar\omega_{eg} - \hbar\omega_1\right)\left(\hbar\omega_{eg} - \hbar\omega_2\right)} \right\}^2 \tag{1.57}$$

where $\bar{\mu}_{ee}^x = \Delta\mu_{eg} = \mu_{ee} - \mu_{gg}$, $\hbar\omega_{eg} = \hbar\omega_1 + \hbar\omega_2$, $\Omega_{eg} = \hbar\omega_{eg} - \Gamma_{eg}$ and $\Gamma_{eg} \ll \hbar\omega_i$.

From the relationship between δ and imaginary parts of γ, we obtain:

$$\delta = \frac{3}{n_1 n_2 c^2 \epsilon_0 \hbar N} \cdot \frac{(\hbar\omega_2)^2 \hbar\omega_1}{\hbar(\omega_1+\omega_2)} \cdot \mathrm{Im}\chi^{(3)}(\omega_2;\ \omega_1, -\omega_1, \omega_2)$$
$$= \frac{3L_1^2 L_2^2}{n_1 n_2 c^2 \epsilon_0 \hbar} \cdot \frac{(\hbar\omega_2)^2 \hbar\omega_1}{\hbar(\omega_1+\omega_2)} \cdot \mathrm{Im}\gamma(\omega_2;\ \omega_1, -\omega_1, \omega_2) \quad (1.58)$$

where n_i is concentration of molecule *i*.

Eqns 1.30 and 32 give the following expression:

$$\delta_{D-term} \propto \frac{3L_1^2 L_2^2}{n_1 n_2 c^2 \epsilon_0 \hbar} \cdot \frac{\mu_{ge}^2 \Delta\mu_{eg}^2}{\Gamma_{eg}} \cdot \frac{\hbar\omega_1 + \hbar\omega_2}{\hbar\omega_1} \quad (1.59)$$

In degenerate process with $\omega_1 = \omega_2$, $L_1 = L_2$ and $n_1 = n_2$, the imaginary part of γ for D-term simply becomes $\frac{16\mu_{ge}^2 \Delta\mu_{eg}^2}{\Gamma_{eg}(\hbar\omega_{eg})^2}$, and, therefore, δ writes:

$$\delta_{D-term} \propto \frac{24L^2}{n^2 c^2 \epsilon_0 \hbar} \cdot \frac{\mu_{ge}^2 \Delta\mu_{eg}^2}{\Gamma_{eg}} \quad (1.60)$$

We repeat the same procedure for the T-term from eqns 31 and 32, and obtain:

$$\delta_{T-term} \propto \frac{3L_1^2 L_2^2}{n_1 n_2 c^2 \epsilon_0 \hbar} \cdot \frac{\mu_{ge}^2 \mu_{ee'}^2}{\Gamma_{e'g}} \cdot \frac{(\hbar\omega_2)^2 \hbar\omega_1}{\hbar(\omega_1+\omega_2)} \cdot \left\{ \frac{(\hbar\omega_{eg} - \hbar\omega_1) + (\hbar\omega_{eg} - \hbar\omega_2)}{(\hbar\omega_{eg} - \hbar\omega_1)(\hbar\omega_{eg} - \hbar\omega_2)} \right\}^2 \quad (1.61)$$

The term is further simplified with the imaginary part of γ in a degenerate TPA process $\frac{4\mu_{ge}^2 \mu_{ee'}^2}{\Gamma_{e'g}} \cdot \frac{1}{(\hbar\omega_{eg} - \hbar\omega_{e'g}/2)^2}$:

$$\delta_{T-term} \propto \frac{6L^2}{n^2 c^2 \epsilon_0 \hbar} \cdot \frac{\mu_{ge}^2 \mu_{ee}'^2}{\Gamma_{e'g}} \cdot \frac{(\hbar\omega_{e'g})^2}{(\hbar\omega_{eg} - \hbar\omega_{e'g}/2)^2} \quad (1.62)$$

It is important to note that we only consider xxxx component of γ, as we focus on quasi-one-dimensional molecules. In other instances, we should consider all the combination of Cartesian coordinate of ijkl in γ^{ijkl}.

As can be seen in eqn 1.34, large δ due to D-term using degenerate photons are obtained as we increase the transition dipole and state dipole difference between the ground and final states. Typically, π-conjugated dipolar dyes with push-pull structures assembled with electron donating and acceptor groups present large transition dipoles and dipole differences between the ground and first excited states and, therefore, can display large δ. In such instances, there is no excited state between the ground and final states that would induce undesired optical processes. In π-conjugated centrosymmetric compounds, the state dipole difference is absent and thus no D-term is present. The T-terms involve three states. Figure 1.8 illustrates the degenerate TPA process with the ground state (g), the intermediate excited state (e), and the final excited state (e'). Eqn 1.36 indicates that not only large μ_{ge} and $\mu_{ee'}$ but also small detuning factor Δ_f ($= E_{eg} - E_{e'g}/2$), are required for large δ. In practice, TPA starts being contaminated with OPA when Δ_f becomes very small(double resonance effects), which then limits the applicability of the TPA process.

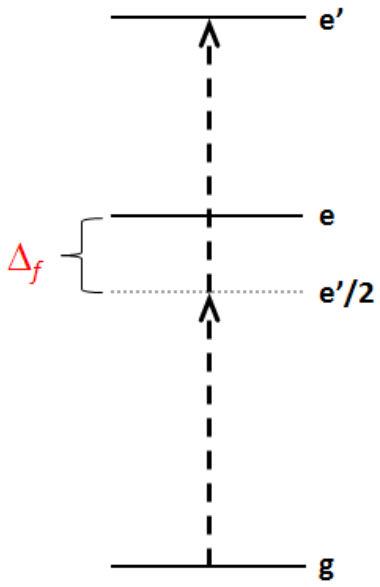

Figure 1.8. The degenerate TPA process with the ground state (g), the intermediate excited state (e), and the final excited state (e'). The detuning factor Δ_f is defined as $\Delta_f = E_{eg} - E_{e'g}/2$.

S-tensor approach

To compute the cross-sections, it is convenient to introduce the following expression called the S-tensor:[13,14]

$$S_{e'}^{ij} = \sum_{e} \frac{\mu_{ge}^{i}\mu_{ee'}^{j}}{E_{eg} - E_{e'g}/2} + \frac{\mu_{ge}^{j}\mu_{ee'}^{i}}{E_{eg} - E_{e'g}/2} \tag{1.63}$$

The TPA cross-sections can be rewritten as:

$$\delta^{S-tensor} = \frac{3L^4}{2n^2c^2\epsilon_0\hbar}\frac{1}{15}\left(\frac{E_{e'g}}{2}\right)\sum_{ij}\left\{S_{e'}^{ii}S_{e'}^{*jj} + 2S_{e'}^{ij}S_{e'}^{*ji}\right\} \tag{1.64}$$

Both SOS and S-tensor methods require to include large number of higher excited states to compute accurate values. However, it is known that the method typically truncated after inclusion of a couple hundred states.

Correction vector method (CVM)

An alternative approach to compute the TPA cross-sections, called the correction vector method (CVM),[15] involves the variational calculations of the first- and second-order correction vectors $\phi_i^{(1)}$ and $\phi_{ij}^{(2)}$. Using perturbation theory, we obtain the following equation that gives the first-order correction vector:

$$(H_0 - E_0 + \hbar\omega_1)|\phi_i^{(1)}(\omega_1)\rangle = -\mu_i|0\rangle \tag{1.65}$$

Both the first-order correction vector and the ground state are expanded as a linear combination of the same basis functions, and the substitution of the expansions for $|0\rangle$ and $|\phi_i^{(1)}(\omega_1)\rangle$ gives:

$$\boldsymbol{H}\cdot\boldsymbol{C_i} = \boldsymbol{\mu_i}$$
$$\begin{cases} \boldsymbol{H} = H_{pq}(\omega_1) = \langle\chi_p|(H_0 - E_0 + \hbar\omega_1)|\chi_q\rangle \\ \boldsymbol{\mu_i} = (\mu_i)_p = \langle\chi_p|\mu_i|0\rangle \end{cases} \tag{1.66}$$

where $\phi_i^{(1)}(\omega_1) = \sum_p C_{ip}\chi_p$. By solving the equations for C_i, we can obtain $\phi_i^{(1)}$. The correction vector expanded in terms of the excited states is written as:

$$\phi_i^{(1)}(\omega_1) = \sum_n \frac{\mu_{gn}^i}{\Omega_{gn} + \hbar\omega_1}|n\rangle \tag{1.67}$$

Once $\phi_i^{(1)}$ is known, $\phi_{ij}^{(2)}$ can also be computed from the linear equation:

$$(H_0 - E_0 + \hbar\omega_2)|\phi_{ij}^{(2)}(\omega_1,\omega_2)\rangle = -\mu_j|\phi_i^{(1)}(\omega_1)\rangle \tag{1.68}$$

After expansion of $\phi_{ij}^{(2)}$ in terms of χ, C_{ij} is obtained from $\phi_{ij}^{(2)}$:

$$\boldsymbol{H} \cdot \boldsymbol{C_{ij}} = \boldsymbol{\mu_{ij}}$$

$$\begin{cases} \boldsymbol{H} = H_{pq}(\omega_2) = \langle \chi_p | (H_0 - E_0 + \hbar\omega_2) | \chi_q \rangle \\ \boldsymbol{\mu_i} = \left(\mu_{ij}\right)_p(\omega_1) = \langle \chi_p | \mu_j | \phi_i^{(1)}(\omega_1) \rangle \end{cases} \tag{1.69}$$

The second-order correction vector expanded in terms of the excited states is:

$$\phi_{ij}^{(2)}(\omega_1, \omega_2) = \sum_m \frac{\langle m | \mu_i | \phi_j^{(1)}(\omega_1) \rangle}{\Omega_{mg} + \hbar\omega_2} | m \rangle \tag{1.70}$$

From eqns 1.25 and 1.26, the first- and third-order NLO coefficients can be written in terms of the correction vectors:

$$\alpha_{ij}(-\omega_\sigma; \omega_1) = -\frac{1}{\hbar} \langle 0 | \mu_i | \phi_j^{(1)}(\omega_1) \rangle \tag{1.71}$$

and

$$\begin{aligned} &\gamma_{ijkl}(-\omega_\sigma; \omega_1, \omega_2, \omega_3) \\ &= (-\hbar)^{-3} \mathcal{P} \left\langle \phi_i^{(1)}(-\omega_1 - \omega_2 - \omega_3) \middle| \mu_j \middle| \phi_{kl}^{(2)}(-\omega_1 - \omega_2, -\omega_1) \right\rangle \end{aligned} \tag{1.72}$$

From the imaginary part of these expressions, we can obtain the linear and nonlinear absorption cross-sections.

While with the SOS method one can take into account only a finite number of excited states due to the large memory requirement of the calculations, in CVM, the TPA calculation requires only the lowest eigenvalue and eigenvector. Therefore, a larger number of configurations compared with the SOS method can

be handled. The disadvantage of using this method is that we can no longer investigate strongly coupled excited states that are involved in the TPA process.

1.3 Goal of the dissertation

Organic materials with large TPA cross-sections are of interest due to application in the optical, materials fabrication, and biological fields.[18-29] The purpose of this dissertation is to contribute to the establishment of structure-optical property relationships for π-conjugated chromophores using highly correlated quantum-chemical calculations. An improved knowledge of the relation between the structural properties in a molecule and its optical response will lead to rational design of molecular systems with enhanced nonlinear optical (NLO)properties. Theoretical investigations enable us to study these relationships without the need for organic syntheses and/or characterizations, which are typically difficult and more expensive than computational approaches.

In this dissertation, the NLO properties were investigated in various extended π-conjugated chromophores, and structure-property relationships were established for (i) alkyne carbocations, (ii) porphyrin dimers, and (iii) squaraine compounds. In particular:

(i) We examined the relationship between structure and optical properties in a series of alkyne carbocation dyes that form a new class of cyanine-like dyes and helped assess their potential.

(ii) Porphyrins are an important class of organic systems which, in addition to their biological functions, have been considered as sensitizers in photovoltaic cells, hole-transporting semiconductors, optical limiters, or components in artificial photosynthesis or molecular-scale electronics due to their attractive spectroscopic and photophysical properties. Recently, a number of butadiyne-linked and other porphyrin oligomers have been shown to possess large third-order molecular polarizabilities and TPA cross-sections. To optimize the TPA cross-sections in porphyrin dimers, we sought to provide the factors determining non-linear absorption in the dimer systems by examining various structural aspects of these dimers.

(iii) The lowest TPA-active state in squaraine compounds is important for optoelectronic applications, since, depending on the molecular structure, their absorption is located close to or within the telecommunications band of the near-infrared (1.30-1.55 μm). TPA in this region can potentially be exploited for applications such as all-optical beam stabilization and dynamic range compression, while the presence of a TPA-allowed state close to this region will affect the telecommunications-band dispersion of the real part of the third-order polarizability γ, which can be exploited for all-optical switching. We studied the origin of the lowest TPA-active state in a series of squaraine molecules.

REFERENCES

(1) Goeppert-Mayer, M. *Annalen der Physik* **1931**, *401*, 273.

(2) Kaiser, W.; Garrett, C. G. B. *Physical Review Letters* **1961**, *7*, 229.

(3) Mataga, N.; Nishimoto, K. *Z Phys Chem* **1957**, *13*, 140.

(4) Becke, A. D. *J. Chem. Phys.* **1993**, *98*, 5648.

(5) Dirac, P. A. M. *Proc. Royal Soc. (London) A,* **1929**, *123*, 714.

(6) Slater, J. C. *Physical Review* **1951**, *81*, 385.

(7) Becke, A. D. *Physical Review A* **1988**, *38*, 3098.

(8) Lee, C.; Yang, W.; Parr, R. G. *Physical Review B* **1988**, *37*, 785.

(9) Ridley, J.; Zerner, M. *Theor. Chim. Acta* **1973**, *32*, 111.

(10) Pople, A.; Beveridge, D. L.; Dobosh, P. A. *J. chem. Phys* **1967**, *47*, 2026.

(11) Zerner, M. C.; Loew, G. H.; Kichner, R. F.; Mueller-Westerhoff, U. T. *J. Am. Chem. Soc.* **1980**, *102*, 589.

(12) Orr, B.; Ward, J. *Mol. Phys.* **1971**, *20*, 513.

(13) Monson, P. R.; McClain, W. M*. J.Chem. Phys.,* **1970**, *53*, 29.

(14) Peticolas, W. L. *Ann. Rev. Phys. Chem.*, *1967*, *16*, 233.

(15) Ramasesha, S.; Shuai, Z.; Bredas, J. *Chem. Phys. Lett.* **1995**, *245*, 224.

(16) Dreuw, A.; Head-Gordon, M. *J. Am. Chem. Soc.* **2004**, *126*, 4007.

(17) Magyar, R. J.; Tretiak, S. *J. Chem. Theory Comput.* **2007**, *3*, 976.

(18) Albota, M.; Beljonne, D.; Brédas, J.-L.; Ehrlich, J. E.; Fu, J.-Y.; Heikal, A. A.; Hess, S. E.; Kogej, T.; Levin, M. D.; Marder, S. R.; McCord-Maughon, D.; Perry, J. W.; Röckel, H.; Rumi, M.; Subramaniam, G.; Webb, W. W.; Wu, X.-L.; Xu, C. *Science* **1998**, *281*, 1653.

(19) Chung, S. J.; Rumi, M.; Alain, V.; Barlow, S.; Perry, J. W.; Marder, S. R. *J. Am. Chem. Soc.* **2005**, *127*, 10844.

(20) Lin, T.-C.; Chung, S.-J.; Kim, K.-S.; Wang, X.; He, G. S.; Swiatkiewicz, J.; Pudavar, H. E.; Prasad, P. N. *Adv. Polym. Sci.* **2003**, *161*, 157.

(21) Pond, S. J. K.; Rumi, M.; Levin, M. D.; Parker, T. C.; Beljonne, D.; Day, M. W.; Bredas, J. L.; Marder, S. R.; Perry, J. W. *J. Phys. Chem. A* **2002**, *106*, 11470.

(22) Strehmel, B.; Sarker, A. M.; Detert, H. *ChemPhysChem* **2003**, *4*, 249.

(23) Marder, S. R.; Brédas, J. L.; Perry, J. W. *MRS Bulletin* **2007**, *32*, 561.

(24) Kim, H.-S.; Kim, C.-H.; Ha, C.-S.; Lee, J.-K. *Synth. Met.* **2001**, *117*, 289.

(25) Campbell, W. M.; Jolley, K. W.; Wagner, P.; Wagner, K.; Walsh, P. J.; Gordon, K. C.; Schmidt-Mende, L.; Nazeeruddin, M. K.; Wang, Q.; Graetzel, M.; Officer, D. L. *J. Phys. Chem. C* **2007**, *111*, 11760.

(26) Savenije, T. J.; Goossens, A. *Phys. Rev. B* **2001**, *64*, 115323.

(27) Calvete, M.; Ying Yang, G.; Hanack, M. *Synth. Met.* **2004**, *141*, 231.

(28) Damasio, H.; Grabowski, T.; Frank, R.; Galaburda, A. M.; Damasio, A. R. *Science* **1994**, *264*, 1102.

(29) Anderson, H. L. *Chem. Commun.* **1999**, 2323.

(30) Rumi, M.; Barlow, S; Wang, J; Perry, J. W.; Marder, S. R. *Adv. Polymer Sci*. **2008,** *213,* 1. (cover picture: available online).

CHAPTER 2:

A new class of cyanine-like dyes with large bond-length alternation

Objective

Polymethine cyanine dyes, which represent a class of charged chromophores with an odd number of π-conjugated carbons, have fascinated chemists for decades.[1-8] Cyanines display unique electronic and optical properties, attributed to the strong electronic delocalization and absence of any significant carbon-carbon bond-length alternation, BLA, along their backbone. The flatness of the corresponding electronic potential, illustrated in Figure 1, and the equivalence of their bond lengths make cyanine dyes the compounds to which simple free-electron theory can be applied in the most relevant way.[2,3,6] Recently, Thorley *et al.*[9] have reported the synthesis of cations of porphyrin dimers linked by a π-conjugated bridge with an odd number of carbons and presenting alternating single and triple bonds. Interestingly, these cations were shown to possess linear and nonlinear optical properties analogous to cyanines.[9] Here, We have used a theoretical approach based on correspondence between the polymethine cyanines and the new class of alkyne carbocations, in spite of their marked difference in BLA.

2.1 Introduction

The degree of electronic delocalization and of BLA along the backbone of π-conjugated molecules and polymers is widely regarded as a critical parameter determining their electronic, electrical, and optical properties.[10-12] In this context, cyanine dyes form a distinct class of compounds as they present a nonalternated geometric structure; this key feature can be viewed as due to the interplay between the two valence bond structures shown in Figure 1, which provides each bond with an intermediate length between single and double bonds. The vanishing BLA in cyanines is confirmed by several crystal structures.[13-16] The resulting fully delocalized electronic potential energy surface[17] depicted in Figure 2.1 imparts cyanines with a set of remarkable properties. In particular the following:

(i) The lowest energy optical bands are intense and very sharp, as the ground-state and excited-state equilibrium geometries are (nearly) identical, see Figure 2.1, bottom.

(ii) Extrapolation of the optical gap in short cyanines would lead to a vanishing optical gap (metallic structure) in long chains, in accordance with the predictions of the simple free-electron model.[4-6] However, beyond some 13-15 carbon atoms, the symmetric structure of cyanines becomes unstable as the charge then localizes on one nitrogen atom; this results in the appearance in long cyanines of an asymmetric, strongly bond-alternated structure with an optical gap similar to regular polyenes.[18,19]

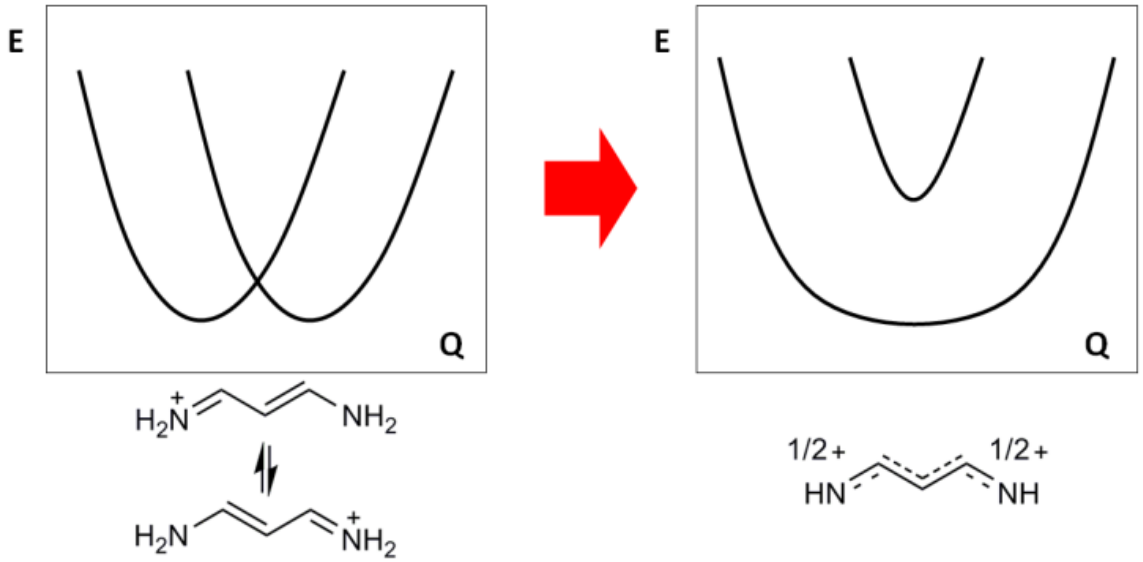

Figure 2.1. Illustration of the resonance forms and potential energy surfaces as a function of nuclear displacement (Q) for typical cyanine dyes. Left: The diabatic surfaces corresponding to each of the individual resonance forms. Right: The resulting adiabatic surfaces of the ground and lowest excited states for the nonalternated structure.

(iii) The molecular polarizabilities steeply increase with molecular length, L, in the way predicted by the free-electron model or Hückel theory;[20,21] the first-order (linear) static polarizability, α, evolves as ~L^3; the third-order static polarizability, γ, is negative, a characteristic of nonalternated structures, and evolves as ~L^{7-8}. In contrast, α evolves as ~$L^{1.5}$ and γ as ~L^{3-4} in polymethine dyes with BLA typical of polyene structures (BLA on the order of 0.1 Å).[22,23] In their unified theory of linear and nonlinear polarization, Marder *et al.*[12] have shown that zero-BLA structures (referred to in their work as the "cyanine limit", which can be considered to correspond to the "polymethine state" described by Dähne and Kulpe[4]), provide for the largest α and γ values at a fixed molecular length, as the

transition dipoles between ground state and excited state are then maximized and the optical gap minimized.

We have used a theoretical approach combining first-principles Hartree–Fock and Density Functional Theory calculations to assess the geometric structures of model cyanines and alkyne carbocations (labeled **Cn** and **ACn**, respectively); cyanine dyes **por-C** and **ind-C**; alkyne carbocations **por-AC** and **ind-AC**; and their alcohol precursor **ind-COH**, **ind-ACOH**, **por-COH** and **por-ACOH** (the newly synthesized indole compounds in the Anderson's group at University of Oxford **por-C** and **por-AC** and porphyrin compounds **ind-C** and **ind-AC**; see Figure 2.2 for chemical structures). Highly correlated INDO/MRD-CI calculations were performed on those compounds to examine the evolution of the optical properties as a function of chain length. We note that, in order to compare the properties of both series of compounds on an equal footing, we only deal here with symmetric geometries.

This section is structured as follows. We first discuss the results of computational studies on the structural properties focusing on bond length alternation in cyanine and alkyne carbocation dyes, comparing simulated IR spectra with the experimental results (2.2). We also present a theoretical understanding of molecular orbital and charge distribution in two series of dyes. We next turn to a theoretical analysis of the evolution of lowest excited state energies and transition dipole moments in the model cyanines and verify the results with the

synthesized compounds (2.3). Finally, we investigate the evolution of the first-, second- and third-order polarizabilities of cyanine and alkyne carbocation dyes and compare to experimental results (2.4).

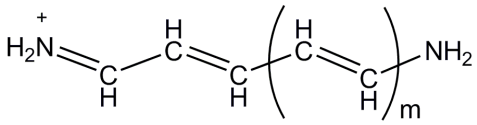

m=1: **C5**; m=3: **C9**; m=5: **C13**; m=7: **C17**

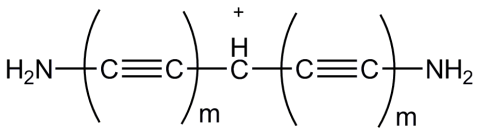

m=1: **AC5**; m=2: **AC9**; m=3: **AC13**; m=4: **AC17**

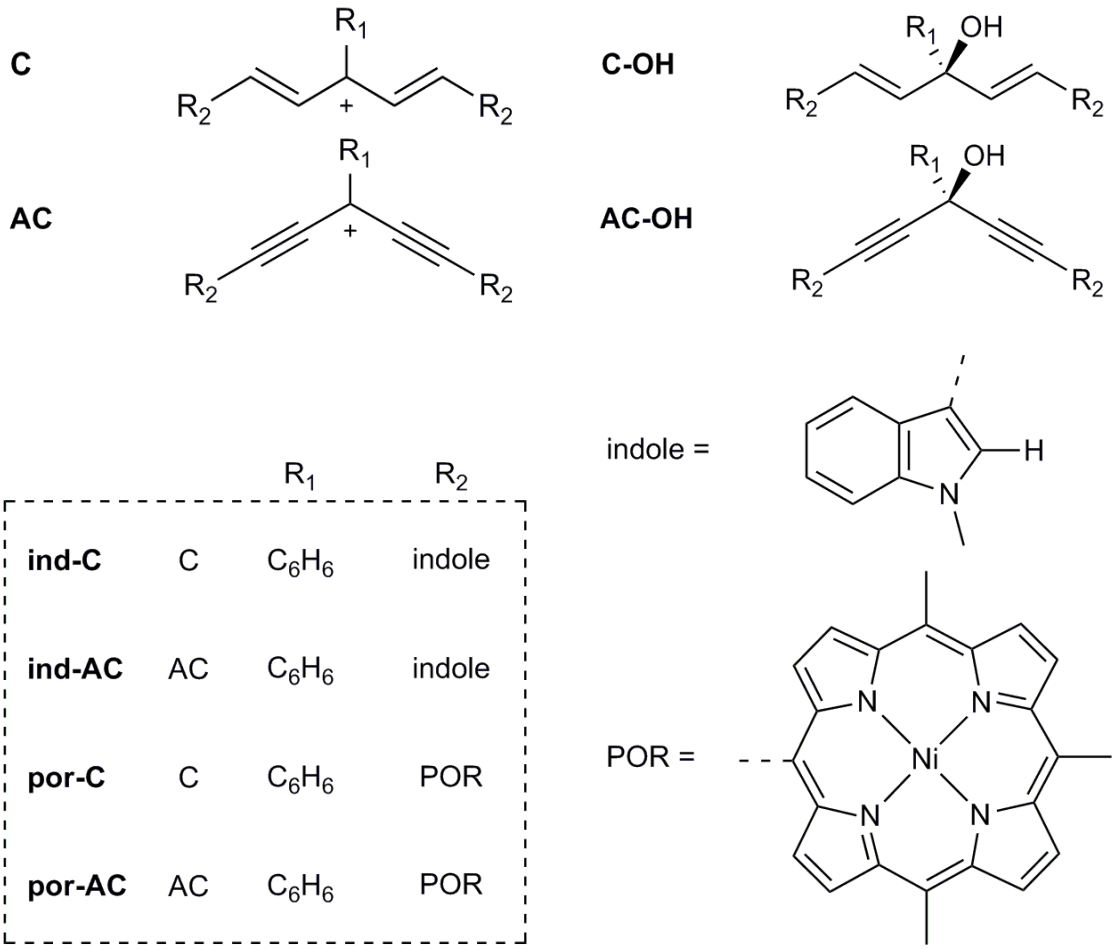

		R_1	R_2
ind-C	C	C_6H_6	indole
ind-AC	AC	C_6H_6	indole
por-C	C	C_6H_6	POR
por-AC	AC	C_6H_6	POR

Figure 2.2. Chemical structures of the compounds considered here: Compounds **1** – **4**; model cyanines **Cn**; and model alkyne carbocations **ACn**; the number n represents the number of carbon atoms between the nitrogen atoms. Characterization of compounds **1** and **2** has not been completed yet.

2.2 Structural properties and IR spectrum

The fully optimized geometries of **ACn**, **ind-AC** and **por-AC** exhibit a strong BLA within the bridge; the average long bonds of **AC5**, **ind-AC** and **por-AC** are calculated to be around 1.38 Å and the short bonds around 1.23 Å, leading to a very large BLA degree of ~0.15 Å. The BLA value for **C5**, **ind-C** and **por-AC** is ~0.02 Å for the single and double bond polymethine bridges. These geometrical features can be understood from a simple analysis of the resonance forms that can be drawn for **C5** and **AC5** (Figure 2.3): in **C5**: with resonance forms (1) and (5) dominant; in **AC5** with resonance forms (1), (3), and (5) dominant. On the basis of these five resonance forms, the average bond orders can be evaluated: they are found to be the same in **C5** and **AC5** for the central bonds (7/5), while they differ by one full bond order for the nominal triple bonds of **AC5** (13/5) compared to the same bonds in **C5** (8/5). It is also important to focus on the resonance forms in which the formal positive charge appears on a carbon; their consideration underlines that the alternation in π-electron densities along the carbon backbone (Figure 2.4), which is a hallmark of cyanine dyes (*i.e.*, zero BLA and π-charge density alternation),[4,5] occurs in the same way in the **ACn** compound.

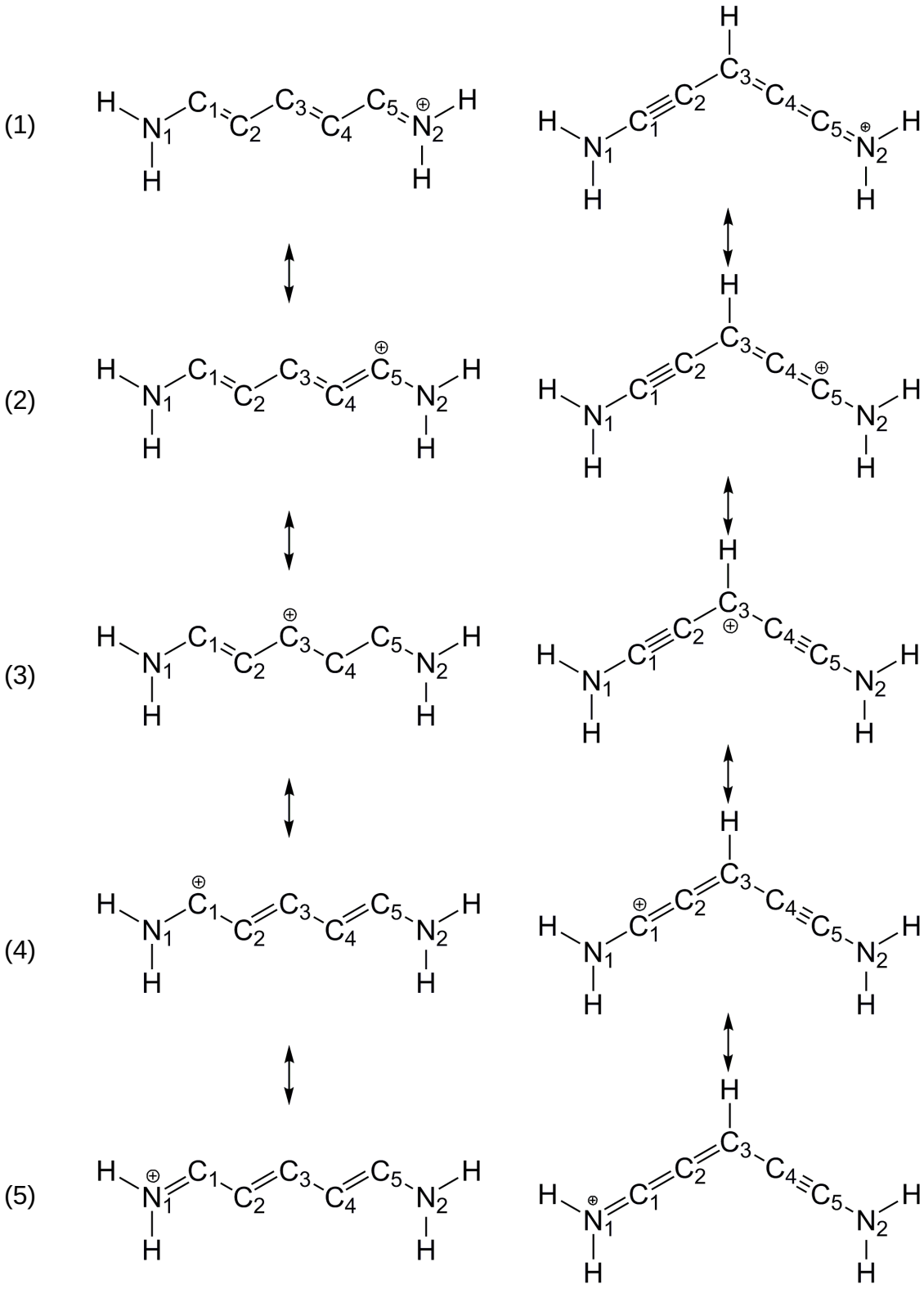

Figure 2.3. Resonance structures of **AC5** and **C5** (the closed-shell octet resonance forms (1) and (5) are expected to be dominant).

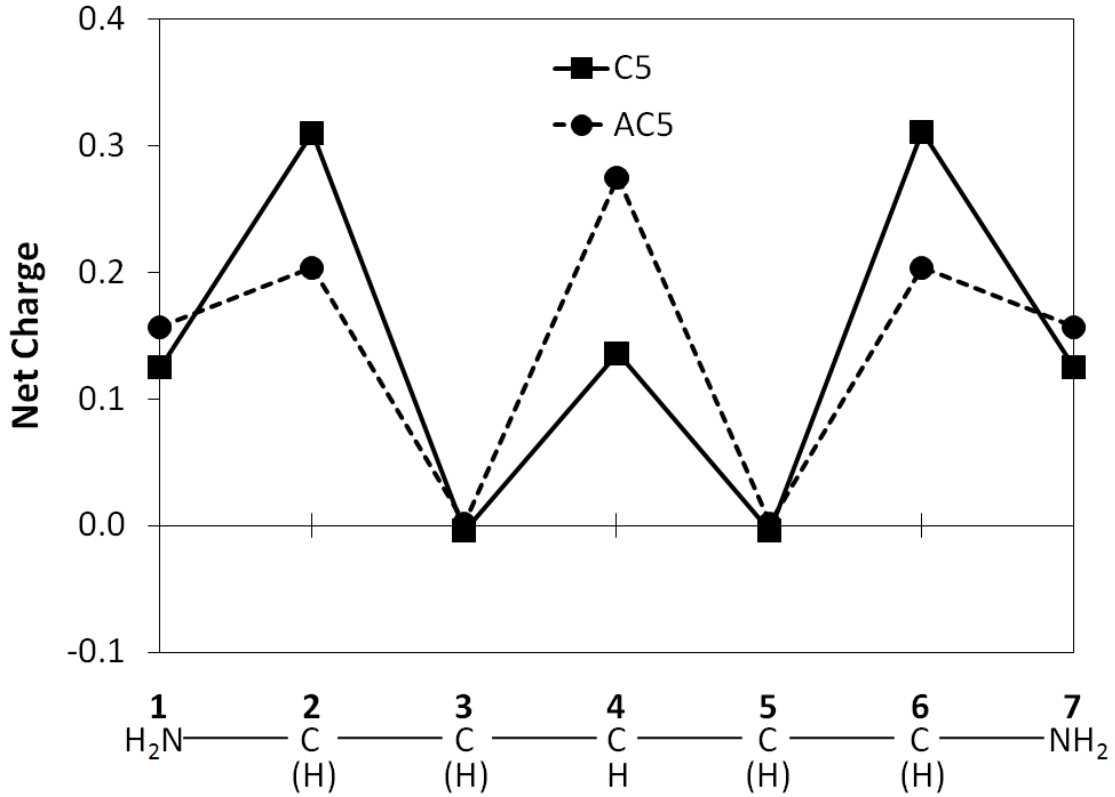

Figure 2.4. Mulliken charge analysis of **C5** and **AC5**. The amount of formal charge are summed at each site; C and H for cite 2, 3, 5, and 6 in **C5**; only C for cite 2, 3, 5, and 6 in **AC5**. The significant charge difference on π-bridges between two compounds is shown at cite 2 and 6 (terminal carbon atoms) and 4 (central carbon atom).

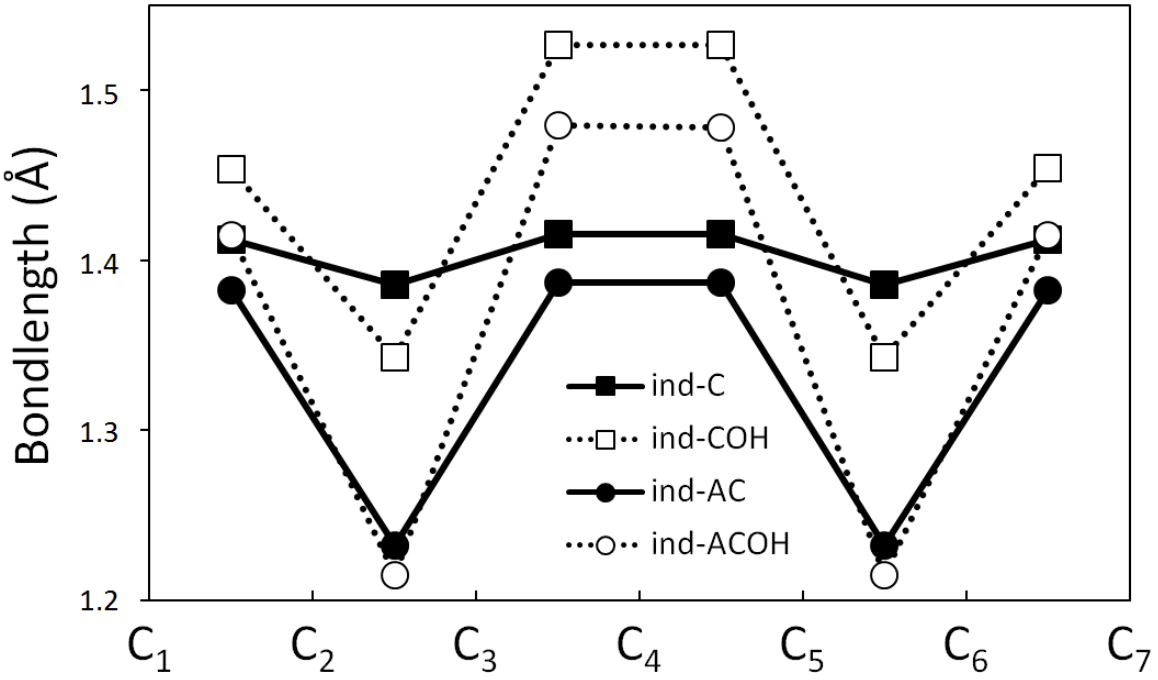

Figure 2.5. Bond lengths for **ind-C**, **ind-COH**, **ind-AC** and **ind-ACOH** computed at the B3LYP/6-31G** level.

Upon cation formation from their alcohol precursors, the central carbon atoms in the **C** and **AC** compounds change hybridization from sp^3 to sp^2. On the basis of this change in hybridization, the evolution of the bond lengths were investigated in **ind-C** and **ind-AC** with their alcohol precursors **ind-ACOH** and **ind-ACOH** (Figure 2.5). Both cyanine and alkyne carbocation dyes significantly shorten their bond lengths at C_3-C_4 and C_4-C_5 as dehydroxylation proceeds. However, the cation formation has a rather small impact on the bond lengths at C_2-C_3 and C_5-C_6 in **ind-AC,** while the elongation of those bonds is observed in **ind-C**. To investigate how the charge is distributed within the π-bridge, the ground-state Mulliken charge distribution in the large cyanine and alkyne carbocation model compounds **C5** and **AC5** are computed using INDO/MRDCI (Figure 2.4). This

result describes the different charge localizations in the two systems: the positive charge is localized on the central part, site 4 in **AC5** and it is more localized on the terminal carbon atoms, site 2 and 6 in **C5**.

To investigate the structural properties of the newly synthesized **C** and **AC** compounds, the IR spectra of **ind-C**, **ind-AC**, **por-C** and **por-AC** were computed based on the DFT-optimized geometries. The carbocation spectrum, in general, has more intense peaks than its neutral compounds as expected from the presence of a net charge.[24] The **AC** spectrum presents an intense band and another relatively small band around 2000—2300 cm^{-1}. This IR region corresponds to vibrational modes in conjugated alkynes and substituted allenes (the latter appearing due to the resonance forms of the molecule, see above). The peaks were observed in **ind-AC**: at 2179 and 2264 cm^{-1} and in **por-AC**: 2060 and 2161 cm^{-1} (Figure 2.6). The **C** compounds **ind-C** and **por-C** have strong peaks from in-plane C-H and conjugated alkene stretches around 1300—1600 cm^{-1}.

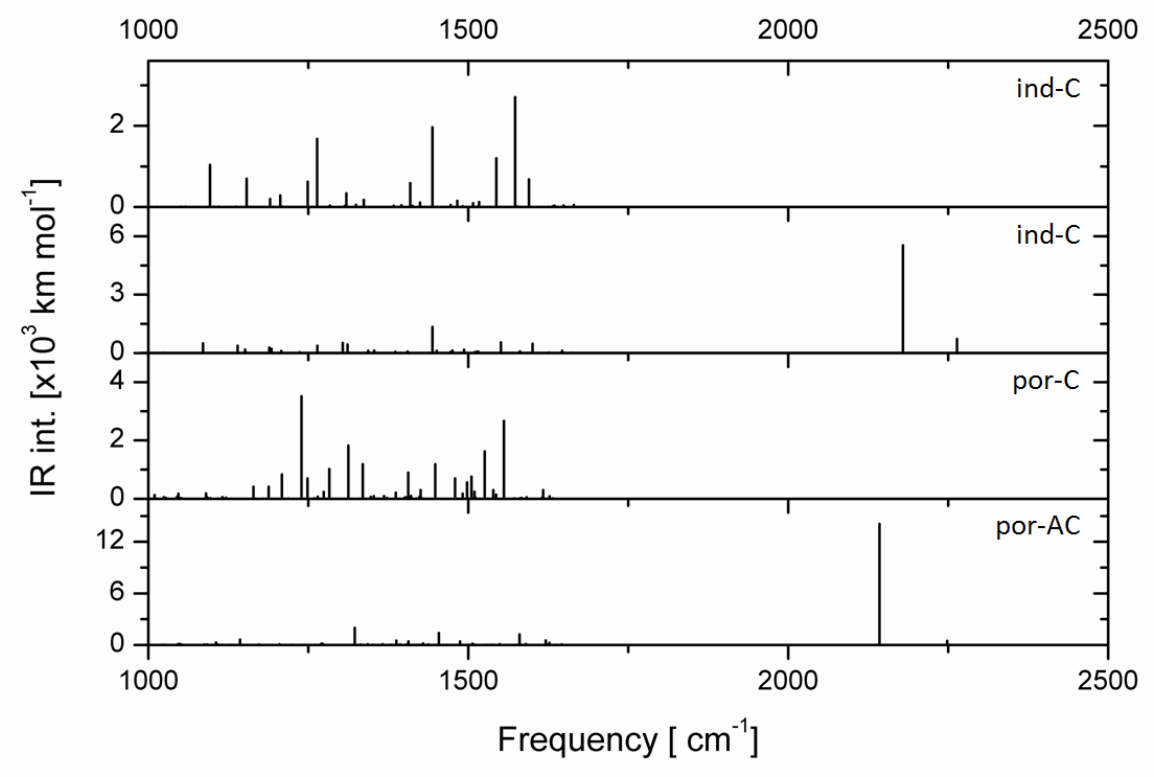

Figure 2.6. Simulated IR spectra for **1** – **4** computed at the B3LYP/6-31G** level. The **AC** spectra presents an intense band and another relatively small band around 2000—2300 cm^{-1}, which are absent in **C** spectra.

Figure 2.7 collects the FTIR spectra of **por-AC** in chloroform: 2% trifluoroacetic acid and **por-ACOH** in chloroform, together with the DFT-calculated spectra. The carbocation spectrum presents a major new band at 2008 cm^{-1} and another new band at 2152 cm^{-1}. These bands are well reproduced in the calculations (carried out on isolated molecules), with bands at 2060 and 2161 cm^{-1}, as is the ratio of their intensities, 27.6 in experiment vs. 28.3 in the simulated spectra. The normal mode coordinates for the calculated bands at 2060 and 2161 cm^{-1} are illustrated in Figure 2.8; the origin of these modes is due mainly to antisymmetric and symmetric stretches of the triple-like bonds, respectively. This very good

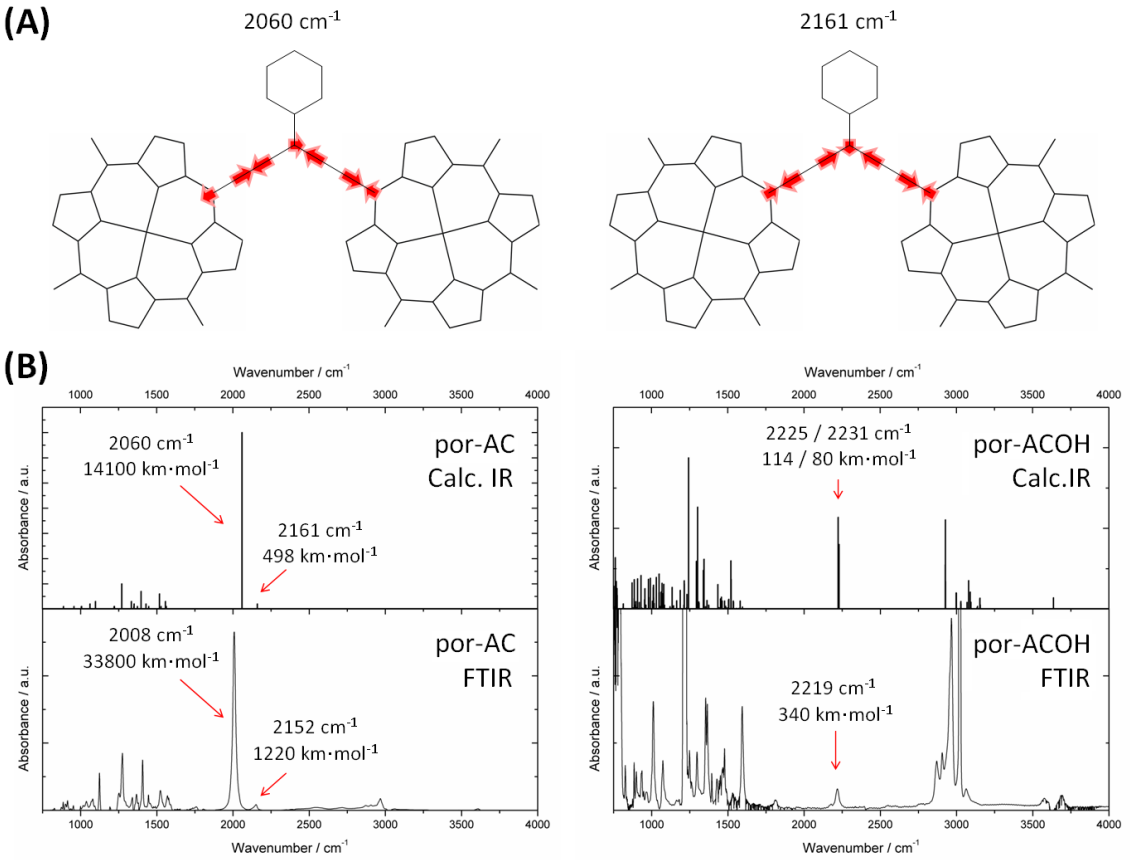

Figure 2.7. (A) Illustration of the normal modes of the DFT-calculated bands at 2060 cm^{-1} and 2161 cm^{-1} for **4**. (B) Calculated IR (top) and experimental FTIR spectra in $CHCl_3$ (bottom) of **4** (left) and **4-OH** (right). The signals at ~1750 cm^{-1} and between 2500-3500 cm^{-1} in the FTIR spectrum of **4** are residual peaks from trifluoroacetic acid.

agreement between theory and experiment confirms that compounds **1** and **ACn**, whose (fully-optimized) calculated geometric structures can be simply viewed as averages over the sets of resonance structures, correspond to strongly bond-alternated structures.

The similarities between the **Cn** and **ACn** series can be rationalized when considering the bonding-antibonding patterns in the π-molecular orbitals of, for example, **C5** and **AC5** (Figure 2.8). All MO's are essentially identical in the two compounds. Interestingly, except in the case of the fully bonding, most stable π-MO, the π-bonding remains weak between the carbons nominally bearing the triple bonds in **AC5** and the corresponding carbons in **C5**. This feature could explain why the shortening of these bonds due to the perpendicular π-system in **AC5** has only a weak impact on the electronic properties.

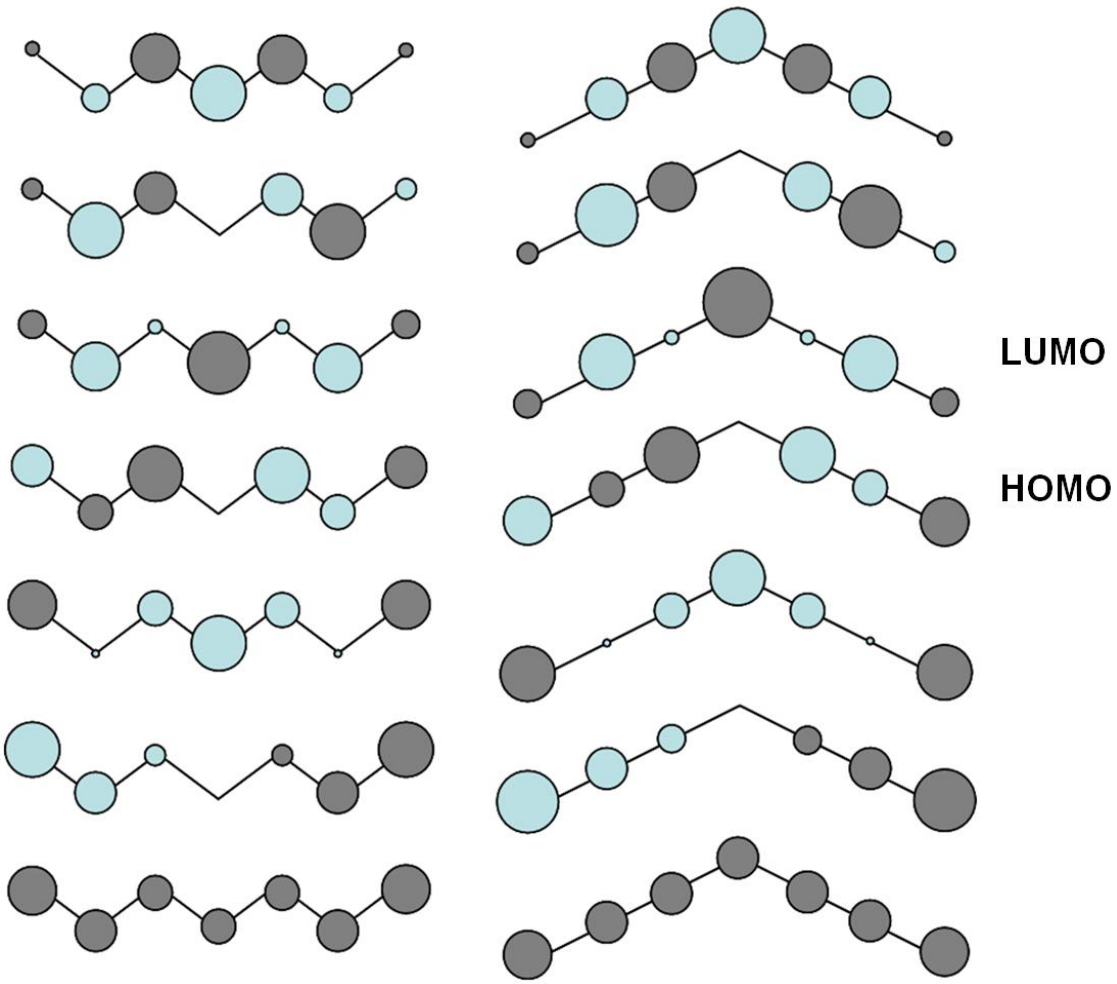

Figure 2.8. Comparison of the DFT π wavefunctions for C5 (left) and AC5 (right) the four lowest wavefunctions correspond in each case to the four doubly-occupied π levels.

2.3 The first excited state energy and the transition dipole moment

The next step was to compare the optical properties of cyanine dyes and alkyne carbocations as a function of the physical length, *d*, of the molecules (taken as the distance between the two nitrogen atoms in **Cn** and twice the distance between one of the nitrogen atoms to the central carbon atom in **ACn**). Here, we have relied on the highly correlated INDO-MRDCI technique coupled to the sum-over-states (SOS) perturbative approach.

The electric dipole moment associated with the transition between two states. $|e\rangle$ and $|g\rangle$ is defined as:

$$\mathrm{M}_{eg} = \int \Psi_e^* e\vec{\mathrm{r}}\Psi_g \mathrm{d}\vec{\mathrm{r}} = \int \Psi_e^*(\vec{\mathrm{r}})\Psi_g(\vec{\mathrm{r}})\, e\vec{\mathrm{r}}\, \mathrm{d}\vec{\mathrm{r}}$$

where $\int \Psi_e^*(\vec{\mathrm{r}})\Psi_g(\vec{\mathrm{r}})\mathrm{d}\vec{\mathrm{r}}$ denotes the overlap between $|e\rangle$ and $|g\rangle$; and $e\vec{\mathrm{r}}$ denotes the charge e separation with the distance vector $\vec{\mathrm{r}}$. Thus, the transition dipole moment is large when: (i) both $|e\rangle$ and $|g\rangle$ wavefunctions delocalized over the whole molecule; and (ii) there is a larger charge separation $e\vec{\mathrm{r}}$. Here, the large M_{eg} for **AC5** and **C5** is explained by the efficient charge-separation qr compared with polyene, $NH_2(CH)_6NH_2$, shown in Figure 2.10 on the basis of an analysis of the transition densities. Furthermore, the transition dipole vectors is the larges in the molecular length is maximized as is in **Cn** compounds.

The evolution with model cyanines and alkyne carbocations is fully consistent with the optical characterization of compounds **ind-C**, **ind-AC**, **por-C**, and **por-AC**. Table 2.1 shows that the INDO/MRDCI results with two reference

determinants for the compounds are in good agreement with the experimental values. It is important to note that there is a significant contribution from doubly-excited configurations in the lowest excited state for all of the cyanines and alkyne carbocations, a feature that INDO/S and TD-DFT methods cannot capture.

Table 2.1. The first excited state energy and transition dipole moments of **1** – **4** computed at the INDO/S 50x50, INDO/MRDCI with two references, INDO/MRDCI with five references and TD-DFT B3LYP/6-31G**.

		INDO/S 50x50	INDO/MRDCI with 2ref[a]	with 5ref[a]	B3LYP 6-31G**	Exp.
1	E (eV)	2.22	1.55	1.52	2.37	
	TDM (D)	14.3	13.0	14.5	12.5	
2	E (eV)	2.25	1.56	1.70	2.11	1.63[b]
	TDM (D)	11.7	10.9	11.9	10.0	
3	E (eV)	1.41	0.95	1.27	1.49	1.03[b]
	TDM (D)	19.3	16.9	18.6	15.9	
4	E (eV)	1.49	1.03	1.37	1.45	1.00[c]
	TDM (D)	16.8	15.3	15.8	16.5	16.8[c]

(a) Larger MO-active space was used for the INDO/MRDCI calculations with two reference determinants than that with five reference determinants.
(b) Unpublished data from the Anderson's group at University of Oxford.
(c) Ref. 9

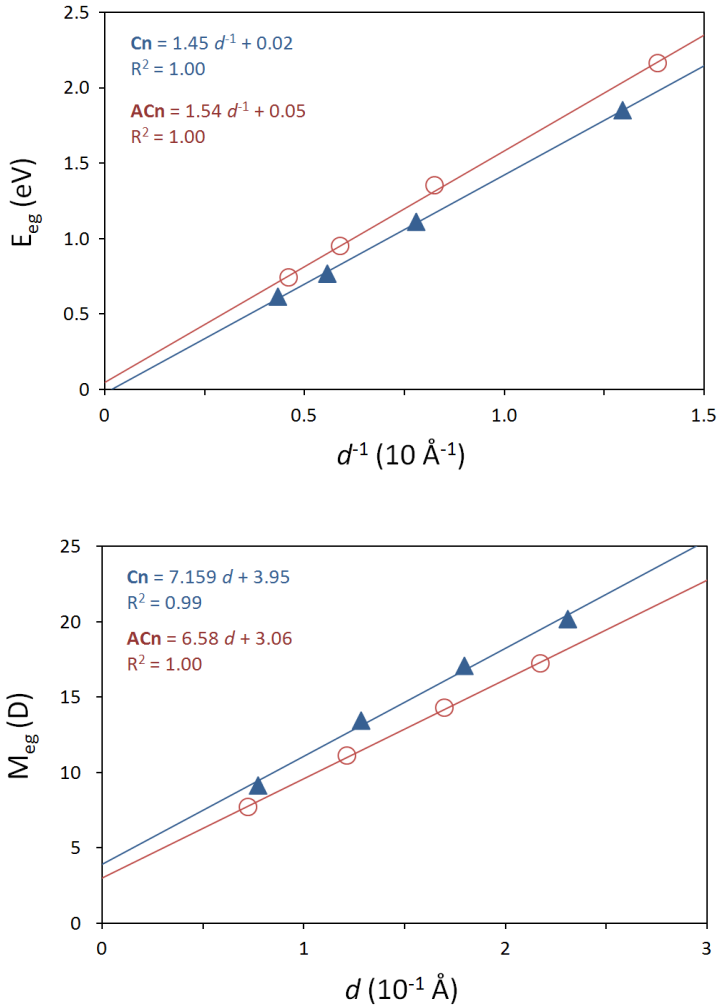

Figure 2.9. Evolution of the S_0-S_1 energy gap (E_{eg}), and S_0-S_1 transition dipole (M_{eg}), as a function of d^{-1}, and d, respectively (where d is the length of the π-system, see text for detail) for the **Cn** (triangles) and **ACn** (circles) compounds.

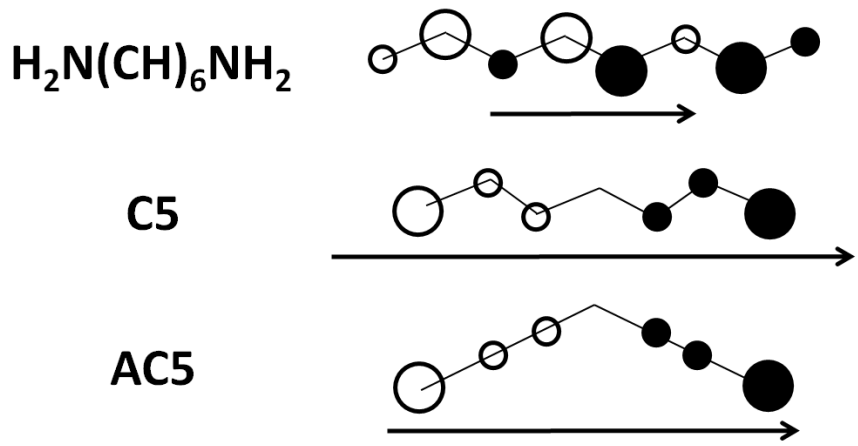

Figure 2.10. Transition dipole moment M_{eg} vector and atomic transition density for polyene $H_2N(CH)_6NH_2$, **C5** and **AC5**.

2.4 First- and third-order polarizabilities

We now turn to an analysis of the first- and third-order polarizabilities computed at the highly correlated INDO-MRDCI technique coupled to the sum-over-states (SOS) perturbative approach. In the SOS framework, when a single excited state dominates the optical response, the static polarizability expressions can be simplified with M_{eg} and E_{eg}: $\alpha \approx M_{eg}^2/E_{eg}$; $\gamma \approx M_{eg}^4/E_{eg}^3$ (although a significant $\Delta\mu_{eg}$ is present in **ACn**, we confirmed that $\Delta\mu_{eg}$ is much smaller than M_{eg} and neglected the dipolar term in the γ expression). The first- and third-order polarizabilities are predicted to grow (in absolute values) as the third and seventh power of the molecular length, respectively.

Table 2.2. The first-, and third-order static polarizabilities for **ind-C, ind-AC, por-C** and **por-AC** computed at the INDO/MRDCI-SOS level.

	α (10^{-24} esu)	γ (10^{-36} esu)
ind-C	70	-3.6×10^3
ind-AC	66	-1.5×10^3
por-C	219	-5.5×10^4
por-AC	203	-3.2×10^4

Table 2.3. Experimental static third-order polarizability $\langle\gamma\rangle$ values (in esu) for polyenes as a function of the number n of double bonds.[25]

n	10^{-36} esu
4	50
5	99
6	180
7	280
8	400
9	570
10	830
11	1100
12	1500
13	1900
14	2400
15	2900

A number of conclusions can be drawn from the results in Figure 2.11:

(i) It is remarkable to note that, for similar molecular lengths, the α values in the **ACn** compounds are basically identical to those in the **Cn** counterparts due to the similar M_{eg} and E_{eg}. The traditional cyanines show slightly higher α values, since they exhibit somewhat smaller E_{eg} and larger M_{eg} in comparison to the **ACn** compounds.

(ii) The small differences in the M_{eg} and E_{eg} values between two series are enhanced in the γ expression. The γ evolution indicates that γ increases about four times faster in the **Cn** compounds with respect to the **ACn** compounds with larger M_{eg} and smaller E_{eg} in **Cn** compounds.

From Table 2.2, it can be seen that the polarizabilities for the indole and Ni-porphyrin cyanines and alkyne carbocations **ind-C**, **ind-AC**, **por-C** and **por-AC** show the same trends as the model compounds. It is predicted that both C and AC systems will have significantly large third-order polarizability γ as a comparison with the experimental static third-order poralizability $<\gamma>$ values for various length of polyenes in Table 2.3.

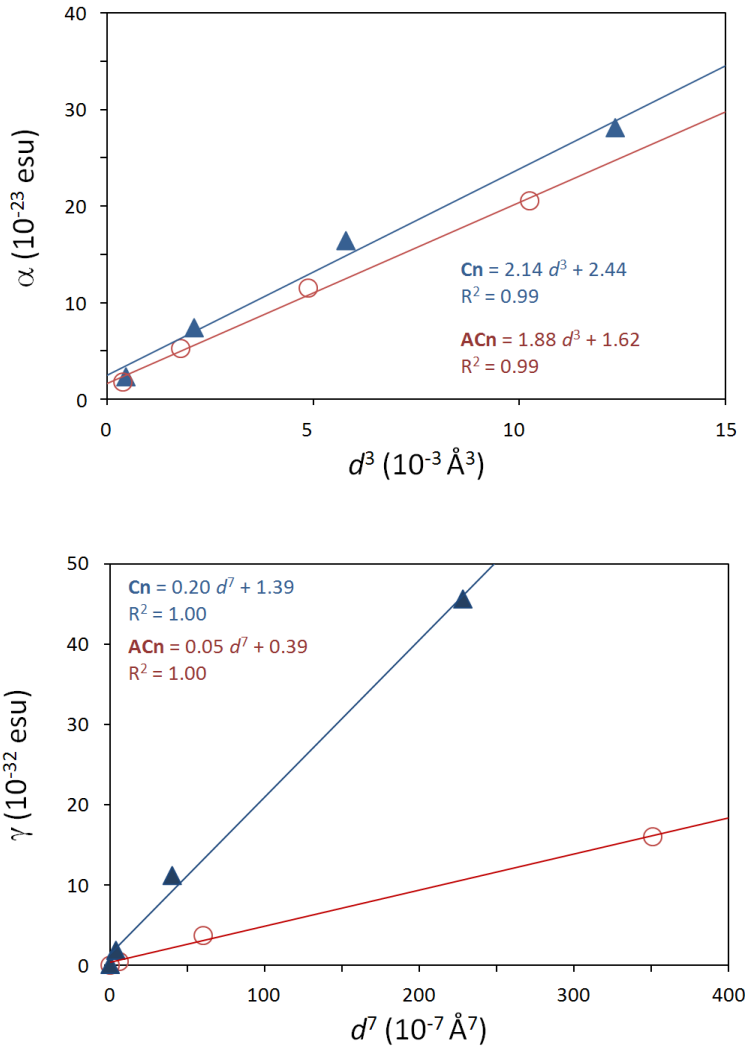

Figure 2.11. Evolution of the first- and third-order polarizabilities α, and γ as a function of d^3, and d^7, respectively (where d is the length of the π-system, see text for detail) for the **Cn** (triangles) and **ACn** (circles) compounds.

2.5 Conclusion

Our theoretical results establish that the alkyne carbocations exhibit very similar optical properties to traditional cyanine dyes, such as the transition dipole moment between the ground state and the lowest excited state, M_{eg}, the transition energy, E_{eg} and the static first-order polarizability, α. However, the NLO properties in alkyne carbocations do not show the typical cyanine character. The new set of compounds have relatively large third-order polarizabilities γ.

The similarities between the **Cn** and **ACn** series can be rationalized when considering the bonding-antibonding patterns in the π-molecular orbitals. All MO's are essentially identical in the two compounds. Interestingly, except in the case of the fully bonding, most stable π-MO, the π-bonding remains weak between the carbons nominally bearing the triple bonds in **AC5** and the corresponding carbons in **C5**. We suggest that this feature is a reason why the shortening of these bonds due to the perpendicular π-system in **AC5** has only a weak impact on the electronic properties.

In conclusion, our theoretical results establish that the *alkyne carbocations, in spite of their significant degree of bond-length alternation, behave in the same way as cyanine dyes*. They confirm that in these compounds (which could be considered as monomethine cyanine dyes such as Michler's hydro blue or Victoria green), the delocalized nature of the electronic structure represents a

more significant characteristic than the degree of BLA. It will be important to determine up to what length the **ACn** compounds can retain full delocalization.

REFERENCES

(1) (a) König, W. *Ber. Deutsch. Chem. Ges.* **1922,** *55*, 3293-3313. (b) König, W. *J. Prakt.Chem.***1926**, *112*, 1-36.

(2) Kuhn, H. *J. Chem. Phys.* **1948**, *16*, 840-841.

(3) Simpson; T., W. *J. Chem. Phys.* **1948**, *16*, 1124-1136.

(4) Dähne, S.; Kulpe, S. *Abh. Akad. Wiss. DDR, Abt. Math. Naturwiss. Tech.* **1977**, *8*, 1-128 and references therein.

(5) Fabian, J.; Hartmann, H. *J. Mol. Struct.* **1975**, *27*, 67-78.

(6) Salem, L. *The Molecular Orbital Theory of Conjugated Systems*; W.A. Benjamin: New York, 1966.

(7) Chemla, D. S.; Zyss, J. *Nonlinear Optical Properties of Organic Molecules and Crystals*; Academic: New York, 1987.

(8) Marder, S. R.; Sohn, J. E.; Stucky, G. D.; American Chemical Society: Washington, DC, 1991.

(9) Thorley, K. J.; Hales, J. M.; Anderson, H. L.; Perry, J. W. *Ang. Chem. Int. Ed.* **2008**, *47*, 7095-7098.

(10) Su, W. P.; Schrieffer, J. R.; Heeger, A. *J. Phys. Rev. Lett.* 1979, *42*, 1698-**1701**.

(11) Brédas, J.-L. *J. Chem. Phys* **1985**, *82*, 3808-3811.

(12) Marder, S. R.; Gorman, C. B.; Meyers, F.; Perry, J. W.; Bourhill, G.; Brédas, J.-L.; Pierce, B. M. *Science* **1994**, *265*, 632-635.

(13) Potenza, J. A.; Zyontz, L.; W., B. *Acta Cryst.* **1978**, *B34*, 193-199.

(14) Kulpe, S.; Kuban, R. J.; Schulz, B.; S., D. *Cryst. Res. Tech.* **1987**, *22*, 375-379.

(15) Marder, S. R.; Perry, J. W.; Tiemann, B. G.; Gorman, C. B.; Gilmour, S.; Biddle, S. L.; Bourhill, G. *J. Am. Chem. Soc.* **1993**, *115*, 2524-2526.

(16) Yau, C. M. S.; Pascu, S. I.; Odom, S. A.; Warren, J. E.; Klotz, E. J. F.; Frampton, M. J.; Williams, C. C.; Coropceanu, V.; Kuimova, M. K.; Phillips, D.; Barlow, S.; Brédas, J.-L.; Marder, S. R.; Millar, V.; Anderson, H. L. *Chem. Commun.* **2008**, 2897-2899.

(17) Lu, D.; Chen, G.; Perry, J.W.; Goddard, W.A. *J. Am. Chem. Soc.* **1994,** *116,* 10679-10685.

(18) Tolbert, L. M.; Zhao, X. *J. Am. Chem. Soc.* **1997**, *119*, 3253-3258.

(19) Fabian, J. *J. Mol. Struct. THEOCHEM* **2006**, *766*, 49-60.

(20) Pierce, B. M. *Phys. D* **1993**, *68*, 51-58.

(21) Brédas, J. L.; Adant, C.; Tackx, P.; Persoons, A.; Pierce, B. M. *Chem. Rev.* **1994**, *94*, 243-278.

(22) Bodart, V. P.; Delhalle, J.; André, J. M.; Zyss, J. *Can. J. Chem.* **1985**, *63*, 1631-1634.

(23) Hurst, G. J. B.; Dupuis, M.; Clementi, E. *J. Chem. Phys.* **1988**, *89*, 385-395.

(24) Mele, E. J.; Rice, M. *J. Phys. Rev. Lett.* **1980**, *45*, 926-929.

(25) Craig, G. S. W.; Cohen, R. E.; Schrock, R. R.; Silbey, R. J.; Pucetti, G.; Ledoux, I.; Zyss, J. *J. Am. Chem. Soc.* **1993**, *115*, 860**.**

CHAPTER 3:

Porphyrin Dimers: A Theoretical Understanding of the Impact of Electronic Coupling Strength on the Two-Photon Absorption Properties

Objective

Many porphyrin oligomers exhibit large two-photon absorption (TPA) at fundamental photon energies around 1.5 eV, while the corresponding monomers have negligible TPA cross-sections in that energy range. In general, our understanding of nonlinear absorption in these compounds is rather limited compared to that of linear absorption. Here, we seek to provide insight into this issue by examining various structural aspects of porphyrin dimers and analyzing how they lead to either “pure” or double resonance-enhanced TPA cross-sections. To do so, we have carried out highly correlated quantum-chemical calculations on model chromophores which differ by their central π-conjugated bridges or acceptor moieties. In a number of such dimers, the calculated energies of the lowest two-photon active states are stabilized and display significant cross-sections as the electronic coupling strength between the two porphyrin moieties becomes significant; in these instances, the lowest electronic TPA-active state is located in an energy range preventing contributions from double resonance effects. On the other hand, in dimers in which the porphyrin moieties are either very strongly or very weakly electronically coupled, the TPA cross-sections are mainly due to double resonance effects.

3.1 Introduction

Organic compounds with large two-photon absorption (TPA) cross-sections, δ, are of general interest due to their possible exploitation in optical devices, micro- or nano-fabrication, or bioimaging.[1-7] Porphyrins represent an important class of organic systems which, in addition to their biological functions, have been considered as sensitizers in photovoltaic cells,[8, 9] hole-transporting semiconductors,[10] optical limiters,[11] or components in artificial photosynthesis[12] or molecular-scale electronics,[13] due to their attractive spectroscopic and photophysical properties. Recently, a number of butadiyne-linked and other porphyrin oligomers have been shown to possess large third-order molecular polarizabilities and TPA cross-sections.[14, 15] However, our current understanding of the factors determining non-linear absorption in these systems remains limited. Here, we seek to provide insight into this issue and examine various structural aspects of porphyrin dimers that can lead to either double resonance-enhanced or "pure" TPA cross-sections; in the latter case, the fundamental photon energy is far from the energy of any one-photon optical transition; in the former, it becomes resonant with a one-photon transition, which limits the applicability of the TPA process.

The linear absorption spectra of porphyrins were interpreted some 45 years ago by Gouterman *et al.* on the basis of what is now referred to as the four-orbital model.[16] This model relies on the fact that in porphyrins the highest two occupied molecular orbitals (HOMO and HOMO-1) and lowest two unoccupied molecular

orbitals (LUMO and LUMO+1) are energetically well separated from any other electronic levels. In porphyrins with D_{4h} symmetry, the occupied frontier orbitals belong to a_{1u} and a_{2u} symmetries while the unoccupied levels are doubly degenerate with e_g symmetry, see Figure 3.1. The combination of (HOMO→LUMO) and (HOMO-1→LUMO) transitions yields two electronic states: A higher–energy state with strong oscillator strength (B or Soret band) and a low–energy state with weak oscillator strength (Q band).

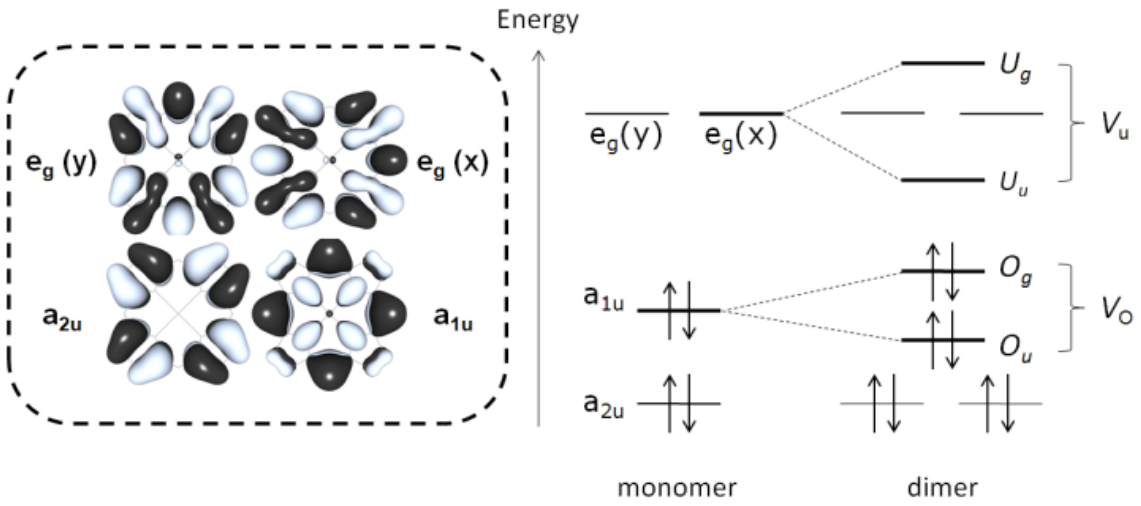

Figure 3.1 Left: Highest two occupied and lowest two unoccupied molecular orbitals in a porphyrin molecule with D_{4h} symmetry: a_{1u}, a_{2u}, $e_g(x)$, and $e_g(y)$. Right: Energy correlation diagram in going from a monomer to a porphyrin dimer: The dimer MO's are labelled $U_{g/u}$ (unoccupied *gerade/ungerade*) and $O_{g/u}$ (occupied *gerade/ungerade*) and originate from a_{1u} and $e_g(x)$ molecular orbitals of the monomer, respectively. The electronic couplings are defined as V_U for the unoccupied MO's and V_O for the occupied MO's.

Porphyrin dimers (and oligomers) are usually linked through their meso positions, along what we define here as the x-axis. The larger electron density at the *meso* (x) binding position in the monomer $e_g(x)$ and a_{1u} molecular orbitals leads to more

substantial energy shifts of these MO's compared to the $e_g(y)$ and a_{2u} MO's, as illustrated in Figure 3.1. This results in Q- and B-band splittings in the linear absorption spectra (Q_x/Q_y- and B_x/B_y-bands). In the case of the dimer, the $e_g(x)$ and a_{1u} MO's originating from the D_{4h} monomer split into two MO's, that present *gerade* or *ungerade* inversion symmetry. The energy splitting between the *gerade* and *ungerade* levels primarily depends on the electronic coupling strength V between the two porphyrin moieties; here, we will therefore take V_O [V_U], see Figure 3.1, as a measure of the electronic coupling for the occupied [unoccupied] MO's. Clearly, these energy splittings and resulting orbital ordering are a function of the nature of the bridges between the porphyrin units (we note that in most of the cases for *meso*-linked porphyrin dimers, the electronic interactions are not strong enough to impact the a_{2u} and $e_g(y)$ MO's, so that each of them remains nearly doubly degenerate).

Symmetrical porphyrin dimers linked by *meso*-butadiyne bridges consistently present the lowest TPA-active state around the Soret-band energy range (around 2.78—3.02 eV), with large cross-sections in the range 3,000—10,000 GM[14, 15] (1 GM [Goeppert-Mayer] =10^{-50} cm^4·s per photon). It is useful to point out that since the Q_x bands in such dimers appear at lower energies (1.67-1.93 eV) than their typical location in the monomers (~2.12 eV),[17] this opens up the possibility in some instances of one-photon resonance enhancement of the TPA signal (double resonance conditions). It has been recently observed that (zinc porphyrin)—(perylene diimide)—(zinc porphyrin) donor-acceptor-donor

(D—A—D) chromophores linked by ethynylene groups show comparatively high TPA cross-sections (2,000—7,000 GM) but at a much lower energy range, 2.07—2.33 eV.[18] Since in these compounds the lowest one-photon absorption (OPA) band is also located around 1.5 eV, this prevents the TPA response to suffer from contributions from double resonance effects.[19] These examples point to the importance of understanding the factors affecting both the one-photon absorption (OPA)- and TPA-peak positions in porphyrin dimers, in order to obtain large and *usable* δ values.

Model zinc porphyrin dimer compounds. Here, we use the results of highly correlated quantum-mechanical calculations to understand the relationship between electronic coupling and OPA and TPA peak positions in porphyrin dimers with various linkages. We have considered a series of metalloporphyrin—π/R—metalloporphyrin complexes with π-conjugated bridges or acceptor R groups that can control the electronic coupling strength between the two porphyrin moieties, see Figure 3.2. The TPA data for compounds **1-0**,[20] **1-1**,[14, 15] **1-2**,[14, 15] **2**,[14, 15] **3**,[14, 15] **4**,[20] **6**,[21] and **7**[18] and the (linear) absorption spectra for **1-0**,[20] **1-1**,[14, 15,22] **1-2**,[14, 15] **1-4**,[22] **2**,[14, 15] **3**,[14, 15] **4**,[20] **6**,[21] and **7**[18] have been reported in the literature; **1-3**, **1-6**, and **5** were used as model compounds. We will first discuss the **1-n** compounds, for which we examine the effect of increasing the π-conjugation length or the torsional angle between the porphyrin units. Then, compounds **1-0**, **2**, **3**, and **4** are used as examples of porphyrin dimers with

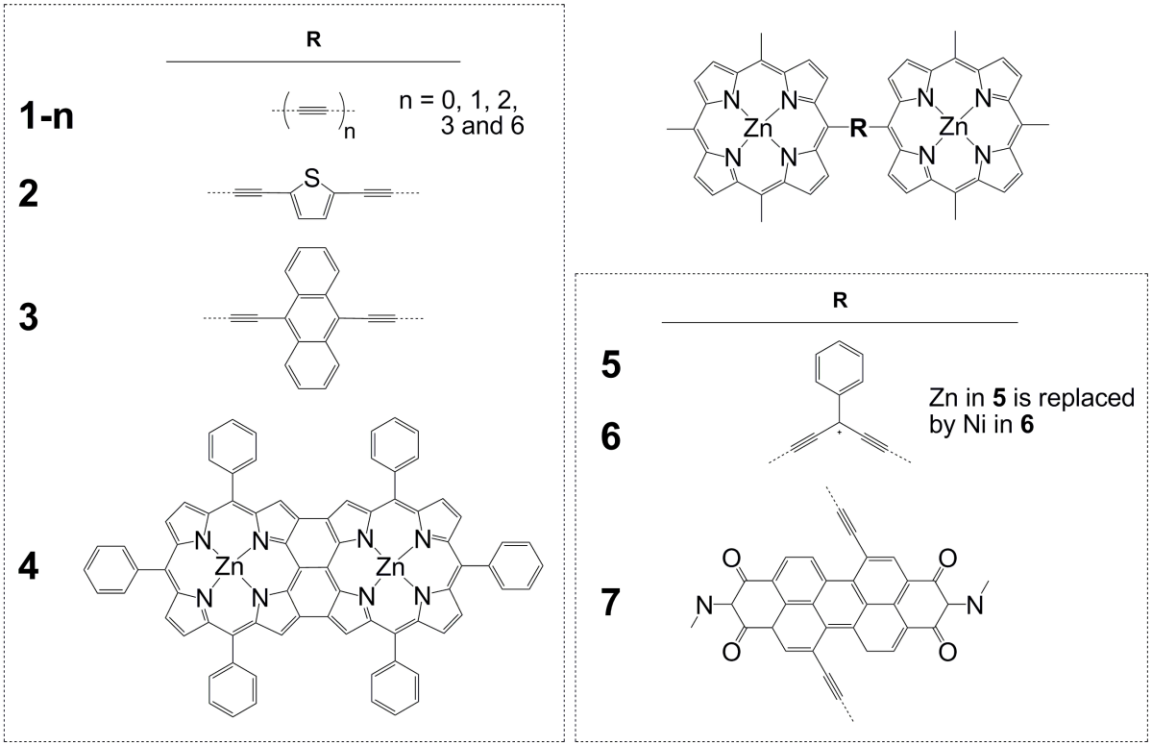

Figure 3.2 Chemical structures of metalloporphyrin—R—metalloporphyrin complexes with π-conjugated bridges or acceptor R groups examined in this work. The TPA data for compounds **1-0**,[20] **1-1**,[14,15] **1-2**,[14,15] **2**,[14,15] **3**,[14,15] **4**,[20] **6**,[21] and **7**[18] and the (linear) absorption spectra for **1-0**,[20] **1-1**,[14,15,22] **1-2**,[14,15] **1-4**,[22] **2**,[14,15] **3**,[14,15] **4**,[20] **6**,[21] and **7**[18] have been reported in the literature; **1-3**, **1-6**, and **5** were used as model compounds; (i) Compounds **1-n** are used to examine the effect of increasing the π-conjugation length or the torsional angle between the porphyrin units; (ii) Compounds **1-0**, **2**, **3**, and **4** are used as examples of porphyrin dimers with varying conjugated bridges; (iii) Compounds **5** – **7** are used to discuss the effect of strong acceptor or cationic R groups.

varying conjugated bridges. Finally, we discuss the effect of strong acceptor or cationic R groups using 5–7.

3.2 Extended Gouterman's model

We first examined how Gouterman's model can be extended to the case of dimers. To do so, we considered the frontier molecular orbitals (FMO's) of the dimers, which are observed to fall into two categories: In the first, with planar **1-2** as an example, there appear four occupied FMO's and four unoccupied FMO's, as illustrated in Figure 3.3. Clearly, these eight FMO's directly come from the splitting of the four corresponding FMO's of the monomers. In the second category, with **5** as an example, nine FMO's need to be considered, four occupied and five unoccupied; in this case, the LUMO does not correspond to any combination among the four monomer FMO's and presents a strong bridge contribution, Figure 3.4.

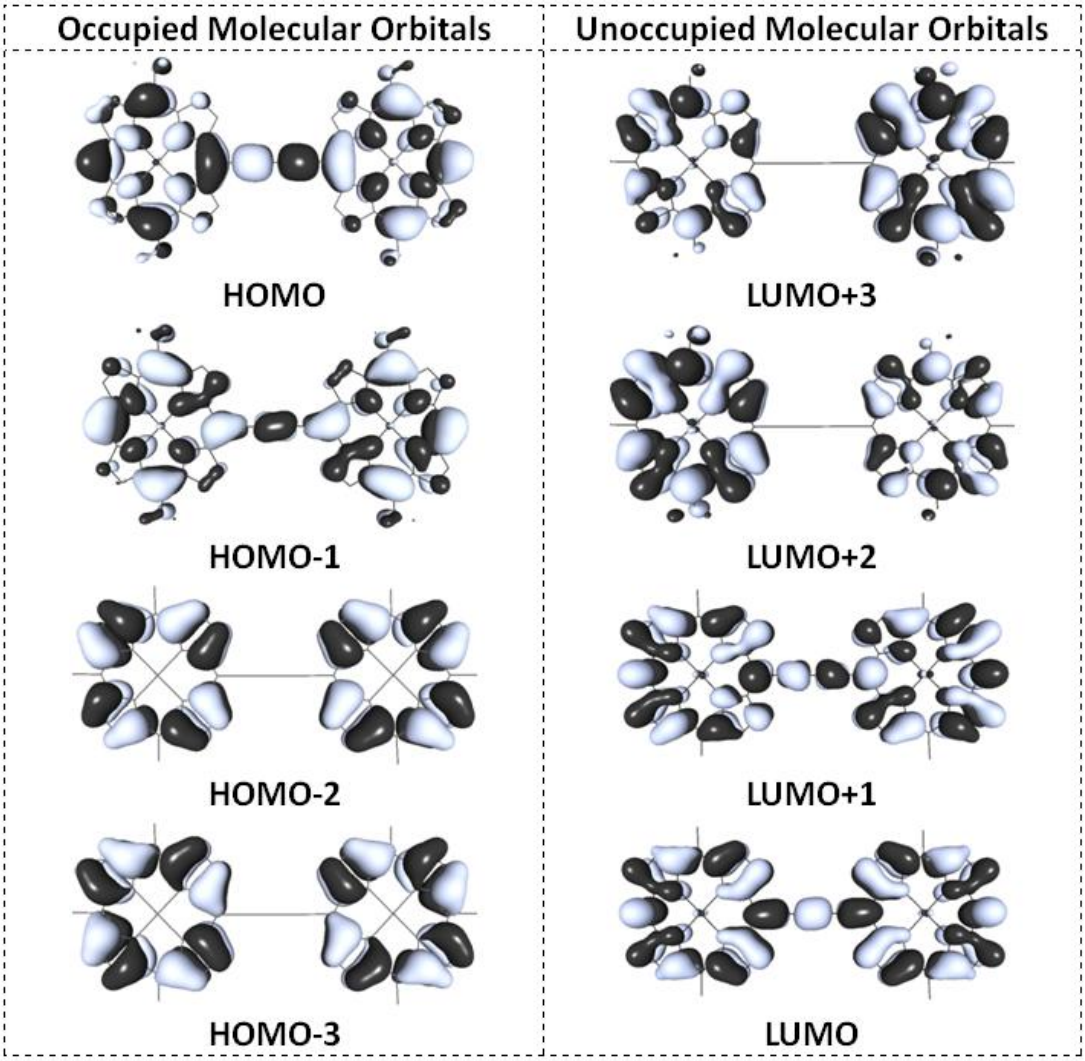

Figure 3.3 The highest four occupied and lowest four unoccupied molecular orbitals of planar **1-2** computed at the B3LYP/6-31G** level.

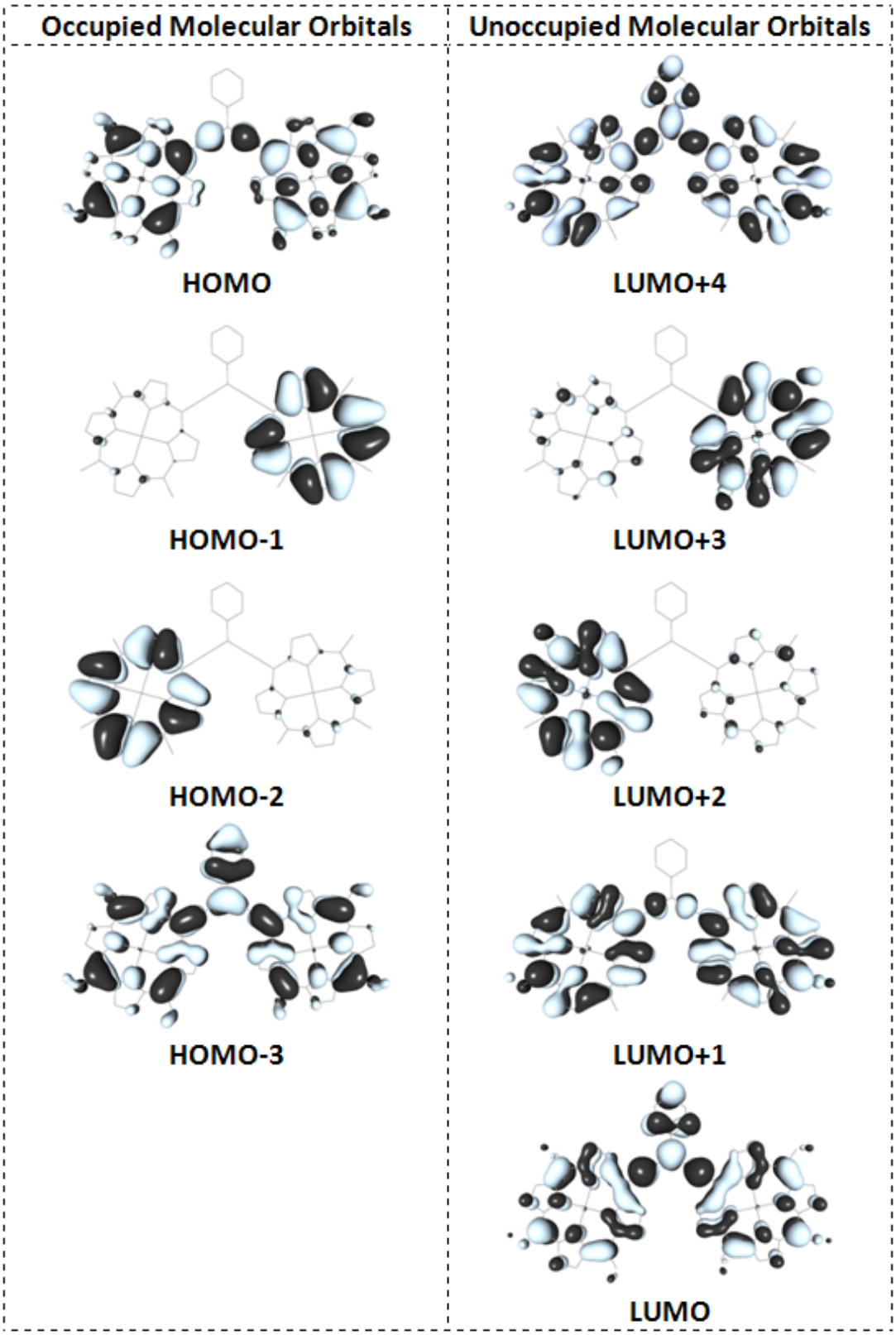

Figure 3.4 The highest four occupied and lowest five unoccupied molecular orbitals of **5** computed at the B3LYP/6-31G** level.

3.3 Porphyrin dimers 1–4

In the case of the series of planar compounds **1-n** with varying π-conjugated bridge lengths between the porphyrin moieties, we observe a decrease in energy splittings of the O_u/O_g and U_u/U_g levels with extension of the bridge (Figure 3.5, top). While in π-conjugated polymers the lowest OPA- and TPA-active states decrease in energy with increasing conjugation length,[38, 39] the state energies in **1-n** are controlled by the coupling strength between the porphyrin end groups.[14, 15, 22] The porphyrin dimers that are separated by long alkyne π-conjugated bridges do interact weakly, so that their electronic and optical properties are actually similar to those of porphyrin monomers. Figure 3.5, bottom, illustrates that, as the size of the conjugated alkyne bridge increases, the lowest TPA-active state energies are destabilized (the OPA-active state energies are as well), while cross-sections (and OPA transition dipole moments) are enhanced. For TPA in the range ~3.5 – 3.6 eV, the fundamental photon energy approaches the OPA-active state energy, so that the TPA cross-section no longer originates from “pure” TPA processes. In **1-6**, which presents a weak coupling between terminal groups, the first TPA-active state energy comes close to the double-resonance energy range, so that some contamination of the TPA from double-resonance effects is expected.

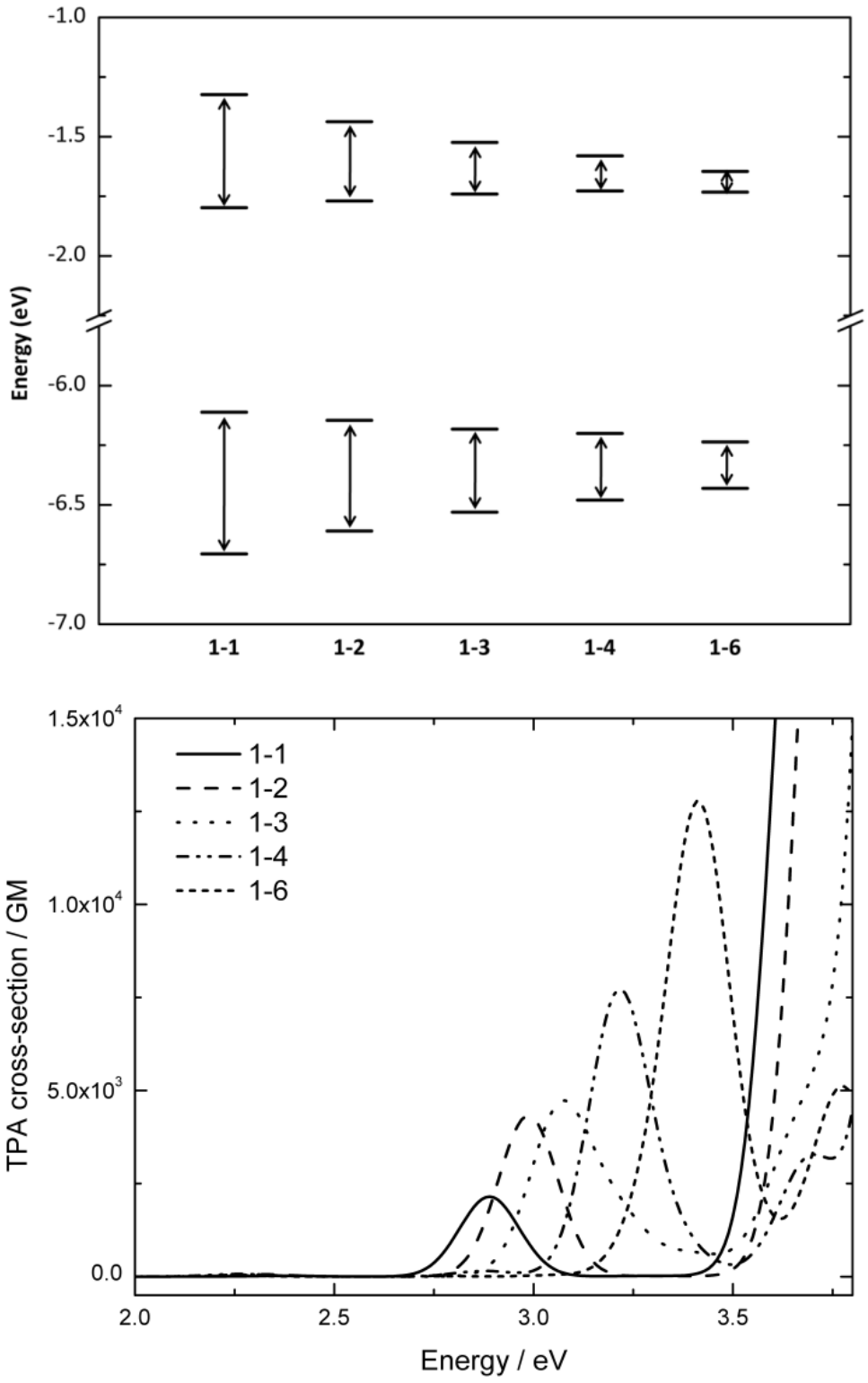

Figure 3.5 Energy splittings V_U and V_O (top) and TPA spectra (bottom) for planar compounds **1-n** as a function of the length of the conjugated bridge, computed at the INDO/S and INDO/MRDCI-SOS levels, respectively.

Table 3.1 First optically allowed transition energies in the planar **1-n** compounds with various alkyne lengths (top) and in **1-2(θ)** with various torsional angles θ (°) (bottom) between the porphyrin units, computed at the B3LYP/6-31G**, INDO/S, and INDO/MRDCI levels. The experimental data are provided as well. All values are in eV.

	B3LYP/ 6-31G**	INDO/S	INDO/ MRDCI	Exp.
1-1	1.82	1.71	2.07	1.74[a]
1-2	1.78	1.74	2.10	1.77[a]
1-3	1.76	1.76	2.12	
1-4	1.77	1.78	2.15	1.85[b]
1-6	1.71	1.79	2.17	
1-2(0)	1.78	1.74	2.10	1.77[a]
1-2(30)	1.80	1.76	2.12	
1-2(45)	1.85	1.77	2.14	
1-2(60)	1.90	1.78	2.18	
1-2(80)	2.00	1.80	2.24	
1-2(90)	2.06	1.80	2.24	

[a] Refs. 14 and 15. [b] Ref. 22.

We note that conventional DFT functionals do not accurately describe long-range correlation effects and the excitation energies of charge-transfer (CT) states.[40, 41] This was also observed in this study: the DFT/B3LYP calculations provide large V_O and V_U values in **1-6**, which results in a significant decrease of the HOMO-LUMO gap and a lowering of the first excited-state energy as the π-conjugated bridge length increases. This trend is completely opposite to the experimental data and the INDO results (Table 1).[15, 22] Therefore, in this work, we focus on the INDO results when considering the excited states and OPA/TPA spectra.

We now turn to a discussion of the electronic structures and OPA/TPA activity for **1-2(θ)** where θ represents the torsional angle between the porphyrin units. The planar geometry, **1-2(0)**, is energetically more favorable than any other

conformation; however, the energy difference computed at the B3LYP/6-31G** level between **1-2(0)** and **1-2(90)** is merely 0.03 eV (equivalent to ~360 K), which is in good agreement with the theoretical work of Winters *et al.*[42] With the shorter π-conjugation length in **1-1**, the energy difference between **1-1(0)** and **1-1(90)** is about twice as large as that of **1-2**, 0.06 eV. The torsion potential remains, however, completely flat up to some 30°. Thus, porphyrin dimers **1-n** should present in solution a wide range of torsional angles at ambient temperature.

The energy level splittings V_O and V_U for the various **1-2(θ)** conformations are given in Figure 3.6. As expected, the largest interaction between the porphyrin units is obtained for θ = 0°; the splitting energies V_U and V_O reach 0.33 and 0.46 eV for θ = 0° and vanish as θ reaches 90°. The Q- and B-bands are most stabilized for θ = 0°, 1.74 and 2.62 eV at the INDO/S level (Table 1); in this conformation, the TPA cross-section occurs at the lowest energy (2.99 eV) and is calculated to reach 4.0×10^3 GM at the INDO/MRDCI level (Figure 3.6, bottom). The calculated values agree very well with the experimental data: Q- and B-bands of 1.77 and 2.57 eV, TPA energy and cross-sections of 2.99 eV and 5,500 GM.[15] We have also considered compound **1** in which **n** = 0, that is the two porphyrin moieties are directly linked to one another. In that case, a DFT geometry optimization indicates that the rings are perpendicular to one another. As a result, the V_O and V_U couplings become vanishingly small and we calculate optical absorption energies (INDO/S: Q-band at 1.86 eV) and TPA cross-sections (INDO/MRDCI: $\delta = 1.0 \times 10^2$ GM) very similar to the monomer case; these

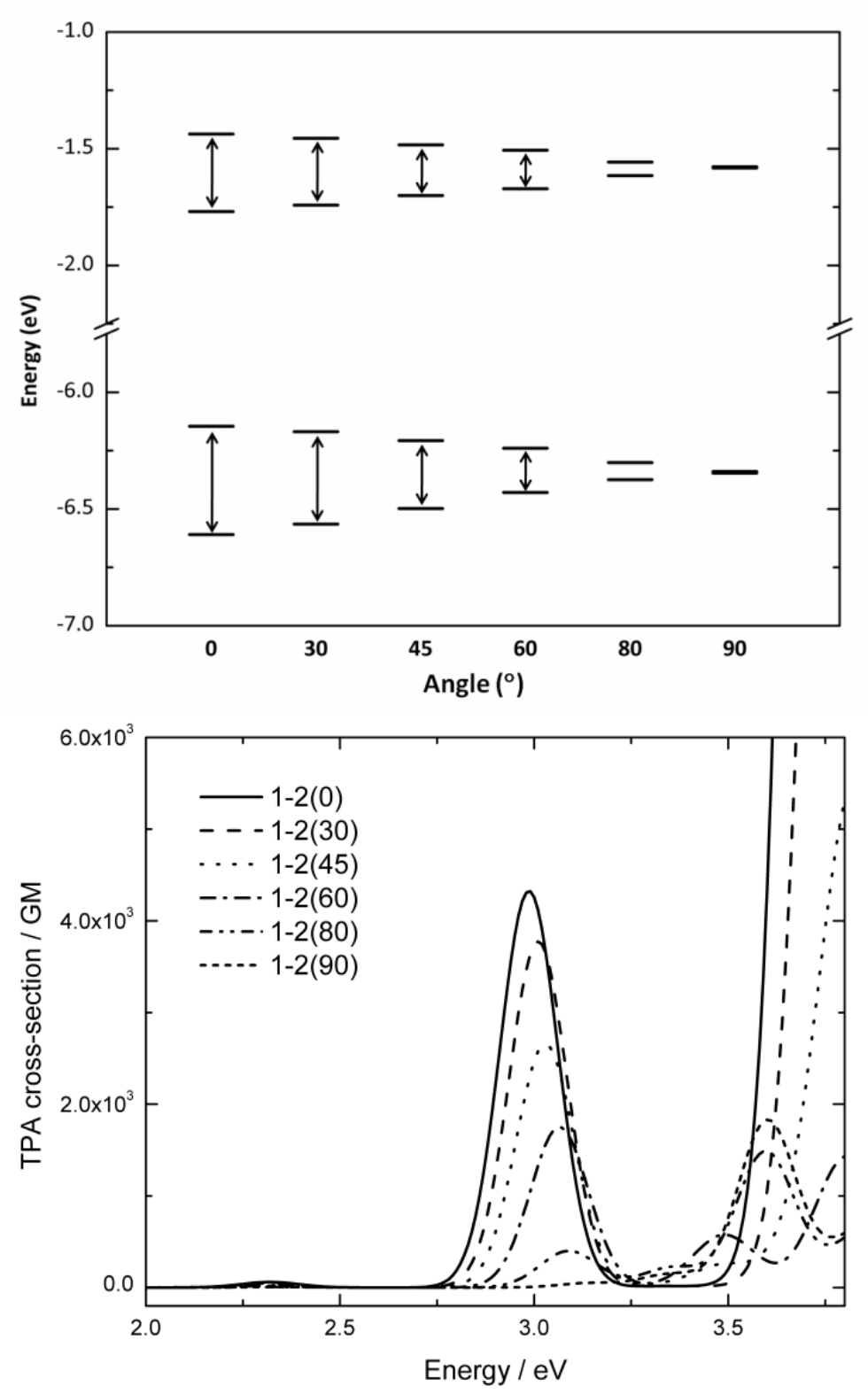

Figure 3.6 Energy splittings V_U and V_O (top) and TPA spectra (bottom) for compound **1-2** as a function of the torsional angle (θ) between the porphyrin units, computed at the INDO/S and INDO/MRDCI-SOS levels, respectively.

values are in good agreement with the experimental data reported by Ahn *et al*.[20]

Despite the presence of the central thiophene or anthracene moieties, compounds **2** and **3** can be classified into the same group as the **1-n** compounds from an FMO analysis. In these compounds, the four-orbital model remains valid, though the levels are shifted due to the central groups. The V_O and V_U values (~ 0.34 — 0.4 eV and ~0.2 eV, respectively) are small and similar to these in **1-3** and **1-4** (Table 2); the Q-bands of **2** and **3** also have the same energies as in the **1-n** series (**2**: 1.81 eV, **3**: 1.81 eV) at the INDO/S level. The OPA and TPA results present similar trends as in the **1-n** series (**2**: 3.11 eV and 5.4×10^3 GM, **3**: 3.01 eV and 4.3×10^3 GM) at the INDO/MRDCI level.

Compound **4** is interesting since it provides for a strong direct coupling between the porphyrin units with the two β-β linkages forcing the dimer to be coplanar. As a consequence, the V_O and V_U splittings are large (1.15 and 1.26 eV, respectively) and the lowest OPA-active state energy comes down to 1.38 eV, in good agreement with the experimental value in the 1.1—1.2 eV range (see Table 2). However, the TPA cross-sections are predicted to be rather small and the values do not exceed 500 GM before the photon energy reaches the double-resonance enhancement range.

In their experimental work, Ahrn *et al*. reported remarkably large TPA cross-section values for **4** (11,900 GM at 2.07 eV).[20] The fundamental photon

frequency is then so close to the Q-band energy that one might suspect strong contributions from double-resonance effects/one-photon absorption (note that the authors of Ref. 20 did not report the intensity dependence of their data to verify the cubic response of the Z-scans, a procedure suggested by Sheik-Bahae *et al*.[43, 44]). Thus, the quantum-chemical calculations underline that a strong coupling between the porphyrins shifts the OPA- and TPA-active state energies in such a way that double-resonance effects become important, which tends to reduce the usefulness of compounds with such characteristics for TPA applications.

In the case of compounds **1** — **4**, the FMO's are thus built from a straight extension of Gouterman's model (Figure 3.3). We now turn to a discussion of compounds **5** — **7**, where the LUMO has a strong bridge character (Figure 3.4).

3.4 Porphyrin dimers 5–7

The porphyrin dimer carbocation, **6**, shows an intense near-IR (NIR) absorption maximum at 1.00 eV[21] and the porphyrin–perylene diimide derivative, **7**, has a broad peak maximum between 1.3–1.7 eV.[18] Their TPA cross-sections are large in the NIR range (**6**: 3,100 GM at 1.60 eV and **7**: 2,000–7,000 GM at 2.07–2.33 eV; these energies refer to the energies of the TPA-active states).[18] Although these cross-sections were measured at a fundamental photon energy approaching the absorption maxima ($E_{TPA}/2 - E_{OPA\text{-}edge}$, **6**: 0.20 eV and **7**: 0.08 – 0.21 eV),[21] their nonlinear spectra were confirmed to be independent from

double-resonance effects. Note that while the carbocation compound **6** which has been experimentally characterized is based on Ni-porphyrins, we have also calculated the optical properties of its Zn analog in order to make an easier comparison with all the other compounds in this work. In fact, as seen from Table 2, the nature of the metal does not alter significantly the electronic and optical properties we are interested in here. The appearance of a bridge-based LUMO in **5**–**7** has important consequences: (i) It reduces the optical gap and shifts the major absorption peaks to lower energies. Depending on the electronic coupling strength between the central unit and the porphyrin moieties, there appears a from occupied levels to the LUMO can mix with other transitions to change the broad low-energy band, akin to a charge-transfer transition. (ii) The transitions

Table 3.2 Electronic couplings V_U and V_O computed at the INDO/S level, lowest optically allowed transition energies E_{OPA} computed at the INDO/S and INDO/MRDCI levels, and TPA-active state energies with "pure" TPA cross-sections at the INDO/MRDCI-SOS level **1-0** and planar **2** – **7**.

	INDO/S		Lowest E_{OPA} (eV)			INDO/MRDCI	
	V_U (eV)	V_O (eV)	INDO/S	INDO/MRDCI	Exp.	E_{TPA} (eV)	δ_{sos} ($\times 10^3$ GM)
1-0	0.00	0.00	1.86	2.24	2.11[a]	3.64	0.1
1-1	0.47	0.59	1.71	2.07	1.74[b]	2.92	2.2
1-2	0.33	0.46	1.74	2.10	1.77[b]	2.99	4.0
1-3	0.22	0.35	1.76	2.12	NA	3.07	3.7
1-4	0.15	0.28	1.78	2.15	1.85[c]	3.21	7.1
1-6	0.09	0.19	1.79	2.17	NA	3.29/3.41	1.6/11
2	0.19	0.40	1.81	2.16	1.74 [b]	3.11	5.4
3	0.17	0.34	1.81	2.19	1.71 [b]	3.01	4.3
4	1.26	1.15	1.38	1.57	1.1 – 1.2 [a]	2.48/2.89	0.2/0.4
5	0.31	0.60	1.53	1.07	NA	2.31	7.4
6	0.34	0.61	1.49	1.03	1[d]	2.25	11
7	0.06	0.12	1.73	2.01	1.38 – 1.65[e]	2.58	3.5

[a] Ref. 20. [b] Refs. 14 and 15. [c] Refs. 14, 15 and 22. [d] Ref. 21. [e] Ref. 18.

peak positions and/or shapes, including those of the OPA- and TPA-active states. Electron correlation effects thus play a significant role.

From the V_U and V_O values and the energy shift of MO's originating from the LUMO of the bridge, it appears that the electronic couplings between the porphyrin moieties and between the porphyrin V_O and the bridge are both much stronger in **5** and **6** than in **7**. This effect translates into markedly different absorption spectra in **6** and **7**: there is an intense B-band-like peak in **7**, while the lowest peak has a higher intensity than that around the B-band energy range in **6**.[18, 21]

3.5 Conclusions

In this chapter, we sought to establish structure-properties relationships in porphyrin dimers. The nature of the bridge between the porphyrin units in the dimers tunes the electronic coupling strength, which in turn determines the splitting of the frontier molecular orbital levels and the excited-state energies. The respective locations of the OPA/TPA-active states control the nonlinear optical properties of the dimers and lead to either double resonance-enhanced or "pure" TPA cross-sections. The TPA-active state energies in **1—3** and **7** are stabilized and exhibit significant cross-sections since the electronic coupling strength between the two porphyrin moieties are significant.

When there is weak interaction between the porphyrin end groups, such as in the case of the non-planar dimers **1-0** and **1-2(90)** or dimers with long π-bridges such as **1-6**, the TPA cross-sections are mainly due to double-resonance effects. The same conclusion actually holds in porphyrin dimers with very strong coupling, **4**–**7**; the TPA-active state energy then appears in the double-resonance energy range, so that significant contamination of the TPA from double-resonance effects is expected.

The results of these calculations have thus allowed us to underline the relationship between the electronic coupling strength and the TPA properties in porphyrin dimers.

REFERENCES

(1) Albota, M.; Beljonne, D.; Brédas, J.-L.; Ehrlich, J. E.; Fu, J.-Y.; Heikal, A. A.; Hess, S. E.; Kogej, T.; Levin, M. D.; Marder, S. R.; McCord-Maughon, D.; Perry, J. W.; Röckel, H.; Rumi, M.; Subramaniam, G.; Webb, W. W.; Wu, X.-L.; Xu, C. *Science* **1998**, *281*, 1653.

(2) Chung, S. J.; Rumi, M.; Alain, V.; Barlow, S.; Perry, J. W.; Marder, S. R. *J. Am. Chem. Soc.* **2005**, *127*, 10844.

(3) Lin, T.-C.; Chung, S.-J.; Kim, K.-S.; Wang, X.; He, G. S.; Swiatkiewicz, J.; Pudavar, H. E.; Prasad, P. N. *Adv. Polym. Sci.* **2003**, *161*, 157.

(4) Pond, S. J. K.; Rumi, M.; Levin, M. D.; Parker, T. C.; Beljonne, D.; Day, M. W.; Bredas, J. L.; Marder, S. R.; Perry, J. W. *J. Phys. Chem. A* **2002**, *106*, 11470.

(5) Strehmel, B.; Sarker, A. M.; Detert, H. *ChemPhysChem* **2003**, *4*, 249.

(6) Marder, S. R.; Brédas, J. L.; Perry, J. W. *MRS Bulletin* **2007**, *32*, 561.

(7) Pawlicki, M.; Collins, H. A.; Denning, R. G.; Anderson, H. L. *Angew. Chem., Int. Ed.* **2009**, *in press*.

(8) Kim, H.-S.; Kim, C.-H.; Ha, C.-S.; Lee, J.-K. *Synth. Met.* **2001**, *117*, 289.

(9) Campbell, W. M.; Jolley, K. W.; Wagner, P.; Wagner, K.; Walsh, P. J.; Gordon, K. C.; Schmidt-Mende, L.; Nazeeruddin, M. K.; Wang, Q.; Graetzel, M.; Officer, D. L. *J. Phys. Chem. C* **2007**, *111*, 11760.

(10) Savenije, T. J.; Goossens, A. *Phys. Rev. B* **2001**, *64*, 115323.

(11) Calvete, M.; Ying Yang, G.; Hanack, M. *Synth. Met.* **2004**, *141*, 231.

(12) Damasio, H.; Grabowski, T.; Frank, R.; Galaburda, A. M.; Damasio, A. R. *Science* **1994**, *264*, 1102.

(13) Anderson, H. L. *Chem. Commun.* **1999**, 2323.

(14) Drobizhev, M.; Stepanenko, Y.; Dzenis, Y.; Karotki, A.; Rebane, A.; Taylor, P. N.; Anderson, H. L. *J. Am. Chem. Soc.* **2004**, *126*, 15352.

(15) Drobizhev, M.; Stepanenko, Y.; Dzenis, Y.; Karotki, A.; Rebane, A.; Taylor, P. N.; Anderson, H. L. *J. Phys. Chem. B* **2005**, *109*, 7223.

(16) Gouterman, M.; Wagnière, G. H.; Snyder, L. C. *J. Mol. Spect.* **1963**, *11*, 108.

(17) Du, H.; Fuh, R. A.; Li, J.; Corkan, A.; Lindsey, J. S. *Photochemistry and Photobiology* **1998**, *68*, 141.

(18) Odom, S. A.; Kelley, R. F.; Ohira, S.; Padilha, L. A.; Huang, C.; Webster, S.; Coropceanu, V.; Barlow, S.; Stryland, E. V.; Brédas, J.-L.; Anderson, H. L.; Wasielewski, M. R.; Marder, S. R. *J. Am. Chem. Soc.* **in preparation**.

(19) Dirk, C. W.; Cheng, L.-T.; Kuzyk, M. G. *International Journal of Quantum Chemistry* **1992**, *43*, 27.

(20) Ahn, T. K.; Kim, K. S.; Kim, D. Y.; Noh, S. B.; Aratani, N.; Ikeda, C.; Osuka, A.; Kim, D. *J. Am. Chem. Soc.* **2006**, *128*, 1700.

(21) Thorley, K. J.; Hales, J. M.; Anderson, H. L.; Perry, J. W. *Angew. Chem., Int. Ed.* **2008**, *9999*, NA.

(22) Aimi, J.; Nagamine, Y.; Tsuda, A.; Muranaka, A.; Uchiyama, M.; Aida, T. *Angew. Chem., Int. Ed.* **2008**, *47*, 5096.

(23) Kohler, B. E. *J. Chem. Phys.* **1990**, *93*, 5838.

(24) Hudson, B. S.; Kohler, B. E.; K. Schulten *Excited States* Academic Press: New York, 1982; Vol. 6.

(25) Dreuw, A.; Head-Gordon, M. *J. Am. Chem. Soc.* **2004**, *126*, 4007.

(26) Magyar, R. J.; Tretiak, S. *J. Chem. Theory Comput.* **2007**, *3*, 976.

(27) Winters, M. U.; Karnbratt, J.; Eng, M.; Wilson, C. J.; Anderson, H. L.; Albinsson, B. *J. Phys. Chem. C* **2007**, *111*, 7192.

(28) Sheik-bahae, M.; Said, A. A.; Van Stryland, E. W. *Opt. Lett.* **1989**, *14*, 955.

(29) Sheik-bahae, M.; Said, A. A.; Wei, T.-H.; Hagan, D. J.; Van Stryland, E. W. *IEEE J. Quantum. Electron.* **1990**, *26*, 760.

CHAPTER 4:

Electronic and vibronic contributions to two-photon absorption in donor-acceptor-donor squaraine chromophores

Objective

Many squaraines have been observed to exhibit two-photon absorption at transition energies close to those of the lowest-energy one-photon electronic transitions. Here, we have sought to elucidate the electronic and vibronic contributions to these low-energy two-photon absorptions by performing correlated quantum-chemical calculations on model chromophores which differ in their terminal donor groups (diarylaminothienyl, indolenylidenemethyl, dimethylaminopolyenyl, or 4-(dimethylamino)phenylpolyenyl). For squaraines with diarylaminothienyl and dimethylaminopolyenyl donors and for the longer examples of 4-(dimethylamino)phenylpolyenyl donors, the calculated energies of the lowest TPA active states approach those of the lowest energy one-photon (OPA) active ($1B_u$) states. This is consistent with the existence of purely electronic channels for low-energy TPA in these types of chromophores. On the other hand, for all squaraines containing indolinylidenemethyl donors, the calculations indicate that there are no low-lying electronic states of appropriate symmetry for TPA. Actually, we have found that the lowest energy TPA transitions can be explained through coupling of the OPA-active $1B_u$ state with b_u vibrational modes. Via implementation of Herzberg-Teller theory, we were able to identify the vibrational modes responsible for the low-energy TPA absorption

peak and to reproduce, at least qualitatively, the experimental TPA spectra of several squaraines of this type.

4.1 Introduction

High TPA cross-sections have been observed for chromophores with various structural motifs, including donor-acceptor-donor (D-A-D) conjugated chromophores. Among this class of chromophores, the linear and nonlinear optical properties of D-A-D squaraines (also known as squarylium dyes) consisting of two electron-donor terminal groups (D) and a central electron-poor 1,3-disubstituted C_4O_2-unit (A) have been extensively studied because of their narrow and intense one-photon absorption (OPA) bands and large real and imaginary third-order non-linear optical (NLO) responses.[1-15]

High two-photon absorption (TPA) cross sections ranging from 750[1] to 33,000[2] GM have been measured at photon energies close to the one-photon absorption edge for a variety of squaraines. Assuming centrosymmetric conformations, this corresponds to excitation to a singlet A_g state referred to here as peak 3 (see Figure 4.1 for general peak labeling). Even though, as discussed in the results and discussion section, squaraine compounds can adopt several non-centrosymmetric conformations, the behavior of their excited states typically remains strongly reminiscent of the properties of strictly *ungerade* and *gerade* states found in the centrosymmetric *conformers;* this is particularly true for extended molecules. We have, therefore, referred to all excited states assuming

inversion symmetry, i.e., as (one-photon active) B_u or (two-photon active) A_g states, even if the structure of a particular conformer deviates from centrosymmetry. Some of these cross-sections are remarkably large, even when normalized for the number of π-electrons in the molecules, and originate largely from resonance enhancement, *i.e.*, from the appropriate photon energy closely approaching the one-photon transition energy.[2] It is worth pointing out that is possible to observe the effects of resonance enhancement, *i.e*., to probe TPA with excitation energies very close to the OPA transition, due to the remarkably sharp OPA absorption edge. However, in squaraines with indolinylidenemethyl-donor groups, in addition to the strong high-energy TPA state, there is evidence for another TPA state (referred to here as peak 2) at state energy similar to that of the lowest energy OPA transition; this lower energy TPA then occurs with maxima in the near-infrared spectral region at photon wavelengths of 1.1-1.4 μm, with cross sections ranging from 45[3] to 500[1] GM. Recently, we have also found a low-energy TPA-active state at energy similar to the lowest OPA-active state in an example of a squaraine in which the donors are substituted pyrroles with extended conjugation, with cross-sections of 800 and 1600 GM at photon wavelengths of 1.3 and 1.5 μm, respectively.[2] Despite the cross-section of peak 2 typically being considerably lower than that of the near-resonant state (peak 3), peak 2 can be of importance for optoelectronic applications, since, depending on the molecular structure, this absorption is located close to or within the telecommunications band of the near-infrared (1.30-1.55 μm). TPA in this region can potentially be exploited for applications such as

all-optical beam stabilization and dynamic range compression, while the presence of a TPA-allowed state close to this region will affect the telecommunications-band dispersion of the real part of the third-order polarizability γ, which can be exploited for all-optical switching.

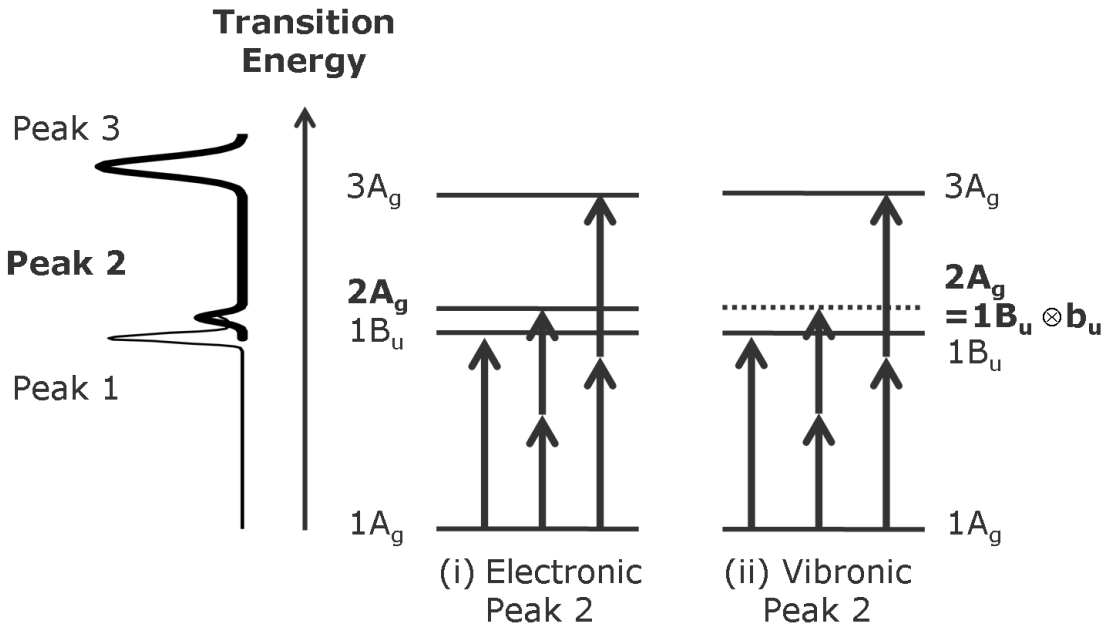

Figure 4.1. Illustration of the one-photon (light line) and two-photon (bold line) absorption processes in squaraines. Left: Sketch of the absorption spectra of squaraines. Middle: Scenario (i), in which peak 2 is purely electronic. Right: Scenario (ii), in which peak 2 has the same electronic nature as the $1B_u$ state.

In order to take full advantage of such TPA in the near–IR region, it is important to better understand the origin of the associated excited state. However, previous quantum-chemical studies on such compounds have considered only purely electronic channels for TPA and have neither addressed the nature of this state in detail nor been successful in reproducing the small energetic separations observed between peak 1 (the OPA peak) and peak 2, *i.e.*, in general < 0.2 eV.[4-7]

Rather than assigning peak 2 to a low-lying electronic state, Scherer *et al*. proposed an alternative origin for peak 2,[1] suggesting the possibility of vibronic coupling between the first excited electronic $1B_u$ state and vibrational modes of b_u symmetry. Furthermore, the presence of both centrosymmetric and non-centrosymmetric conformational isomers, which is supported by NMR experiments for certain squaraines,[8,9] has also been put forward as an explanation for the closely spaced peaks 1 and 2;[7,8] in this case, peak 2 would primarily originate from the lowest electronic excited state, *i.e*., a strongly OPA-active state, of the non-*centrosymmetric* conformers. In such non-centrosymmetric conformers, the OPA-active state is not of strict *ungerade* (*i.e.*, B_u) character and can, therefore, in principle, exhibit a non-zero TPA cross-section due to TPA through purely electronic channels. The observed energetic offset between the OPA peak 1 and TPA peak 2 signals could then potentially be attributed to somewhat different OPA state energies for centrosymmetric and non-centrosymmetric conformers. Moreover, the TPA maximum is typically shifted towards higher energies with respect to the corresponding OPA maximum, since Franck-Condon coupling can redistribute TPA cross-section from the (0-0) into the (0-1) vibrational transition.[10]

Thus, there can be three possible origins for the lowest-energy TPA-active state in squaraines: (i) peak 2 is primarily of electronic nature and due to TPA into the lowest OPA excited states of noncentrosymmetric conformers; (ii) peak 2 is primarily electronic in nature and arises from a TPA-allowed $2A_g$ state close in

energy to the OPA-allowed $1B_u$; or (iii) the state corresponding to peak 2 has the same electronic nature as the OPA $1B_u$ state, but acquires cross-section due to vibronic coupling (non-zero coupling of $1B_u$ state to higher-lying A_g states (Figure 4.1) via b_u modes). In the third scenario, the electronic sum-over-states model must be extended to account for vibronic coupling. In the linear coupling regime, this can be achieved by applying Herzberg-Teller (HT) theory.[11]

Model squaraine compounds. To ease the systematic study of their TPA spectra, the squaraines we have studied have been classified into three groups depending on the nature of their terminal groups (Figure 4.2): (i) group I consists of squaraines with diarylaminothienyl donors, new compound **2** and model compound **1**; (ii) group II consists of squaraines **3**-**5** (**4** being used as a model for **5**), in which the *N*-alkylation of indolinylidenemethyl donors is varied; (iii) group III consists of 6 and new compounds **7-8**, in which the role of attaching additional π-conjugated groups to the 5-position of indolinylidenemethyl donors is investigated. On the theoretical side, we also consider the hypothetical compounds of group IV, in which the effect of increasing the π-conjugation length between the terminal donor and central acceptor units are studied in the model dimethylaminopolyenyl and 4-(dimethylamino)phenylpolyenyl-substituted squaraine series **9-n** and **10-n**. The TPA spectra for **2**, **7**, **8**, **3**, **4**, **5**, and **6** can be found in the literature.[1,3,5,17]

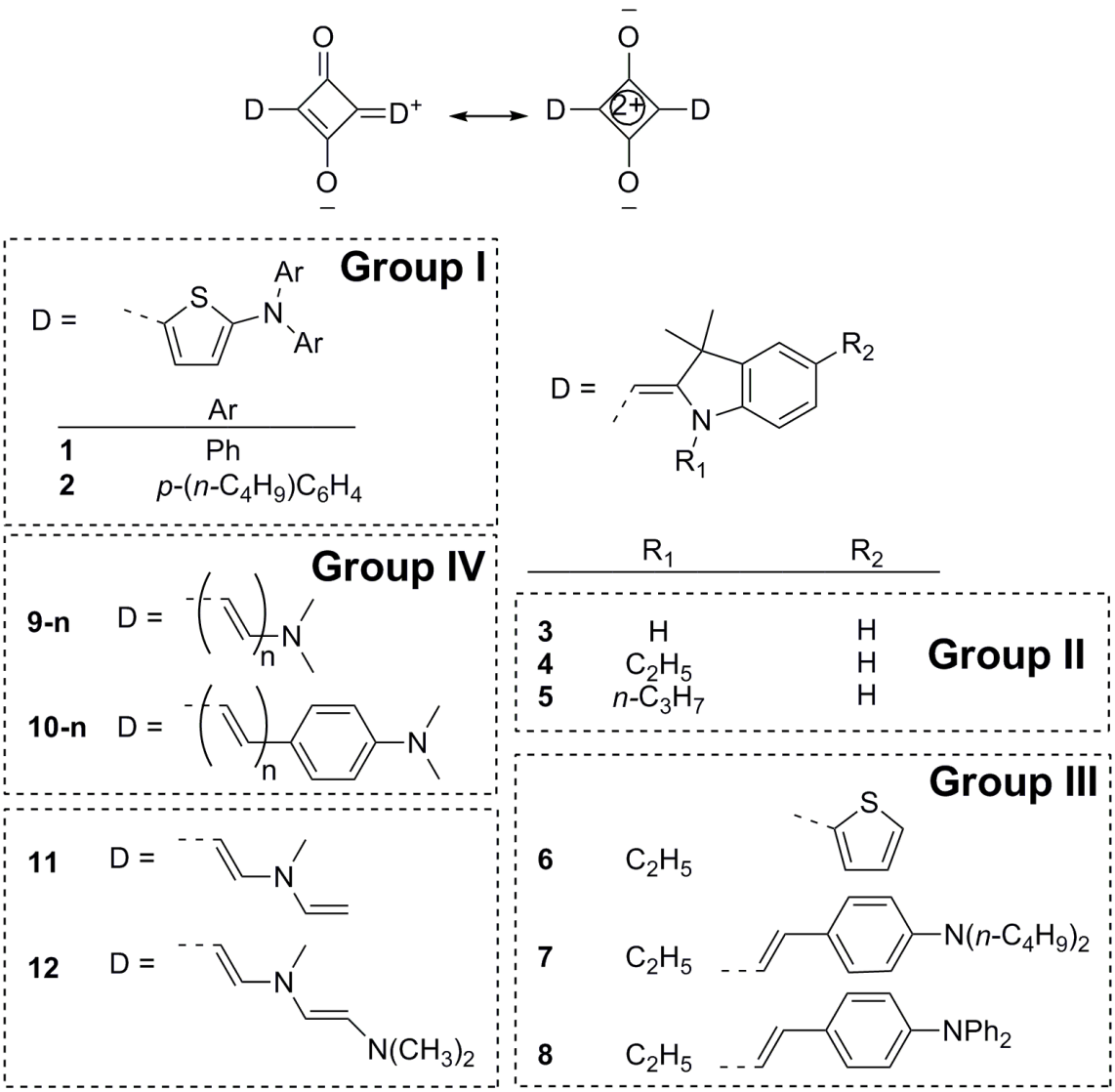

Figure 4.2. Chemical structure of the terminal groups D in the D-π-A-π-D squaraines considered in this study. (i) Group I: Squaraines with diarylaminothienyl donors **2** and model compound **1**. (ii) Group II: Squaraines **3-5** (**4** being used as a model for **5**), in which the N-alkylation of indolinylidenemethyl donors is varied. (iii) Group III: Squaraines **6-8**, in which the role of attaching additional p-conjugated groups to the 5-positionof indolinylidenemethyl donors is investigated. (iv) Group IV: Hypothetical model squaraine series **9-n** and **10-n** (dimethylaminopolyenyl and 4-(dimethylamino)-phenylpolyenely-substituted), in which the effect of increasing the π-conjugation lengths with (**n** = 1−4) between the terminal donor and central acceptor units are studied.

Our discussion is structured as follows. We first discribe the results of computational studies on the effect of molecular conformation on the TPA spectra, focussing on the possibility of TPA into the lowest-lying OPA state of non-centrosymmetric conformers (4.2.1). We turn next to a theoretical analysis of the possibility of low-lying electronically-allowed TPA states in the different types of squaraines under consideration (4.2.2). Finally, we investigate how vibronic coupling of the lowest OPA state to antisymmetric vibrational modes can give rise to low-energy TPA in squaraines with indolinylidenemethyl donors (4.2.3).

4.2 Effect of coexistence of different conformers

We first studied the effect of molecular (centrosymmetric and non-centrosymmetric) conformations on the TPA spectra of squaraines, in order to investigate the likelihood that the experimentally observed lowest lying two-photon active peaks, *i.e*. peak 2, could be attributed to purely electronic TPA into the lowest lying one-photon state of non-centrosymmetric conformers. Roughly planar geometries were observed in NMR experiments by Dirk *et al*.[8] as well as in crystal structures obtained by Kobayashi *et al*.[12] In the case of conformation i of squaraine **3**, semiempirical INDO/MRDCI calculations on the isolated molecule indicate that the conformation with a twist of 10^{o} is 0.12 eV higher in energy than the fully planar conformation, suggesting the existence of mostly planar structures. Among the investigated squaraines, we found that, in general, the approximately planar C_{2h} / C_i centrosymmetric (Figure 4.3, left side, i and iii) and the C_{2v} / C_2 non-centrosymmetric conformers (Figure 4.3, right side, ii and iv) are

more stable relative to conformations with a twisted π-systems and are, thus, likely to predominate at room temperature. Among squaraines **1** (used as a model for experimentally studied compound **2**), **3** and **4**, it is only in the case of **3** that the non-centrosymmetric conformation (**3"** in Figure 4.4, conformation ii in Figure 4.3) is energetically more favorable than the centrosymmetric conformer (**3'** in Figure 4.4, conformation i in Figure 4.3); the energy difference between the **3'** and **3"** isomers calculated at the B3LYP/SV(P) level is 0.06 eV (equivalent to ~700 K). These results are in agreement with those of the theoretical and experimental work of Dirk *et. al*,[8] in which the larger stability of **3"** compared to **3'** had been attributed to the formation of energetically more stable hydrogen bonds in **3"** between both of the indole-ring nitrogen atoms and the same carbonyl oxygen atom of the central unit.

In the case of squaraines **4'** (centrosymmetric) and **4"** (non-centrosymmetric), the possibility for strong hydrogen bonding is removed, while steric hindrance effects between donor and acceptor groups increase as the hydrogen atoms are replaced by alkyl groups. As a result, **4'** is more stable than **4"** by 0.22 eV (equivalent to ~2,500 K). On the other hand, the energy difference between the two isomers of squaraine **1** was computed to be negligibly small. Although our calculations indicate that the non-centrosymmetric conformation iv and centrosymmetric conformation iii (Figure 4.3) have slightly higher energies compared to conformations ii and i for squaraines **3** and **4**, respectively, the possibility of isomeric mixtures (i and iii or ii and iv) cannot be completely ruled

out in solution at ambient temperature. Thus, assuming that solvation does not substantially affect the relative energies of the conformers, squaraines **1**, **3**, and **4** are predicted to be present at ambient temperature as a mixture: *i.e.*, **3** predominantly as C_{2v} / C_2 conformer (mostly ii and probably iv), **4** overwhelmingly as the C_{2h} / C_i conformer (mostly i and probably iii), and **1** as a mixture in which no particular conformer is dominant. We now discuss the electronic structures and TPA activity for these two conformers in squaraines **1**, **3**, and **4**.

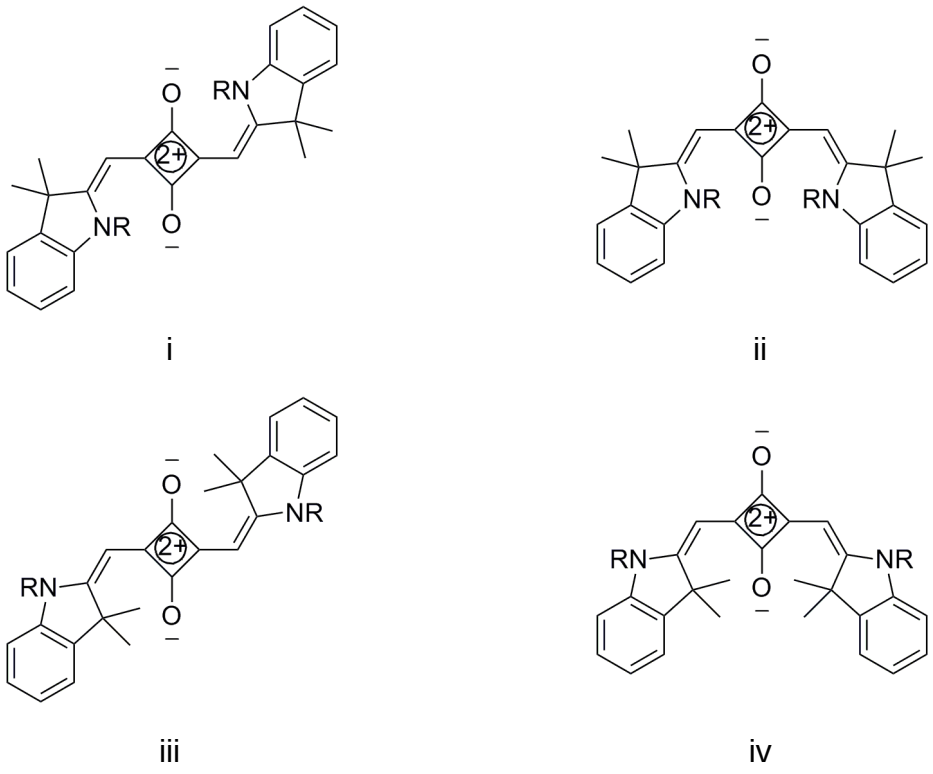

Figure 4.3. Four representive conformational isomers of squaraines in group II.

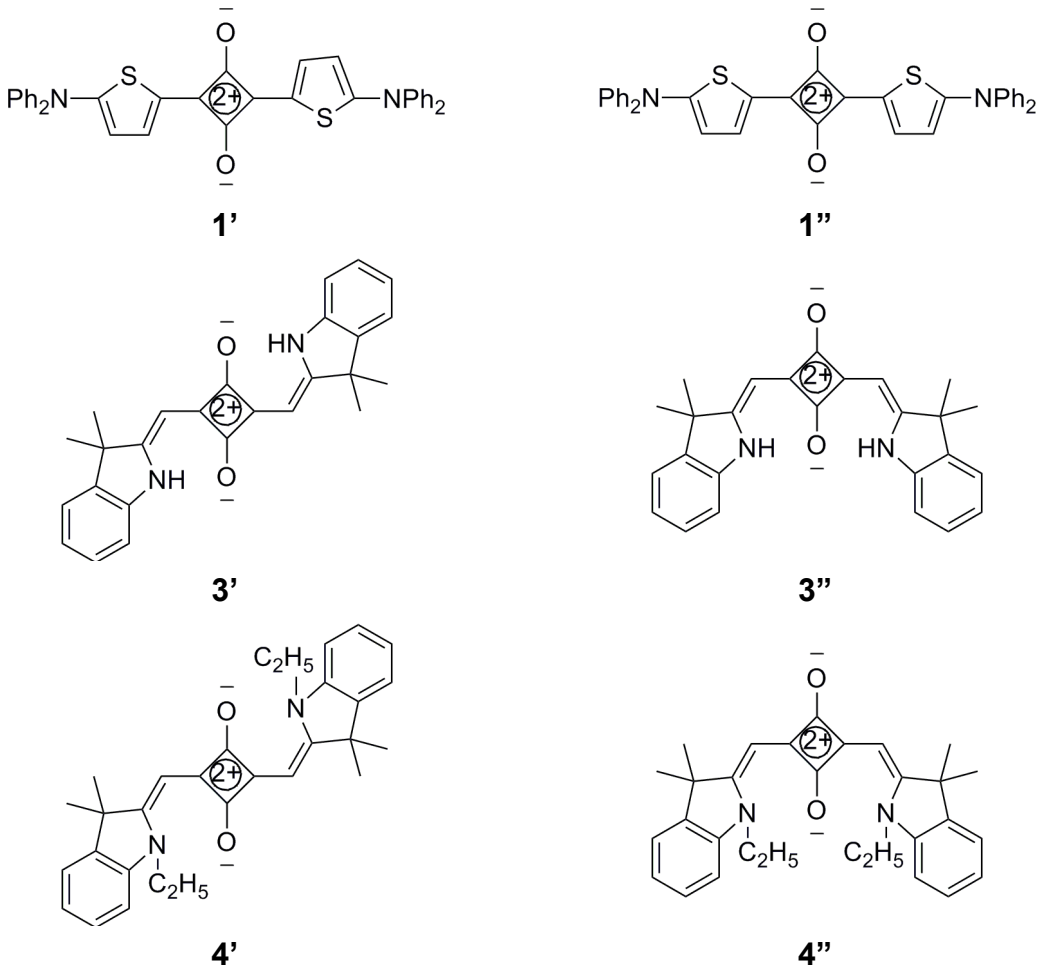

Figure 4.4. Approximate representative conformations of **1**, **3**, and **4**.

INDO/MRDCIS calculations suggest very similar OPA- and TPA spectra for both centro- and non-centrosymmetric conformers of **1**, **3**, and **4** (Table 4.1). This is true irrespective of which isomers (i, ii, iii, and iv in Figure 4.3) are considered (Table 4.2). In particular, the TPA cross-section of the lowest OPA-active state, S_1, remains negligibly small (< 4 GM); therefore, purely electronic TPA channels into S_1 in the non-centrosymmetric conformers can be ruled out as a possible origin of peak 2. By taking squaraine conformers **3'** and **3''** as representative examples, we can distinguish two reasons for this absence of TPA-activity for the

lowest OPA state, despite the lack of an inversion center. Since **3"** has a non-zero static dipole moment, change of this dipole moment upon excitation to the one-photon state could, in principle, give rise to a non-zero TPA cross-section. However, the excited state in both squaraine conformers **3'** and **3"** can be described principally as arising from a HOMO-LUMO transition. The HOMO and LUMO of the molecule (Figure 4.5) indicate rather little change in the spatial extent of the electron-density distribution and, as a result, the change in static dipole moment between the two states ($\Delta\mu_{01}$) is also quite small (~0.1D) while the corresponding transition dipole moment (M_{01}) is large (~10D). Considering the relation between $\Delta\mu_{01}$, M_{01} and TPA cross-section δ according to the two-state model for TPA into the $1B_u$ state,[13-16] $\delta \propto \frac{\Delta\mu_{01}^2 M_{01}^2}{(E_{01}-\hbar\omega)^2}$ (where $\hbar\boldsymbol{\omega}$ is the fundamental photon energy), it can be easily understood why a small $\Delta\mu_{01}$ would result in a very small TPA cross-section for the first excited state of squaraine **3"**.

Table 4.1. Electronic and optical properties of **1**, **3** and **4** calculated with SOS// INDO/MRDCI.

	1'					1"				
N	*E* (eV)	*f*	*δ* (GM)	μ_{0n}	μ_{1n}	*E* (eV)	*f*	*δ* (GM)	μ_{0n}	μ_{1n}
1	1.76	1.4	2	14.5	---	1.76	1.41	0	14.5	---
2	2.02	0	104	0.0	4.1	2.02	0	103	0.0	4.1
3	2.68	0.06	13	2.4	0.7	2.68	0.06	0	2.4	0
4	3.03	0.03	33,526	1.6	14.2	3.03	0	34,962	0.0	14.4
5	3.13	0	409	0.0	1.2	3.14	0	395	0.0	1.1
	3'					3"				
N	*E* (eV)	*f*	*δ* (GM)	μ_{0n}	μ_{1n}	*E* (eV)	*f*	*δ* (GM)	μ_{0n}	μ_{1n}
1	1.8	0.8	3	10.8	---	1.9	1.12	0	12.5	-
2	2.84	0.04	553	1.9	4.1	2.89	0	983	0.0	5.5
3	3.01	0	0	0.0	0	2.92	0	0	0.0	0.1
4	3.24	0.07	5,708	2.4	5.4	3.13	0	0	0.0	0
5	3.34	0	0	0.0	0	3.34	0	11,192	0.0	7.9
	4'					4"				
n	*E* (eV)	*f*	*δ* (GM)	μ_{0n}	μ_{1n}	*E* (eV)	*f*	*δ* (GM)	μ_{0n}	μ_{1n}
1	1.8	1.04	2	12.3	---	1.84	1.19	0	13.0	---
2	2.8	0.01	634	1.0	4	2.87	0	1,376	0.0	5.6
3	2.89	0.01	559	1.0	3.2	2.97	0	1	0.0	0.2
4	3.14	0.01	1,284	0.9	2.8	3.17	0	0	0.0	0
5	3.27	0.04	13,198	1.8	6.3	3.25	0	15,653	0.0	8.4

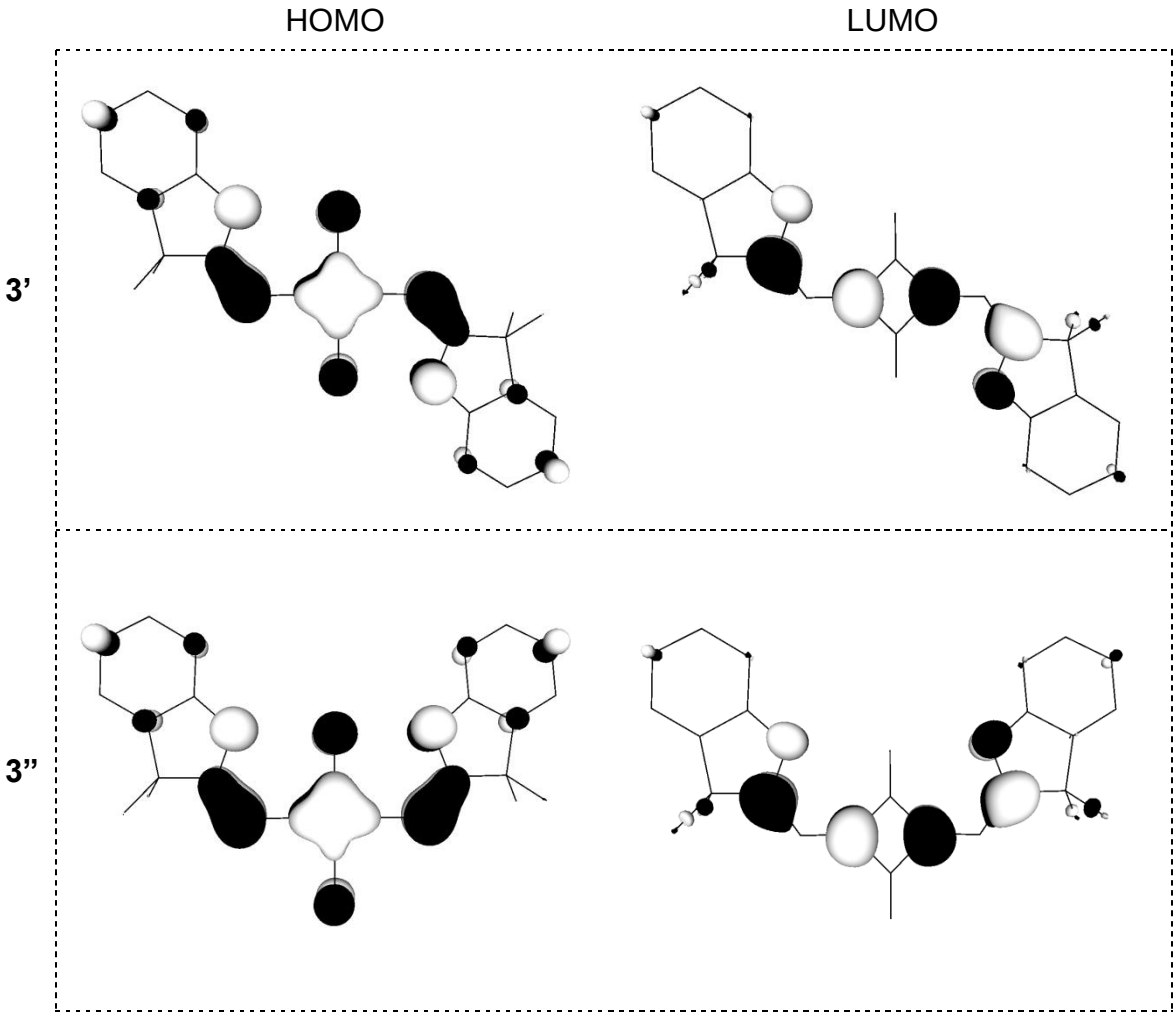

Figure 4.5. Representation of the HOMO (highest occupied molecular orbital) and LUMO (lowest unoccupied molecular orbital) wavefunctions for two conformations of 3, calculated at the DFT-B3LYP/SV(P) level.

Table 4.2. Electronic and optical properties of **4**-i, ii, iii and iv (from top left to bottom right).

n	*E* (eV)	*f*	*δ* (GM)	μ_{0n}	μ_{1n}
1	1.84	1.19	0	13	---
2	2.87	0	1,376	0	5.6
3	2.97	0	1	0	0.2
4	3.17	0	0	0	0
5	3.25	0	15,653	0	8.4

E (eV)	*f*	*δ* (GM)	μ_{0n}	μ_{1n}
1.8	1.04	2	12.3	---
2.8	0.01	634	1	4
2.89	0.01	559	1	3.2
3.14	0.01	1,284	0.9	2.8
3.27	0.04	13,198	1.8	6.3

n	*E* (eV)	*f*	*δ* (GM)	μ_{0n}	μ_{1n}
1	1.96	1.44	0	13.9	---
2	3.13	0	990	0.1	4.1
3	3.15	0	85	0	1.2
4	3.36	0.003	0	0.5	0.1
5	3.78	0	187962	0.1	8.3

E (eV)	*f*	*δ* (GM)	μ_{0n}	μ_{1n}
1.97	1.383	0	13.6	---
3.03	0	0	0.1	0
3.17	0.012	1066	1	4.1
3.42	0.002	566	0.4	1.8
3.78	0.032	182658	1.5	8.6

4.3 Possible Electronic Origin of Lowest TPA State (Peak 2)

In the previous section, we demonstrated that non-centrosymmetric conformers do not exhibit significant TPA cross-sections into S_1, the lowest energy OPA state, through purely electronic channels. Considering the close similarity of the OPA and TPA spectra calculated for centro- and non-centrosymmetric conformers, we will henceforth restrict our discussion to the centrosymmetric conformers. In the context of having multiple species (such as conformers) possibly simultaneously present, it is worth noting that the existence of broken-symmetry structures (in either ground or first excited states), analogous to those seen in a few cyanines, can be ruled out due to the absence of substantial solvatochromism in absorption or fluorescence spectra.[10]

To find out whether structural modifications of the terminal donor group can result in a TPA-active electronic state at the position of peak 2, we now turn to a systematic study of the OPA and TPA spectra of squaraines belonging to groups I, II, III, and IV. As in the previous section, we use squaraine **1** to model new compound **2**. The INDO/MRDCI computed energies of the lowest OPA- and TPA-active states of **1** are 1.76 and 2.02 eV, respectively, which are in good agreement with the experimental peaks 1 and 2 maxima of 1.77 and 1.92 eV, respectively, found for **2** (Figure 4.6). A second TPA peak between 2.8 and 3.7 eV is consistent with the experimental feature at higher energy, which apparently represents the tail of a TPA feature with a maximum at a state energy of ca. 3 eV or higher. It is interesting to note that the lowest TPA-active state is quite close in energy (calculated to be within 0.26 eV) to the OPA-active $1B_u$ state. We would like to point out that a similar energy-level alignment of peak 2 (with TPA cross-section less than 100 GM) with respect to peaks 1 and 3 was calculated for some extended pyrrole-substituted squaraines (Table 4.1). The similar behavior of the compounds discussed in Ref. [2] to that of **1** and **2**, in contrast to that for group-II and III squaraines (*vide infra*), thus suggests that they can also be classified as group I compounds. Note that, although the calculations suggest that peak 2 for this group is principally electronic in origin, some contributions from vibronic coupling cannot be ruled out. The model squaraines of group IV also exhibit low-energy 2PA active states (see Figure 4.7). In general, the lowest TPA state falls in energy with conjugation length more rapidly than the OPA state.

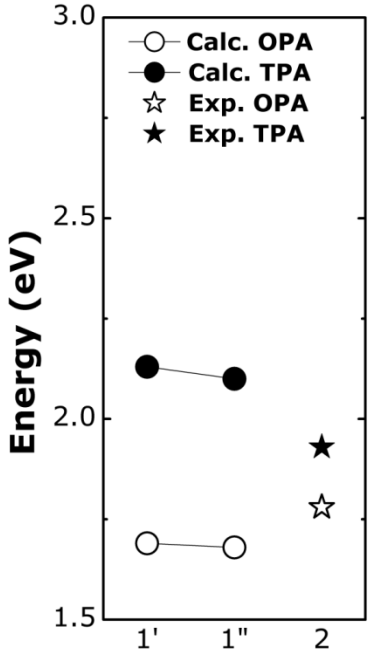

Figure 4.6. INDO/MRDCIS-calculated state energies for two conformers of **1**. The experimental spectra of **2** is available in the literature. [17]

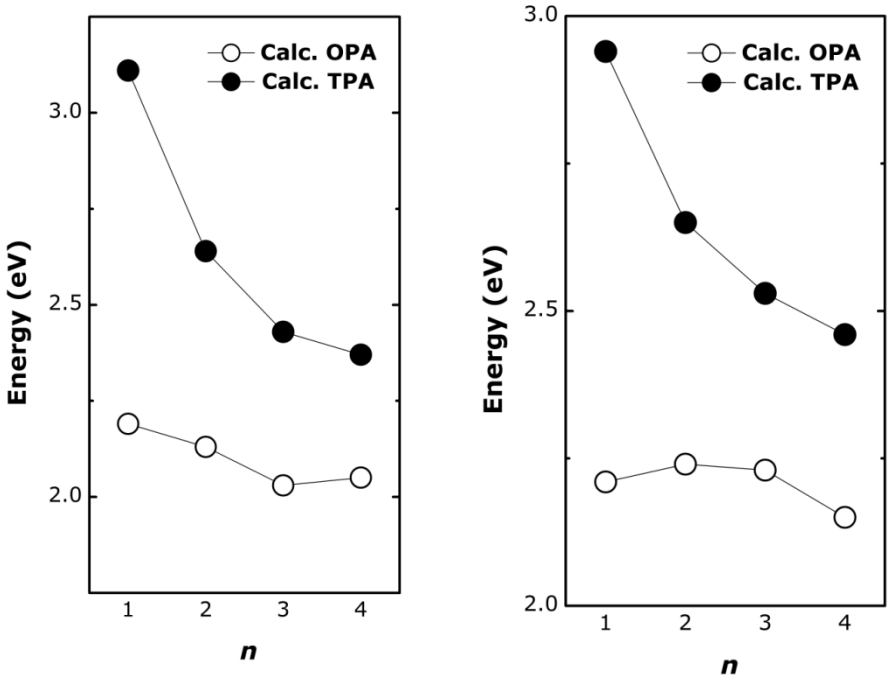

Figure 4.7. INDO/MRDCIS-calculated state energies of **9-n** (left) and **10-n** (right) as a function of size of the polyenic segment.

In contrast to groups I and IV, a TPA-active electronic state was not calculated to appear in the vicinity of experimental peak 2 (*i.e*., close to peak 1) in the bis(indolinylidenemethyl) species of groups II and III. Instead, the calculated OPA state energies and the lowest electronic TPA-active state energies of the molecules were consistent with the experimental values for peaks 1 and 3, with two TPA states appearing in the vicinity of the experimentally observed peak 3 (Figure 4.8). The energies of both transitions are rather insensitive to alkylation on the indole nitrogen atoms (**4** vs. **3**) and also to extension of conjugation at the 4-position of the indole ring system in series III. The insensitivity to extended conjugation reflects the lack of a direct conjugation pathway from the six-membered ring of the indole to the squarylium acceptor; this can be seen from the localization of the HOMO and LUMO (which are the key orbitals involved in the lowest OPA and TPA transitions) in the central unit between the two indole nitrogen atoms (Figure 4.6). The insensitivity to extended conjugation in compounds of group III can be contrasted to that in the group-IV model squaraines in which the terminal donor is in direct conjugation with the acceptor, as shown in Figure 4.7. The insensitivity of both peak-1 and peak-3 states to extension in group-III compounds is fully reproduced in D'-D-π-C_4O_2-π-D-D'-type model structures. In a series of compounds constructed in this way, **9-1**, **11**, and **12** (Figure 4.9), the evolution of the first and second TPA-active state energies remained essentially independent of the length of π-conjugation beyond the primary donor group. Thus, a π-conjugation extension of the molecules beyond the primary donor group cannot participate effectively in the conjugation with the

core moiety and, thus, is not able to sufficiently stabilize the lowest TPA state to explain the origin of peak 2.

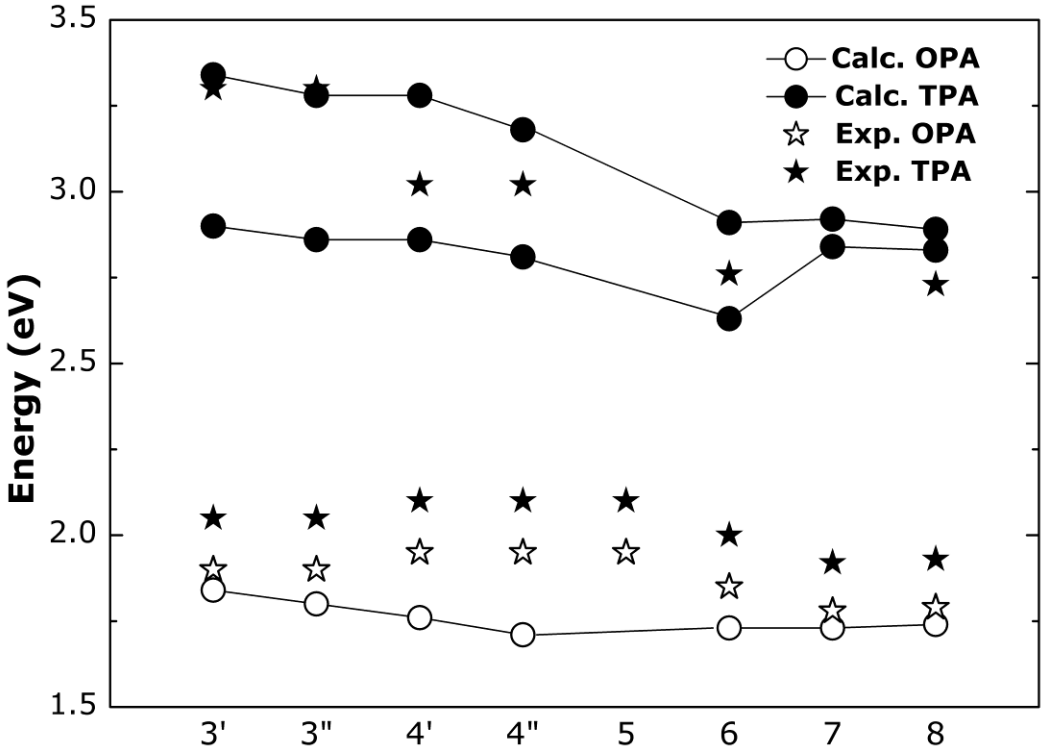

Figure 4.8. INDO/MRDCIS-calculated OPA and TPA state energies for compounds **3-8** and experimental values for **3**[5], 4 and **6**,[1] 5,[3] and **7** and **8**.[17] For **3** and **4**, the theoretical data are obtained for two conformations while the same experimental data (which refer to an equilibrium mixture of conformations) are plotted twice.

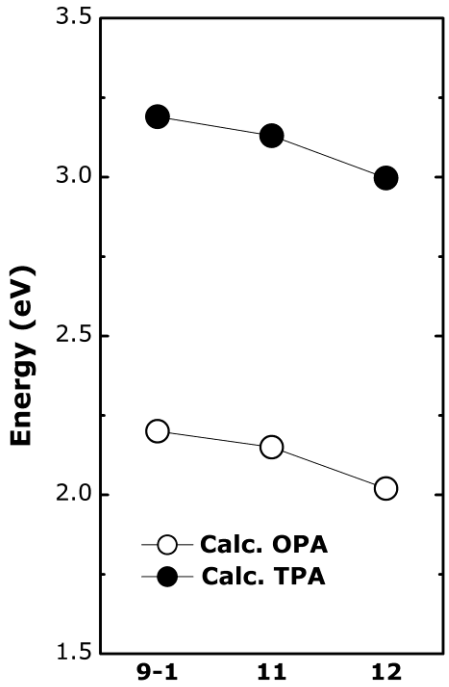

Figure 4.9. OPA- and TPA-active state energies of compounds **9-1**, **11** and **12**.

Even though indole groups block through-conjugation into the thienyl and aminostyryl substituents of the group-III chromophores, the actual structure of the terminal groups nonetheless plays an important role in quantitatively determining the overall nonlinear optical properties. In order to get a better quantitative understanding of the δ values calculated with the correction-vector method (CVM), see Table 4.3, we also used the three-state model,

$$\delta_{3-state} \sim \mu_{01}^2 \times \mu_{12}^2 \times \left(\frac{E_{02}}{E_{01} - {}^{E_{02}}/_{2}}\right)^2 \quad (1)$$

which includes the transition dipole moments between the initial and intermediate states, μ_{01}, and between the intermediate and final states, μ_{12}, and the transition energies E_{01} and E_{02} between the relevant excited states and the ground state.

From Table 4.3, it can be seen that both the simple 3-state model and CVM approach predict an increase in TPA cross-section into the $3A_g$ state (peak 3) with conjugation length, *i.e.,* in going from **4** to **8**. From the parameters entering eq (1), is it clear that this increase in δ upon extending the conjugated bridge is caused by an increase in the transition dipole moments μ_{01} and μ_{12} and, to a much lesser extent, by a slightly enlarged resonance enhancement factor, $E_{02}/(E_{01}-E_{02}/2)$. This calculated trend is in agreement with experiment[3] as the cross-section associated with the second TPA peak (peak 3) is measured to be higher for **8** than for **5** (δ = 4,000 and ~750[3] GM, respectively). It is important to note that the number of π-electrons has direct impact on the nA_g states (n>2), but relatively little effect on the strength of peak 2, *i.e.*, transitions to the $2A_g$ state. However, the significantly higher computational cost associated with modeling the NLO properties of complexes with such large numbers of π-electrons makes a *quantitative* comparison between theory and experiment a challenging task.

Table 4.3. TPA cross-section values into the 3Ag state in **4** (top) and **8** (bottom) calculated with the correction vector method (CVM), δ_{CVM}, and a three-state model, $\delta_{3\text{-state}}$, with the corresponding three-state parameters from MR-DCI calculations with singles.

	E (eV)	μ_{01} (D)	μ_{12} (D)	$\delta_{3\text{-state}}$ (GM)	δ_{CVM} (GM)
$1B_u$	1.76	13			
$3A_g$	2.86		5.6	4.0×10^5	2.8×10^3
	E (eV)	μ_{01} (D)	μ_{12} (D)	$\delta_{3\text{-state}}$ (GM)	δ_{CVM} (GM)
$1B_u$	1.74	15			
$3A_g$	2.89		7.1	1.1×10^6	7.7×10^3

The contribution of the donor group to the major molecular orbitals of the low-lying excited states determines the electronic properties of the squaraines in groups I, II and III. From our studies, we conclude that peak 2 in group-I squaraines can be attributed to an electronically TPA-allowed state ($2A_g$) lying close in energy to the lowest energy OPA state (although the possibility of additional vibronic contributions cannot be ruled out). In contrast, the experimentally observed peak 2 in squaraines from groups II and III with indolinylidenemethyl donor fragments cannot be explained in terms of an electronic origin. We now turn to an examination of the role of vibronic coupling.

4.4 Formation of a low-lying TPA-active state (peak 2) due to vibronic coupling

To obtain a physical insight into the origin of peak 2 in group II and III compounds, we have explored vibronic coupling within Herzberg-Teller (HT) theory as a possible mechanism. Note that, given the approximations related to the implementation of HT theory, it is not expected that the absolute values of the TPA cross-sections computed by this means be quantitatively accurate;[18] also, the experimental cross-sections cannot directly be compared in all cases to the calculated degenerate TPA cross-sections, since the experimental data for peak 2 in some of the compounds are based on non-degenerate TPA measurements. Nevertheless, a qualitative description of vibrational coupling can be achieved, in particular, since our implementation of HT theory allows us to investigate the

relevance of the various vibrational modes and electronic states in enabling TPA-activity.

Due to the C_{2h} symmetry of squaraine 3, only vibrational modes of b_u symmetry can mix with the OPA-active $1B_u$ state to result in a TPA-active $2A_g$ state. Theoretically, vibrational modes of both b_u and a_u symmetries can lead to TPA transitions: $A_g \rightarrow A_g$ and $A_g \rightarrow B_g$, respectively. However, as pointed out by Scherer *et al*.[1], one can rule out the possibility that peak 2 is due to an $A_g \rightarrow B_g$ transition in centrosymmetric squaraine molecules such as **4** from an analysis of the polarization ratio (ratio of TPA cross-sections in circularly and linearly polarized lights) obtained with the two-photon fluorescence technique. Therefore, only b_u vibrational modes are considered here in our study of the vibronically allowed TPA process. From an examination of the adiabatic vibronic coupling constants, we found that in squaraine **3** very few (only 5 out of 48) b_u normal modes strongly couple the one-photon active $1B_u$ state with the TPA-active $3A_g$ state. We note that, although additional b_u modes could, in principle, strongly couple the $1B_u$ state with higher lying nA_g states, their contributions to the two-photon cross-section will be relatively small due to the larger energy differences from the $1B_u$ state. Table 4.4 provides the adiabatic vibronic coupling constant values between the $1B_u$ and $3A_g$ states. We identified that mode 113 (illustrated in Figure 4.10) gives rise to a significantly higher TPA cross-section for the $1A_g \rightarrow 2A_g$ (= $1B_u \times nb_u$) transition than all the other b_u modes. Table 4.5 demonstrates the effect of vibronic coupling: the TPA transition $1A_g \rightarrow 2A_g$ around 2.05 eV (δ ~ 8 GM) is due

to mode 113. According to our calculations, the separation between $1B_u$ and $2A_g$ is 0.18 eV; this is in very good agreement with the experimental difference in state energy between peak 1 and peak 2, especially considering the approximations involved in our vibronic calculation. It is interesting to note that mode 113 is also strongly IR-active.

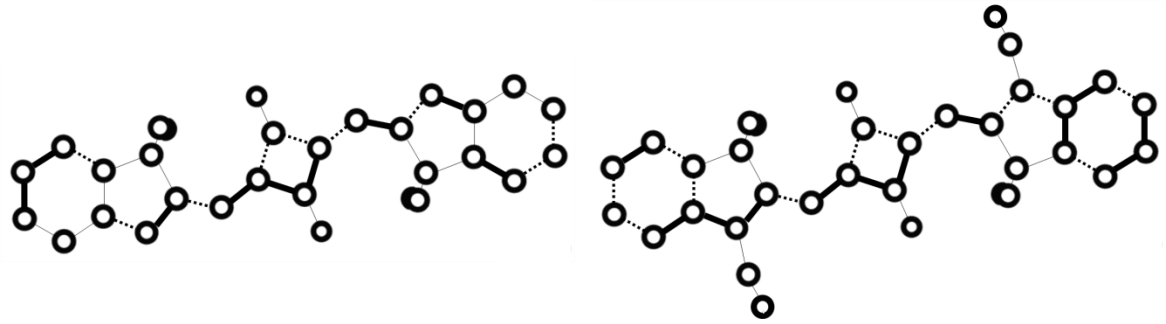

3 (Mode 113) **4** (Mode 159)

Figure 4.10. Schematic representation of the b_u stretching mode 113 in **3** (left) and mode 159 in **4** (right); elongated [compressed] bonds are shown with bold [dotted] line.

Table 4.4. Strongly coupled b_u modes with their coupling strength between the $1B_u$ and $2A_g$ (= $1B_u$ x b_u) state.

Mode No.	Frequency (cm^{-1})	Adiabatic Coupling (cm^{-1})
99	1,240	-566
107	1,362	-681
113	1,417	1,161
123	1,493	510
131	1,590	-2,098

Table 4.5. Electronic and vibronic contributions to TPA cross section values in **3** (top) and **4** (bottom) computed at the B3LYP/SV(P)//INDO/MR-DCI singles level, using the HT vibronic coupling model.

Peak		*E* (eV)	$\delta^{[a]}$ (GM)	$\delta^{[b]}$ (GM)
1	$1B_u$	1.87	---	---
2	**$2A_g = 1B_u \times b_u$**	**2.05**	---	**7.61**
3	$3A_g$	2.89	122	N/A
Peak		*E* (eV)	$\delta^{[a]}$ (GM)	$\delta^{[b]}$ (GM)
1	$1B_u$	2.08	---	---
2	**$2A_g = 1B_u \times b_u$**	**2.27**	---	**33.9**
3	$3A_g$	3.16	244	N/A

[a] Without HT-coupling. [b] With HT-coupling.

HT vibronic coupling was also investigated in squaraine **4**. Unlike squaraine **3**, the centrosymmetric conformer of this compound shown in Figure 4.5 does not have C_{2h} but C_i symmetry due to a slight twist from planarity; thus, all the normal modes were taken into account to compute the vibronic coupling. The top panel in Figure 4.11 shows the TPA cross-section values due to HT vibronic coupling in molecule **4**. Although strictly speaking the TPA-active vibronic states do not have b_u symmetry, we can get an indication from the IR spectrum (considering the correlation between strength of IR activity and magnitude of vibronic coupling constant in squaraine **3**) of which modes could yield large TPA cross-section values through HT vibronic coupling. We observe that the effect of vibronic coupling on TPA cross-section is significantly higher in mode 159 (see Figure 4.10) compared to other normal modes. As with squaraine **3**, inclusion of vibronic coupling in squaraine **4** leads to a predicted peak 2 0.19 eV higher in state energy than peak 1; in this case, the predicted TPA cross-section is somewhat

larger (34 GM). Further analysis of mode 113 in squaraine **3** and mode 159 in squaraine **4** indicates that they both correspond to stretching modes impacting the degree of bond-length alternations; it is expected that the extent of bond-length alternation can affect both IR intensity and vibronic coupling strength (Figures 4.10 and 4.11).

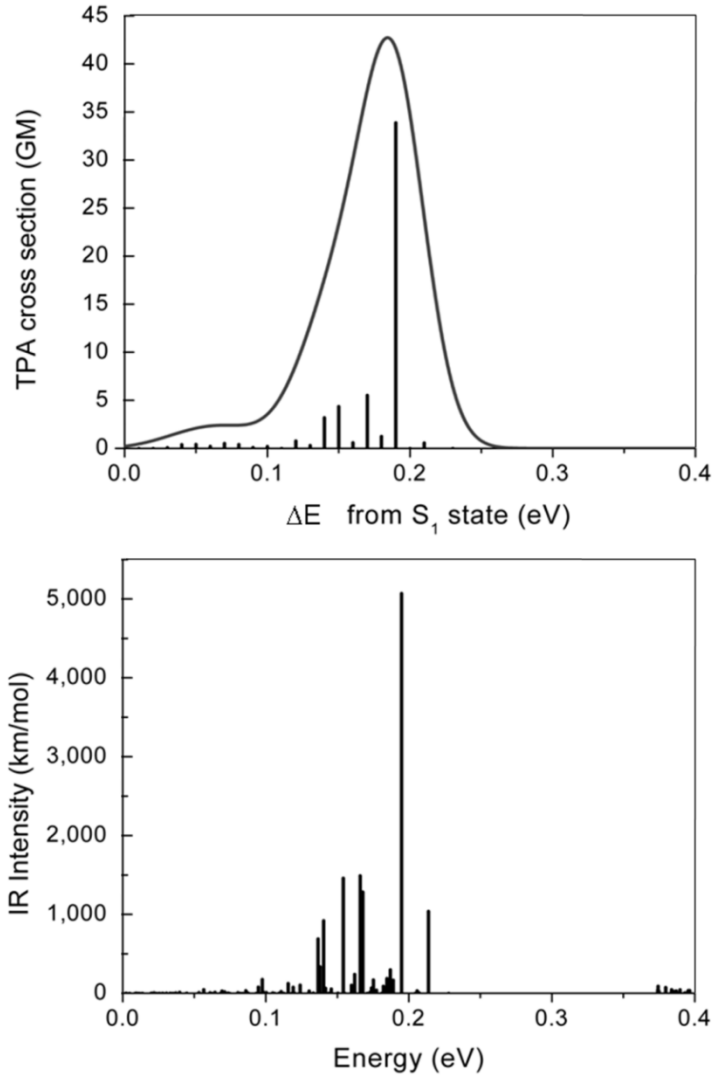

Figure 4.11. TPA cross-section values obtained at the B3LYP/SV(P)//INDO/MR-DCI singles level using the HT vibronic coupling model (top) and IR spectrum computed at the B3LYP/SV(P) level (bottom) for **4**. Also shown is the Gaussian convolution of the calculated TPA spectrum using a FWHM of 5 meV.

To demonstrate that the vibrational characteristics of these molecules are computationally well-described, the experimental IR spectrum of **4** is shown in Figure 4.12. The computed frequencies are slightly overestimated relative to the experimental values, as is typical for the method. There is also an apparent discrepancy in the relative intensities of different modes between the experimental and theoretical spectra; in particular, in contrast to theory, the experimental peak at 0.19 eV is not the most intense peak. However, it should be noted that the 0.19 eV band is broader than all the others in the experimental spectrum, while the theory includes no broadening; when properly considering integrated oscillator strengths, the theoretical spectrum is in considerably better agreement with experiment than a cursory inspection of peak intensities might suggest. Thus, overall, the experimental and computational spectra are indeed in good agreement.

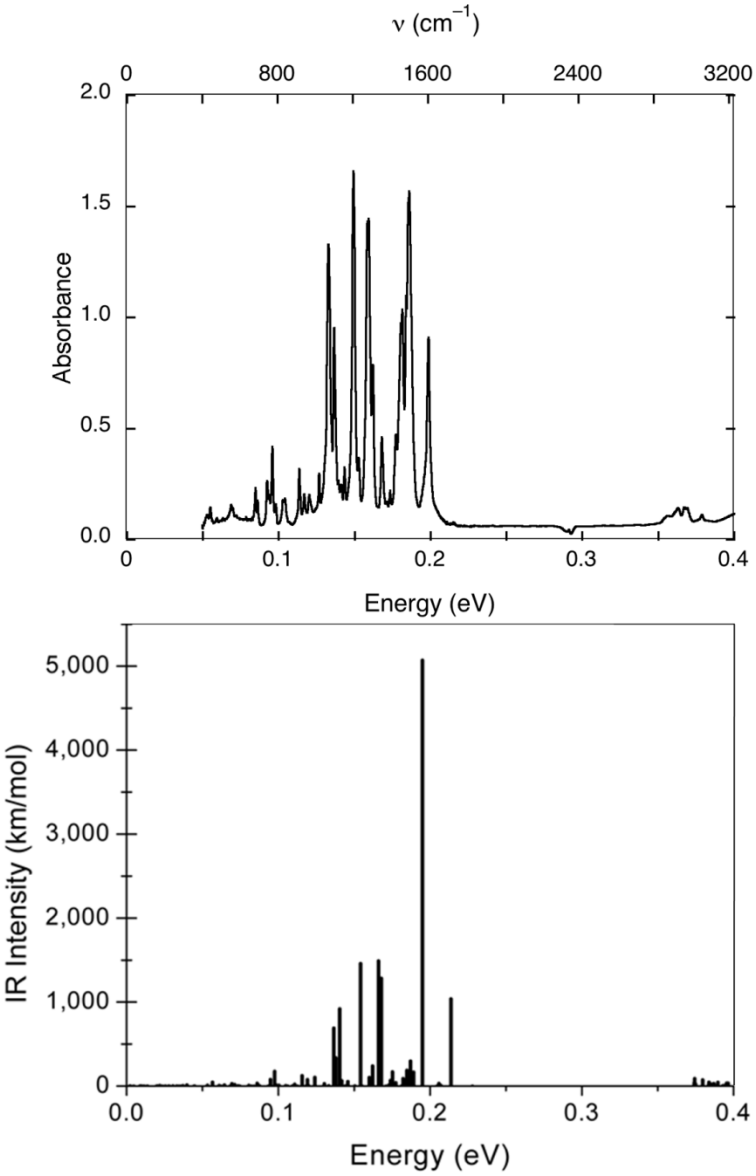

Figure 4.12. Experimental IR spectrum of **4** in KBr and IR spectrum computed at the B3LYP/SV(P) level (bottom) for **4**.

4.5 Conclusions

We have shown that the origin of peak 2 in squaraines is dependent on the nature of substituent donor moiety, changing from predominantly electronic (*e.g.*, in diarylaminothienyl donors) to vibronic (*e.g.*, in indolinylidenemethyl donors) in character. For squaraines with diarylaminothienyl donors (group I), the lowest electronic TPA-active state ($2A_{g,}$ peak 2) is located close in energy to the $1B_u$ (peak 1) state, thus providing a purely electronic channel for TPA into peak 2 (although one cannot rule out additional contributions from vibronic coupling), scenario (i) in Figure 1. On the other hand, the lowest electronic TPA-active state ($3A_g$) is energetically well-separated from the $1B_u$ state for all squaraines containing indolinylidenemethyl donors (groups II and III), which corresponds to scenario (ii) in Figure 4.1.

The possibility of a vibronic origin for peak 2 in group II and III molecules was investigated using an efficient implementation of HT theory in conjunction with the ZINDO Hamiltonian. These calculations confirmed the previous suggestion of Scherer and co-workers[1] of a vibronic origin for peak 2 in this class of chromophores. The experimental TPA absorption peak 2 in compounds of groups II and III is rather sharp, which suggests that only a few modes are strongly coupled with the $1B_u$ state and dominate contributions to the TPA cross-section. Our calculations confirm that this is indeed the case with squaraine molecules containing indolinylidenemethyl fragments and provide an explanation

for the energy and lineshape of the experimentally observed peak 2 in these compounds.

REFERENCES

(1) Scherer, D.; Dorfler, R.; Feldner, A.; Vogtmann, T.; Schwoerer, M.; Lawrentz, U.; Grahn, W.; Lambert, C. *Chem. Phys.* **2002**, *279*, 179.

(2) Chung, S. J.; Zheng, S. J.; Odani, T.; Beverina, L.; Fu, J.; Padilha, L. A.; Biesso, A.; Hales, J. M.; Zhan, X. W.; Schmidt, K.; Ye, A. J.; Zojer, E.; Barlow, S.; Hagan, D. J.; Van Stryland, E. W.; Yi, Y. P.; Shuai, Z. G.; Pagani, G. A.; Bredas, J. L.; Perry, J. W.; Marder, S. R. *J. Am. Chem. Soc.* **2006**, *128*, 14444.

(3) Fu, J.; Padilha, L. A.; Hagan, D. J.; Van Stryland, E. W.; Przhonska, O. V.; Bondar, M. V.; Slominsky, Y. L.; Kachkovski, A. D. *J. Opt. Soc. Am. B-Opt. Phys.* **2007**, *24*, 67.

(4) Andrews, J.; Khaydarov, J.; Singer, K. *Opt. Lett.* **1994**, *19*, 984.

(5) Andrews, J.; Khaydarov, J.; Singer, K.; Hull, D.; Chuang, K. *J. Opt. Soc. Am. B* **1995**, *12*, 2360.

(6) Yu, Y.; Shi, R.; Garito, A.; Grossman, C. *Opt. Lett.* **1994**, *19*, 786.

(7) Poga, C.; Brown, T.; Kuzyk, M.; Dirk, C. *J. Opt. Soc. Am. B* **1995**, *12*, 531.

(8) Dirk, C. W.; Herndon, W. C.; Cervanteslee, F.; Selnau, H.; Martinez, S.; Kalamegham, P.; Tan, A.; Campos, G.; Velez, M.; Zyss, J.; Ledoux, I.; Cheng, L. T. *J. Am. Chem. Soc.* **1995**, *117*, 2214.

(9) Kazmaier, P. M.; Hamer, G. K.; Burt, R. A. *Can. J. Chem.* **1990**, *68*, 530.

(10) Terenziani, F.; Painelli, A.; Katan, C.; Charlot, M.; Blanchard-Desce, M. *J. Am. Chem. Soc.* **2006**, *128*, 15742.

(11) Herzberg, G.; Teller, E. *Z. Physik. Chem.* **1933**, *B21*, 410.

(12) Kobayashi, Y.; Goto, M.; Kurahashi, M. *Bull. Chem. Soc. Jap.* **1986**, *59*, 311.

(13) Dirk, C. W.; Cheng, L. T.; Kuzyk, M. G. *Int. J. Quant. Chem.* **1992**, *43*, 27.

(14) Heflin, J. R.; Garito, A. F. *Electroresponsive Molecular and Polymeric Systems* Marcel Dekker: New York, **1991**; Vol. 2.

(15) Kuzyk, M. G.; Dirk, C. W. *Phys. Rev. A* **1990**, *41*, 5098.

(16) Pierce, B. M. *J. Chem. Phys.* **1989**, *91*, 791.

(17) Ohira, S.; Rudra, I.; Schmidt, K.; Barlow, S.; Padilha, L. A.; Fu, J.; Chung, S.-J.; Zhang, Q.; Matichak, J.; Hagan, D. J.; Stryland, E. W. V.; Marder, S. R.; Brédas, J.-L. *Chem.–Eur. J.* **2008**, *14*, 11082-11091.

(18) Marconi, G.; Orlandi, G. *J. Chem. Soc., Faraday Trans.2* **1982**, *78*, 565.

CHAPTER 5:

Conclusions

The nonlinear optical (NLO) properties were investigated in various extended π-conjugated chromophores: (i) cyanine and alkyne carbocations; (ii) porphyrin dimers; and (iii) squaraine compounds that possess electronic, double resonance, and vibronic based NLO properties. In summary:

(i) It was demonstrated that the alkyne carbocations have very similar optical properties to traditional cyanine dyes, such as the nature of the transition dipole moment between the ground state and the lowest excited state M_{eg}, the transition energy E_{eg}, and the static first-order polarizability α; the new set of compounds do not exhibit as large third-order polarizabilities γ. The similarities between two series can be rationalized when considering the bonding-antibonding patterns in the π-molecular orbitals. Our theoretical results establish that the *alkyne carbocations, in spite of their significant degree of bond-length alternation, behave in the same way as cyanine dyes*. The delocalized nature of the electronic structure represents a more significant characteristic than the degree of BLA. It will be important to determine up to what length the alkyne cyanine compounds can retain full delocalization.

(ii) The nature of the bridge between the monomer moieties in the porphyrin dimers tunes the electronic coupling strength, which in turn determines the splitting of the frontier molecular orbital levels and the excited-state

energies. The respective locations of the OPA/TPA-active states control the nonlinear optical properties of the dimers and lead to either double resonance-enhanced or “pure” TPA cross-sections. In the porphyrin dimers with significant electronic coupling strength TPA-active state energies are stabilized and exhibit significant cross-sections. When there is weak interaction between the porphyrin end groups, the TPA cross-sections are mainly due to double-resonance effects. The same conclusion holds in porphyrin dimers with very strong coupling; the TPA-active state energy then appears in the double-resonance energy range, so that significant contamination of the TPA from double-resonance effects is expected.

(iii) We have shown that the origin of the lowest TPA-active states in squaraines is dependent on the nature of substituent donor moiety, changing from predominantly electronic (*e.g.*, in diarylaminothienyl donors) to vibronic (*e.g.*, in indolinylidenemethyl donors) in character. For squaraines with diarylaminothienyl donors, the $2A_g$ state is located close in energy to the $1B_u$ state, thus providing a purely electronic channel for TPA into the lowest TPA-active state. On the other hand, the lowest electronic TPA-active state ($3A_g$) is energetically well-separated from the $1B_u$ state for all squaraines containing indolinylidenemethyl donors. Using an implementation of HT theory with the ZINDO Hamiltonian, these calculations confirmed a vibronic origin for the TPA peak, and the energy

and lineshape of the experimentally observed lowest TPA peak in these compounds.

The results presented in this thesis have raised several questions which should be pursued. The non-linear optical properties in those compounds should be understood for assessing their potential. We underline the following points:

(i) As traditional cyanine compounds get longer, $\Delta\mu_{eg}$ tends to vanish. However, unlike traditional cyanines, the V-shape structure of alkyne carbocations can lead to significant $\Delta\mu_{eg.}$ This can result in an increased second-order polarizability β. For a more complete characterization of the NLO properties of the compounds, we should evaluate β as a function of length in the alkyne carbocations. Also, an analysis of the length at which a symmetric structure might become unstable in these systems would be of interest.

(ii) Odom *et al* reported that the δ_{max} value for porphyrin—squaraine—porphyrin complex[11] is as large as 1.1×10^4 GM. The value is similar in magnitude to those measured for several other porphyrin dimers with conjugated bridges, for which, however, the maxima are observed at much shorter wavelengths –even shorter than the porphyrin dimers with an acceptor central moiety as discussed in Chapter 3. It would be of

[1] Odom, S. A.; Webster, S.; Padilha, L. A.; Peceli, D.; Hu, H.; Nootz, G.;Chung, S.-J.; Ohira, S.; Matichak, J. D.; Przhonska, O. V.; Kachkovski, A. D.; Barlow, S.; Brédas, J.-L.; Anderson, H. L.; Hagan, D. J.; Van Stryland, E. W.; Marder, S. R. *J. Am. Chem. Soc.* **2009**, in press. See Appendix B for the theoretical details in the paper.

interest to extend our model for the dimers that have strong interactions between the porphyrin and central moieties in both occupied and unoccupied levels, such as Odom’s squaraine complexes.

For all model systems we have analyzed, the structure-property relationships we've identified will aid in the design of molecular systems with enhanced NLO responses.

List of Publications

1. "Electronic and vibronic contributions to two-photon absorption in donor-acceptor-donor squaraine chromophores," S. Ohira, I. Rudra, K. Schmidt, S. Barlow, S.-J. Chung, Q. Zhang, J. Matichak, S. R. Marder and J.-L. Brédas. *Chem.—Eur. J*, **2008**, *14*, 11082-11091.

2. "A spray-processable, low bandgap, and ambipolar donor-acceptor conjugated polymer," T. T. Steckler, X. Zhang, J. Hwang, R. Honeyager, S. Ohira, X.-H. Zhang, A. Grant, S. Ellinger, S. A. Odom, D. Sweat, D. B. Tanner, A. G. Rinzler, S. Barlow, J.-L. Brédas, B. Kippelen, S. R. Marder and J. R. Reynolds. *J. Am. Chem. Soc.* **2009**, *131*, 2824-2826.

3. "A new class of cyanine dyes with large bond-length alternation," S. Ohira, J. M. Hales, K. J. Thorley, H. L. Anderson, J. W. Perry, and J.-L. Brédas. *J. Am. Chem. Soc.* **2009**, *131*, 6099-6101.

4. "Synthesis and two-photon spectrum of a bis(porphyrin)-substituted squaraine," S. A. Odom, S. Webster, L. A. Padilha, D. Peceli, H. Hu, G. Nootz, S.-J. Chung, S. Ohira, J. D. Matichak, O. V. Przhonska, A. D. Kachkovski, S. Barlow, J.-L. Brédas, H. L. Anderson, D. J. Hagan, E. W. Van Stryland and S. R. Marder. *J. Am. Chem. Soc.*, Articles ASAP

5. "Porphyrin dimers: A theoretical understanding of the impact of electronic coupling strength on the two-photon absorption properties," S, Ohira and J.-L. Brédas. *J. Mater. Chem.* Accepted.

6. "Computation of vibronic contribution to two-photon absorption in polymethine and squaraine molecules," I. Rudra, S. Ohira, K. Schmidt, and J.-L. Brédas. Submission to *J. Chem. Phys*. is expected soon.

7. "Synthesis and photophysical properties of an alkyne-bridged bis(zinc porphyrin)–perylene diimide derivative," S. A. Odom, R. F. Kelley, S. Ohira, T. Ensley, C. Huang, L. A. Padilha, S. Webster, V. Coropceanu, S. Barlow, D. J. Hagan, E. W. Van Stryland, J.-L. Brédas, H. L. Anderson, M. R. Wasielewski, S. R. Marder. Submission to *J. Phys. Chem*. is expected soon.

8. “Dithienopyrrole-based donor-acceptor copolymers: synthesis, optical and electronic properties,” X. Zhang, T. T. Steckler, R. R. Dasari, J. Hwang, S. Ohira, W. Postcavage, S. P. Tiwari, S. Coppee, S. Ellinger, D. B. Tanner, A. G. Rinzler, S. Barlow, J.-L. Brédas, B. Kippelen, J. R. Reynolds, and S. R. Marder. Submission to *Chem. Mater.* is expected soon.

9. “Using end groups to tune the linear and nonlinear optical properties of bis(dioxaborine)-terminated polymethine dyes,” J. D. Matichak, J. M. Hales, S. Ohira, S. Barlow, J.-L. Brédas, J. W. Perry, S. R. Marder, S.–H. Jang, and A. K.–Y. Jen. Submission is expected soon.

APPENDIX A:

A spray-processable, low bandgap, and ambipolar donor—acceptor conjugated polymer

Steckler, T. T.; Zhang, X.; Hwang, J.; Honeyager, R.; Ohira, S.; Zhang, X.-H.; Grant, A.; Ellinger, S.; Odom, S. A.; Sweat, D.; Tanner, D. B.; Rinzler, A. G.; Barlow, S.; Brédas, J.-L.; Kippelen, B.; Marder, S. R.; Reynolds, J. R. *J. Am. Chem. Soc.*, **2009**, *131*, 2824–2826

Narrow bandgap conjugated polymers can provide a unique set of redox and optoelectronic properties, including broad and long wavelength light absorption, solid-state transport of both holes and electrons, and access to multiple charge states in a small potential window. In ground-breaking work, Wudl *et al.* demonstrated that polyisothianaphthene exhibited a bandgap of ~1 eV due to the appended benzene ring forcing the thiophene into a quinoid-like ground-state geometry.[1] Multiple researchers have also sought to reduce the band gap by using a donor-acceptor (DA) approach.[2] This method has proven to be an effective strategy for tailoring the properties of oligomers and polymers for applications in photovoltaics,[3] OLEDs,[4] electrochromics,[5] and OFETs.[3a,4e,6]

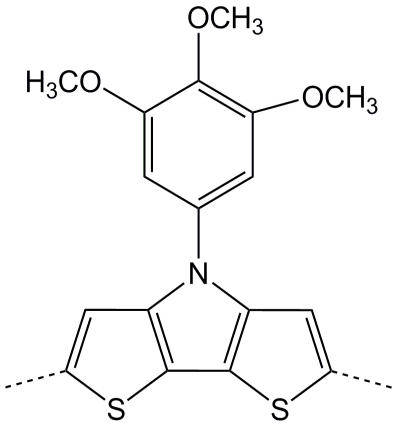

Donor(DTP):
Dithieno[3,2-*b*:2′,3′-*d*]pyrrolefunctionalized with a trialkoxyphenyl group[6d,7]

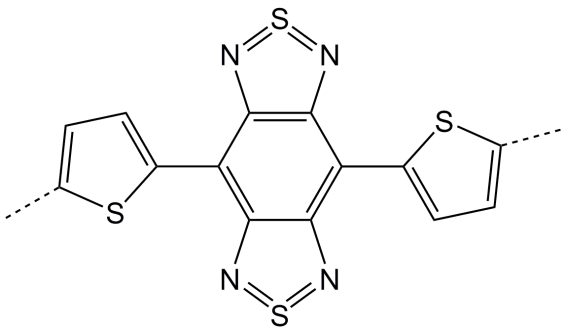

Acceptor (BBT):
Benzo[1,2-*c*;4,5-*c*′]bis[1,2,5]thiadiazole[8]

To enhance the D-A interaction and simultaneously produce soluble low band gap polymers, the polymer P(DTP-BThBBT) consists of the strong donor DTP combined with a strong acceptor BBT. The DTP moiety provides a high-lying HOMO level, planarity for π stacking, and solubility in the polymers due to the long-chain alkoxy substituents.

To aid for investigation of the polymer P(DTP-BThBBT), its electronic properties, including the lowest excited-state energies, were calculated at the density functional theory and time-dependent (TD-)DFT B3LYP/3-21G* levels using model oligomers $(DTP\text{-}BThBBT)_n$ with n = 1, 2, 3, 4, and 6. The HOMO and LUMO of $(DTP\text{-}BThBBT)_2$ are illustrated in Figure 1. As in several similar polymers with alternating donor and acceptor units,[7] while the HOMO wavefunction is delocalized over the whole π system, the LUMO wave function is localized on the acceptor units. The calculated lowest excited-state energy,

obtained by extrapolation (see Figure A.1) to $n = \infty$, is 0.50 eV (Table A.1). Since the lowest lying transition is primarily of HOMO → LUMO character, this points to intramolecular charge-transfer and suggests that P(DTP-BThBBT) will have an especially low onset for optical absorbance. The results are confirmed for polymer films spray cast onto indium tin oxide (ITO), single walled carbon nanotubes (SWCNT),[8] and gold electrodes on glass. The polymer shows an onset of absorption at ~2260 nm giving a bandgap of 0.54 eV, which is close to the calculated S_1 excited-state energy of 0.50 eV.

Table A.1. The summary of the electronic properties (in eV) of P(DTP-BThBBT) computed from the oligomer approach with n = ∞ at the (TD-)DFT B3LYP/3-21G* level.

HOMO (eV)	-4.16
LUMO (eV)	-3.67
HOMO-LUMO gap (eV)	0.47
S_0-S_1 transition energy (eV)	0.50

It was reported that: (i) the polymer P(DTP-BThBBT) is spray-processable and shows an optical bandgap of 0.5-0.6 eV, which is the lowest value reported for a soluble spray processable polymer; (ii) its four differently colored redox states are accessible at moderate potentials and have good stability; and (iii) it exhibits potential for use in ambipolar OFETs with respectable mobilities for a solution-processed device.

Figure A.1. The evolution of HOMO/LUMO levels and the lowest excited state of oligomers $(DTP\text{-}BThBBT)_n$ as a function of $1/n$ (left) and the HOMO/LUMO wavefunctions of $(DTP\text{-}BThBBT)_2$ at the (TD-)DFT B3LYP/3-21G* level.

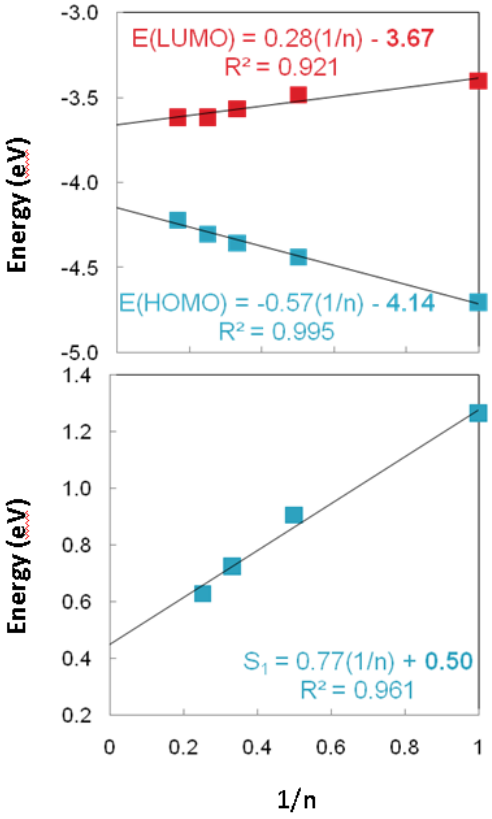

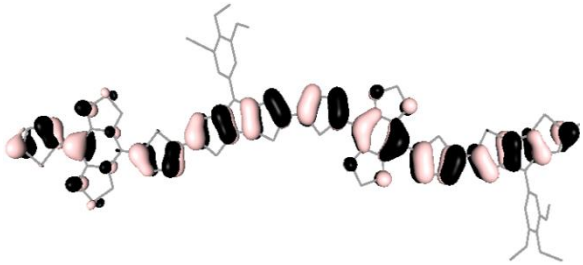

HOMO

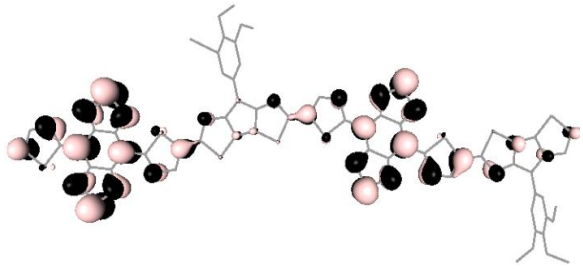

LUMO

REFERENCES

(1) (a) Wudl, F.; Kobayashi, M.; Heeger, A. J. *J. Org. Chem.* **1984**, *49*, 3382–3384. (b) Brédas, J. L.; Heeger, A. J.; Wudl, F. *J. Chem. Phys.* **1986**, *85*, 4673–4678. (c) Hoogmartens, I.; Adriaensens, P.; Vanderzande, D.; Gelan,J.; Quattrocchi, C.; Lazzaroni, R.; Brédas, J. L. *Macromolecules* **1992**, *25*,7347–7356. (d) Kertesz, M.; Choi, C. H.; Yang, S. *Chem. Rev.* **2005**, *105*, 3448–3481.

(2) (a) Brédas, J. L. *J. Chem. Phys.* **1985**, *82*, 3808–3811. (b) Havinga, E. E.;Hoeve, W.; Wynberg, H. *Polym. Bull.* **1992**, *29*, 119–126. (c) Roncali, J.*Chem. Rev.* **1997**, *97*, 173–206. (d) van Mullekom, H. A. M.; Vekemans,J. A. J. M.; Havinga, E. E.; Meijer, E. W. *Mater. Sci. Eng.: R* **2001**, *32*, 1–40. (e) Ajayaghosh, A. *Chem. Soc. Rev.* **2003**, *32*, 181–191.

(3) (a) Zhu, Z.; Waller, D.; Gaudiana, R.; Morana, M.; Muhlbacher, D.;Scharber, M.; Brabec, C. *Macromolecules* **2007**, *40*, 1981–1986. (b)Mammo, W.; Admassie, S.; Gadisa, A.; Zhang, F.; Ingana¨s, O.; Andersson,M. R. *Sol. Energy Mater. Sol. Cells* **2007**, *91*, 1010–1018. (c) Colladet, K.; Fourier, S.; Cleij, T. J.; Lutsen, L.; Gelan, J.; Vanderzande, D.;HuongNguyen, L.; Neugebauer, H.; Sariciftci, S.; Aguirre, A.; Janssen,G.; Goovaerts, E. *Macromolecules* **2007**, *40*, 65–72. (d) Blouin, N.; Leclerc,M. *Acc. Chem. Res.* **2008**, *41*, 1110–1119. (e) Li, Y.; Zou, Y. *Adv. Mater.* **2008**, *20*, 2952–2958. (f) Wienk, M. M.; Turbiez, M.; Gilot, J.; Janssen,R. A. J. *Adv. Mater.* **2008**, *20*, 2556–2560. (g) Huo, L.; Tan, Z. a.; Wang,X.; Zhou, Y.; Han, M.; Li, Y. *J. Polym. Sci., Part A* **2008**, *46*, 4038–4049.

(4) (a) Chen, M. X.; Perzon, E.; Robisson, N.; Jönsson, S. K. M.; Andersson,M. R.; Fahlman, M.; Berggren, M. *Synth. Met.* **2004**, *146*, 233–236. (b) Kulkarni, A. P.; Kong, X.; Jenekhe, S. A. *Macromolecules* **2006**, *39*, 8699–8711. (c) Kulkarni, A. P.; Zhu, Y.; Babel, A.; Wu, P.-T.; Jenekhe, S. A.*Chem. Mater.* **2008**, *20*, 4212–4223. (d) Yang, Y.; Farley, R. T.; Steckler,T. T.; Eom, S.-H.; Reynolds, J. R.; Schanze, K. S.; Xue, J. *Appl. Phys.Lett.* **2008**, *93*, 163305. (e) Zaumseil, J.; McNeill, C. R.; Bird, M.; Smith,D. L.; Ruden, P. P.; Roberts, M.; McKiernan, M. J.; Friend, R. H.; Sirringhaus, H. *J. Appl. Phys.* **2008**, *103*, 064517.

(5) (a) Thompson, B. C.; Kim, Y. G.; McCarley, T. D.; Reynolds, J. R. *J. Am.Chem. Soc.* **2006**, *128*, 12714–12725. (b) Gunbas, G. E.; Durmus, A.;Toppare, L. *Adv. Mater.* **2008**, *20*, 691–695. (c) Beaujuge, P. M.; Ellinger,S.; Reynolds, J. R. *Nat. Mater.* **2008**, *7*, 795–799. (d) Beaujuge, P. M.; Ellinger, S.; Reynolds, J. R. *Adv. Mater.* **2008**, *20*, 2772–2776.

(6) (a) Mas-Torrent, M.; Rovira, C. *Chem. Soc. Rev.* **2008**, *37*, 827–838. (b) Usta, H.; Facchetti, A.; Marks, T. J. *J. Am. Chem. Soc.* **2008**, *130*, 8580–8581. (c) Letizia, J. A.; Salata, M. R.; Tribout, C. M.; Facchetti, A.; Ratner,M. A.; Marks, T. J. *J. Am. Chem. Soc.* **2008**, *130*, 9679–9694. (d) Liu, J.; Zhang, R.; Sauve´, G.; Kowalewski, T.; McCullough, R. D. *J. Am. Chem. Soc.* **2008**, *130*, 13167–13176. (e) Zhu, Y.; Champion, R. D.; Jenekhe,S. A. *Macromolecules* **2006**, *39*, 8712–8719. (f) Yamamoto, T.; Yasuda,T.; Sakai, Y.; Aramaki, S. *Macromol. Rapid Commun.* **2005**, *26*, 1214–1217.

(7) Zhou, E.; Nakamura, M.; Nishizawa, T.; Zhang, Y.; Wei, Q.; Tajima, K.; Yang, C.; Hashimoto, K. *Macromolecules* **2008**, *41*, 8302–8305.

(8) Wu, Z.; Chen, Z.; Du, X.; Logan, J. M.; Sippel, J.; Nikolou, M.; Kamaras, K.; Reynolds, J. R.; Tanner, D. B.; Hebard, A. F.; Rinzler, A. G. *Science* **2004**, *305*, 1273–1276.

APPENDIX B:

Synthesis and two-photon spectrum of a bis(porphyrin)-substituted squaraine

Odom, S. A.; Webster, S.; Padilha, L. A.; Peceli, D.; Hu, H.; Nootz, G.;Chung, S.-J.; Ohira, S.; Matichak, J. D.; Przhonska, O. V.; Kachkovski, A. D.; Barlow, S.; Brédas, J.-L.; Anderson, H. L.; Hagan, D. J.; Van Stryland, E. W.; Marder, S. R. *J. Am. Chem. Soc.* **2009**

Organic materials with large two-photon absorption (TPA) cross sections, δ, are of interest for applications including fluorescence microscopy,[1] microfabrication,[2] and optical pulse suppression.[3] One of the design strategies that have been used to achieve large δ values is the use of π-conjugated molecules with donor acceptor donor (D-A-D) structural motifs.[4] Squaraines can be considered as examples of D-A-D chromophores and have been found to exhibit large values of δ at wavelengths close to their one-photon absorption (OPA) edges,[5] especially when bearing substituents with extended conjugation.[6] Dimers and oligomers of conjugated zinc porphyrins have also been shown to exhibit very strong TPA, with δ_{max} values up to 500 times those of monomeric analogues.[7] Moreover, linear absorption spectra of both squaraines and porphyrins exhibit bands characterized by large transition dipole moments, a key prerequisite for obtaining strong TPA. In addition, the S_0-S_1 transition energies of bis(indolinylidenemethyl) squaraines closely match those of zinc porphyrins, suggesting the possibility of substantial excitonic electronic coupling in a π-conjugated hybrid of these two components. On the basis of these observations, we were interested in

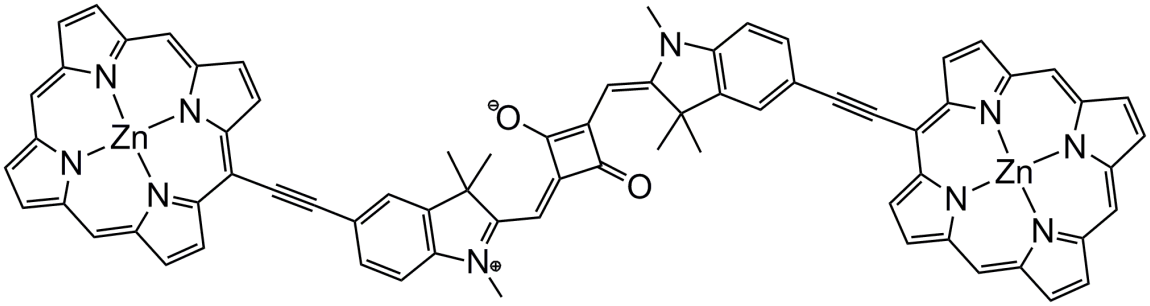

D-A-D bis(porphyrin)-substituted squaraines

investigating whether the electronic coupling between the constituent subunits of D-A-D bis(porphyrin)substituted squaraines could be sufficiently strong to result in enhanced TPA.

Using density functional theory (DFT)-optimized (B3LYP/6-31G**) geometries, we calculated the OPA and TPA properties of the compound, following the INDO/MRD-CI methodology. The frontier orbitals (Figure B.1) show significant delocalization across the whole molecular backbone. The OPA calculations indicate the presence of three main peaks in the visible region, with the lowest-energy feature primarily due to a mixing of HOMO-to-LUMO and (to a lesser extent) HOMO-1-to-LUMO+1 transitions (Table B.1). We note that the best agreement between the calculated OPA and TPA spectra and the experimental data is obtained when the electronic coupling between porphyrin and squaraine units is modulated by setting the degree of bond-length alternation within the acetylenic linkages to 0.10 Å.

The enhancement of δ_{max} for the compound suggests substantial electronic coupling between the porphyrin and squaraine moieties, which is confirmed by the DFT frontier orbitals. The complexity of the molecule and the porphyrin squaraine coupling is anticipated to lead to a large number of low-lying excited states. Therefore, the broad TPA peak is likely to arise from overlap of several transitions. The calculations support this idea, as they reproduce the main features of the experimental spectrum, indicating peaks with δ ~6.9×10^3 and 9.7×10^3 GM at transition energies between those of the two strong OPA states. The observation of large δ over a 750 nm-wide wavelength range suggests that the compound could have applications in broadband NIR pulse suppression.

Table B.1. The lowest 14 singlet excited state energy E, oscillator strength f, transition dipole between ground μ_{0n} and the first excited state (OPA1) μ_{1n} and TPA cross section δ computed at the INDO/MRDCI level.

State n	E / eV	f	μ_{0n} / D	μ_{1n} / D	δ / GM
1 (OPA1)	2.07	1.33	13.0	1.5	0
2	2.16	0.01	1.1	0.3	12
3	2.18	0.00	0.7	0.3	5
4	2.19	0.00	0.6	0.1	7
5	2.41	1.56	13.0	10.7	0
6 (TPA1)	3.05	0.00	0.5	1.6	6927
7	3.10	0.32	5.2	12.8	45
8 (TPA2)	3.17	0.01	1.0	0.7	9733
9	3.32	1.01	9.0	2.6	14
10	3.35	0.08	2.5	0.6	176
11	3.46	0.82	7.9	0.3	3
12	3.47	0.00	0.3	0.5	12
13 (Soret1)	3.48	1.04	8.9	0.4	4
14 (Soret2)	3.52	2.85	14.6	0.2	17

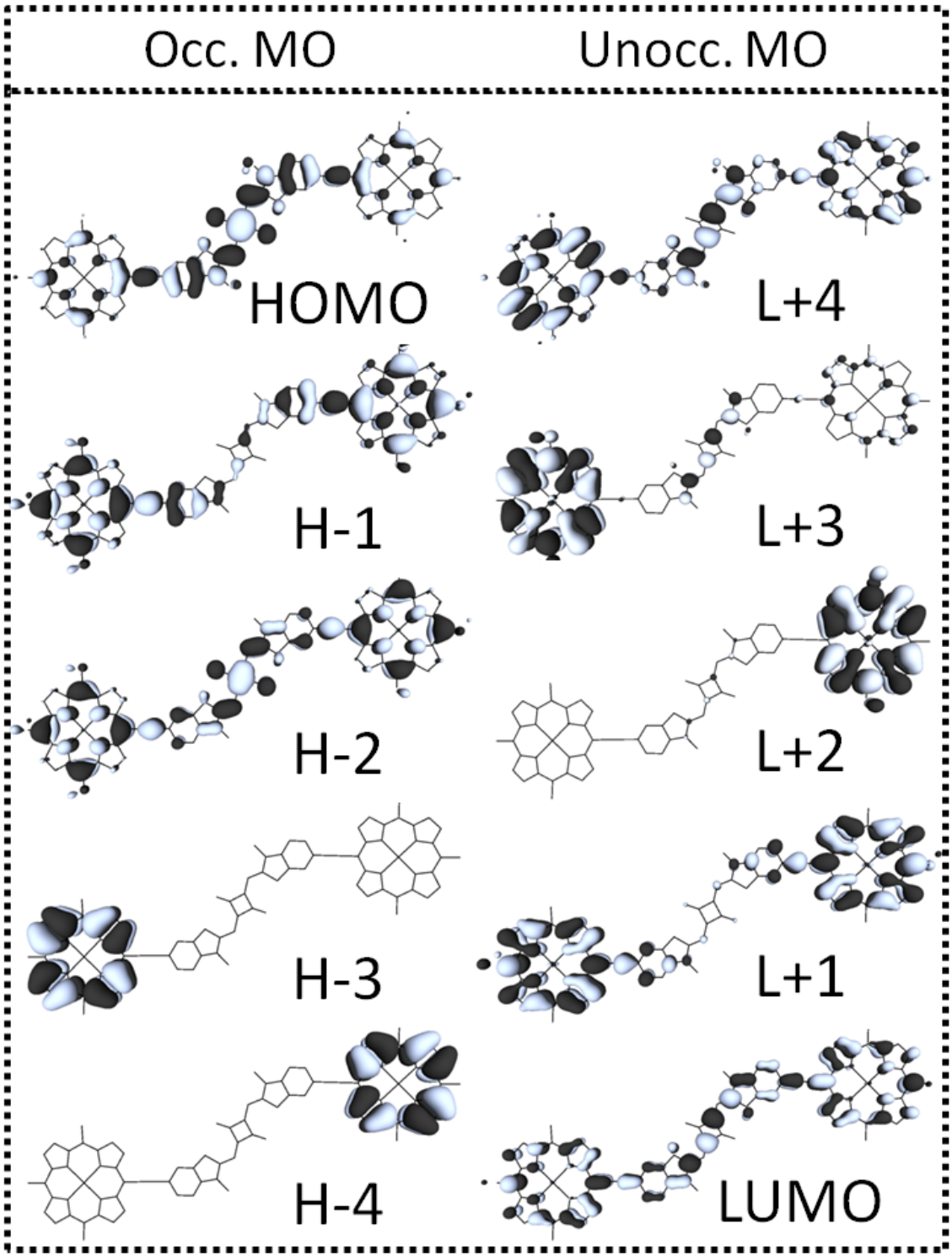

Figure B.1. DFT-B3LYP-calculated frontier orbitals of 1 (with all alkyl groups replaced by methyl groups).

REFERENCES

(1) Denk, W.; Strickler, J. H.; Webb, W. W. *Science* **1990**, *248*, 73.

(2) Cumpston, B. H.; et al. *Nature* **1999**, *398*, 51.

(3) Ehrlich, J. E.; Wu, X. L.; Lee, L. Y. S.; Hu, Z. Y.; Ro ¨ckel, H.; Marder,S. R.; Perry, J. W. *Opt. Lett.* **1997**, *22*, 1843.

(4) (a) Albota, M.; et al. *Science* **1998**, *281*, 1653. (b) Pond, S. J. K.; Rumi, M.; Levin, M. D.; Parker, T. C.; Beljonne, D.; Day, M. W.; Bre ´das, J. L.; Marder, S. R.; Perry, J. W*. J. Phys. Chem. A* **2002**, *106*, 11470. (c) Bartholomew, G.; Rumi, M.; Pond, S. J. K.; Perry, J. W.; Tretiak, S.; Bazan, G. C*. J. Am. Chem. Soc*. **2004**, *126*, 11529. (d) Chung, S.-J.; Rumi, M.; Alain, V.; Barlow, S.; Perry, J. W.; Marder, S. R. *J. Am. Chem. Soc.* **2005**, *127*, 10844. (e) Huang, P. H.; Shen, J. Y.; Pu, S. C.; Wen, Y. S.; Lin, J. T.; Chou, P. T.; Yeh, M. C. P. *J. Mater. Chem*. **2006**, *16*, 850.

(5) (a) Scherer, D.; Dorfler, R.; Feldner, A.; Vogtmann, T.; Schwoerer, M.; Lawrentz, U.; Grahn, W.; Lambert, C. *Chem. Phys.* **2002**, *279*, 179. (b) Fu, J.; Padilha, L.; Hagan, D. J.; Van Stryland, E. W.; Przhonska, O. V.; Bondar, M. V.; Slominksy, Y. L.; Kachkovski, A. D. *J. Opt. Soc. Am. B* **2007**, *24*, 67.

(6) (a) Chung, S. J.; Zheng, S. J.; Odani, T.; Beverina, L.; Fu, J.; Padilha, L. A.; Biesso, A.; Hales, J. M.; Zhan, X. W.; Schmidt, K.; Ye, A. J.; Zojer, E.; Barlow, S.; Hagan, D. J.; Van Stryland, E. W.; Yi, Y. P.; Shuai, Z. G.; Pagani, G. A.; Bredas, J. L.; Perry, J. W.; Marder, S. R. *J. Am. Chem. Soc.* **2006**, *128*, 14444. (b) Ohira, S.; Rudra, I.; Schmidt, K.; Barlow, S.; Chung, S.-J.; Zhang, Q.; Matichak, J.; Marder, S. R.; Brédas, J.-L. *Chem.—Eur. J*. **2008**, *14*, 11082.

(7) (a) Drobizhev, M.; Stepanenko, Y.; Dzenis, Y.; Karotki, A.; Rebane, A.; Taylor, P. N.; Anderson, H. L. *J. Am. Chem. Soc.* **2004**, *126*, 15352. (b) Karotki, A.; Drobizhev, M.; Dzenis, Y.; Taylor, P. N.; Anderson, H. L.; Rebane, A. *Phys. Chem. Chem. Phys.* **2004**, *6*, 7. (c) Drobizhev, M.; Stepanenko, V.; Dzenis, Y.; Karotki, A.; Rebane, A.; Taylor, P. N.; Anderson, H. L. *J. Phys. Chem. B* **2005**, *109*, 7223.